HYDROGEN GENERATION FROM ALUMINUM-WATER SYSTEMS

by

EDITH BARBARA CZECH

Diplom, The Rheinische Friedrich-Wilhelms-University of Bonn, 1988

A THESIS SUBMITTED IN PARTIAL FULFILMENT OF
THE REQUIREMENTS FOR THE DEGREE OF

MASTER OF SCIENCE

in

THE FACULTY OF GRADUATE STUDIES

(Materials Engineering)

THE UNIVERSITY OF BRITISH COLUMBIA

April 2006

Abstract

Aluminum is one of the most active metals with high affinity to oxygen. In reality however, its reactivity is drastically reduced by the presence of a nanometer-thin oxide film which prevents (or slows down) its corrosion in environments in which the pH ranges from about 4 to 9. Increased reactivity and uniform corrosion is observed typically only in high alkaline or high acidic solutions in which the film dissolves.

It has been recently discovered at UBC that the passivation of aluminum in aqueous solutions of neutral and near-neutral pH can be prevented when Al is mechanically alloyed with a non-metallic second phase, such as alumina, carbon or metal oxides [1, 2]. In this work another variant of this system, the Al-WIS (Water-soluble Inorganic Salts such as KCl or NaCl) system, is introduced. The rapid and massive corrosion reaction of the mechanically alloyed Al-WIS system, which takes place in tap (or marine, or ground) water, releases remarkably high amounts of hydrogen gas. This system can therefore be utilized as in situ, on demand hydrogen generation method through aluminum-assisted water split reaction.

Al-WIS powders were prepared by high-energy ball-milling. Powder mixtures as well as salt-free (leached-out) Al powders were characterized using SEM, EDS, XRD, XPS and BET methods. Reaction enthalpy was determined using DSC and the pH shift during the reaction was monitored with a pH meter. The effects of WIS concentration, chemistry of other additives, powder particle size, temperature, and milling conditions on the reaction kinetics were investigated. The H_2 yield and Al-WIS reaction efficiency were high. From 1 g of mechanically alloyed Al powder, up to 1.25 litres of hydrogen gas were generated in the first hour of the reaction, i.e. efficiency up to 92% was achieved. Besides pure gaseous hydrogen, only pure solid aluminum hydroxides were formed as the reaction products. Bayerite ($Al(OH)_3$) was predominantly formed at $T < 60°C$ whereas boehmite (AlOOH) at $T > 100°C$. Both phases were present in the temperature range between $60°C < T < 100°C$.

Table of Contents

Abstract ii

Table of Contents iii

List of Tables vii

List of Figures viii

List of Equations xi

Acknowledgements xiii

1. Introduction and Objectives 1

2. Literature Review 3

2.1. Hydrogen as Fuel 3

2.2. Hydrogen Generation Methods 4

2.2.1. Steam Reforming 4

2.2.2. Coal Gasification 4

2.2.3. Water Electrolysis 5

2.2.4. Biomass Gasification 5

2.2.5. Other Methods 6

2.3. Hydrogen Storage 6

2.3.1. On-demand Hydrogen Generation by Water Splitting 6

2.4. Aluminum and its Production 9

2.5. Reaction of Aluminum with Water - Corrosion of Aluminum 11

2.5.1. Surface Oxide Film on Aluminum and its Formation 12

2.5.2. Kinetics of Oxide Film Formation 13

2.5.3. Anomalies in the Oxide Film on Aluminum 14

2.5.4. Surface Oxide Charge 15

2.5.5. Dissolution of the Aluminum Oxide Film 16
2.5.6. Precipitates in Al-O-H System and their Thermal Decomposition 17
2.5.7. Localized Corrosion of Al in Solutions of Neutral and Near-Neutral pH 19
2.5.7.1. Localized Corrosion in the Presence of Metallic Impurities 19
2.5.7.2. Localized Corrosion in Presence of Ions in the Aqueous Solution 20
2.5.7.3. Corrosion of Al in Presence of Alumina Particles and Chloride Ions 25
2.5.8. Influence of Microstructure and Deformation on Aluminum Corrosion 26
2.6. High Energy Ball-Milling 27
2.6.1. Factors Affecting Mechanical Milling 28
2.6.2. High Energy Ball-Milling with SPEX 8000 30
3. Experimental Procedures 32
3.1. Materials 32
3.2. Powder preparation 32
3.2.1 Leaching of Ball-Milled Al-Salt Powder Mixtures 36
3.2.2 Annealing of Ball-Milled Powders 37
3.3. Microstructural Characterization 37
3.3.1. Scanning Electron Microscopy (SEM / EDS) 37
3.3.2. X-Ray Powder Diffractometry (XRD) 38
3.3.3. X-Ray Photoelectron Spectroscopy (XPS) 39
3.3.4. Surface Area Measurement by BET Analysis 39
3.4. Reaction Characterization 40
3.4.1. Differential Scanning Calorimetry (DSC) 40
3.4.2. pH Measurements 41
4. Results and Discussion 42
4.1. Characterization of As-Received Materials 42

4.2. Characterization of Ball-Milled Powders 48
4.2.1. Surface Morphology and Particle Size Analysis 48
4.2.2. Elemental Analysis of Ball-Milled Composite Powders 57
4.2.2.1. X-Ray Photoelectron Spectroscopy (XPS) of Powder Surface 57
4.2.2.1.1. XPS Survey Scans 57
4.2.2.1.2. High Resolution XPS of O 1s and Al 2p 60
4.2.2.2. Energy Dispersive X-Ray Analysis of Ball-Milled Composite Powders 63
4.3. Hydrogen Generation through Al-assisted Water Split Reaction 65
4.3.1. Influence of the Additive on Hydrogen Generation 66
4.3.1.1. Additive - free Aluminum-H_2O Systems 66
4.3.1.2. Aluminum-Additive-H_2O Systems 70
4.3.1.3. Aluminum-H_2O Systems with Leached-out Additive 73
4.3.2. Influence of Additive Concentration on Hydrogen Generation 75
4.3.3. Influence of Additives and Impurities on Hydrogen Generation 76
4.3.3.1. Influence of Other Additives on Hydrogen Generation 76
4.3.3.2. Influence of Water Quality on Hydrogen Generation 80
4.3.4. Influence of Ball-Milling Time on Hydrogen Generation 81
4.3.5. Influence of Aluminum Heat Treatment on Hydrogen Generation 84
4.3.6. Influence of Temperature on Hydrogen Generation 88
4.3.6.1. Influence of Water Temperature 88
4.3.6.2. Influence of Reaction Heat 89
4.3.7. Influence of Solution pH on Hydrogen Generation 92
4.4. Characterization of Reaction Products 96
5. Conclusions and Recommendations 100

6. References 104

Appendix A 113

Appendix B 115

List of Tables

Table 2.1: Aluminum oxides and hydroxides 18

Table 2.2: Standard electrode potentials vs. SHE at 25°C for some metals. 20

Table 2.3: Corrosion rates of Al-6061 alloy in NaCl aqueous solutions 23

Table 2.4: Corrosion of pure Al and Al-6061 alloy in NaCl solutions of different pH 23

Table 2.5: The anodic, cathodic and oxide dissolution reactions of Al 25

Table 3.1: Ball-milling parameters for Al-additive systems. 35

Table 3.2: Ball-milling parameters and experimental conditions for hydrogen generation 35

Table 4.1: The elemental composition of the Al powder surface obtained by XPS and EDX 48

Table 4.2: Crystallite size and microstrain of ball-milled Al in Al-KCl powder mixtures 56

Table 4.3: The elemental composition of the Al and Al-NaCl powders obtained by XPS. 59

Table 4.4: Reference binding energies for the O 1s core-level. 60

Table 4.5: Aluminum oxide film thickness estimated from Al 2p peaks intensities. 63

Table 4.6: Gross oxygen concentration in fresh milled and 3 weeks aged Al-KCl(50wt%) 64

Table 4.7: Hydrogen generation from as-received and ball-milled additive-free Al powders 67

Table 4.8: Initial particle size of additives and the effect of additives on hydrogen yield 71

Table 4.9: Effect of water temperature on induction time and the amount of H_2 produced 88

Table 4.10: Estimation of the Al amount reacted with water using DSC data 92

Table 4.11: pH shift during Al-H_2O reaction in aqueous solutions of different start pH 96

List of Figures

Figure 2.1: Primary aluminum production (schematically). 10

Figure 2.2: Potential versus pH diagram for Al-H_2O system at 25°C. 16

Figure 3.1: Ball mill SPEX 8000. 33

Figure 3.2: Vial, grinding media and Al-additive powders. 34

Figure 4.1: SEM micrograph of as-received Al. 42

Figure 4.2: SEM micrograph of as-received KCl. 43

Figure 4.3: SEM micrograph of KCl after ball-milling (BM = 5 min). 43

Figure 4.4: SEM micrograph of as-received Al_2O_3 A16 (x1000). 44

Figure 4.5: SEM micrograph of as-received Al_2O_3 A16 (x30 000). 44

Figure 4.6: XPS survey scan of as-received Al powders. 46

Figure 4.7: High resolution Al 2p core–level XPS spectrum of as-received Al powders 46

Figure 4.8: XRD pattern of as-received Al powder. 47

Figure 4.9: SEM micrograph of Al-KCl (1:1) after 15 min ball-milling (x1000). 50

Figure 4.10: SEM micrograph of Al-KCl (1:1) after 15min ball-milling (x5000). 50

Figure 4.11: SEM micrograph of 15 min ball-milled and leached-out Al (x1000). 51

Figure 4.12: SEM micrograph of 15 min ball-milled and leached-out Al (x5000). 51

Figure 4.13: SEM micrograph of Al–Al_2O_3 A16 powder mixture after ball-milling 52

Figure 4.14: SEM micrograph of Al–Al_2O_3 A16 powder mixture after ball-milling 52

Figure 4.15: SEM micrographs of Al-KCl(50wt%) powder mixtures after mechanical alloying 53

Figure 4.16: Spatial element distribution in Al-KCl(50wt%) after mechanical alloying 54

Figure 4.17: XRD diffractograms of non-milled and mechanically alloyed Al-KCl(50wt%) 55

Figure 4.18: (111) Al diffraction peak of annealed and non-annealed Al-NaCl(50wt%) 57

Figure 4.19: XPS survey scan of Al-NaCl(50wt%) powder mixture, ball-milled for 15 min. 58

Figure 4.20: XPS survey scan of 15 min ball-milled and leached-out Al powder. 59

Figure 4.21: High resolution (a) O 1s and (b) Al 2p core–level XPS spectra of ball-milled Al . 62

Figure 4.22: Net increase in oxygen concentration in fresh ground and aged Al-KCl(50wt%)... 65

Figure 4.23: H_2 generation from as-received and ball-milled Al-only powders 68

Figure 4.24: SEM micrograph of ball-milled Al-only powders 69

Figure 4.25: XRD diffractograms of as-received and ball-milled Al-only powders. 69

Figure 4.26: Effect of various Al-additive-H_2O systems on the amount of generated H_2 gas 70

Figure 4.27: Typical stages of hydrogen generation during the first hour of Al-H_2O reaction.... 73

Figure 4.28: Comparison of H_2 generation from Al-NaCl-H_2O and leached-out Al-H_2O 75

Figure 4.29: Effect of the amount of KCl in Al-KCl powder mixture on the total amount of H_2 76

Figure 4.30: Effect of Mg on the induction time and reaction rate of the Al(Mg)-KCl-H_2O..... 78

Figure 4.31: Effect of $NaNO_3$ on the induction time and reaction rate of the Al-KCl($NaNO_3$)... 79

Figure 4.32: Influence of water quality on H_2 generation of the Al-KCl(50wt%) system..... ...81

Figure 4.33: Effect of grinding time on the amount of hydrogen produced from 1g Al powder. 82

Figure 4.34: Effect of regrinding of partly reacted powder mixtures..... 84

Figure 4.35: Hydrogen generation from annealed and standard Al-NaCl(50wt%) powder..... 86

Figure 4.36: Hydrogen generation from heat-treated and standard Al-Al_2O_3(50%) powder..... 86

Figure 4.37: Al-Al_2O_3 before and after heat treatment..... 87

Figure 4.38: Temperature change during the hydrogen generation reaction..... 90

Figure 4.39: Heat flow change as function of time during the hydrogen generation reaction 91

Figure 4.40: pH and T change during H_2 generation reaction of the Al-KCl(50wt%) system..... 94

Figure 4.41: pH shift during H_2 generation reaction of different Al-additive-H_2O systems..... 94

Figure 4.42: H_2 generation from ball-milled Al-KCl(50wt%) in solutions of different pH..... 95

Figure 4.43 XRD patterns of reaction products formed during the Al-KCl-H_2O reaction 97

Figure 4.44: SEM of reaction products formed during the Al-KCl(50wt%)-H_2O reaction 98

Figure 4.45: XRD diffractograms of reacted Al-KCl($NaNO_3$)(50wt%) powders 99

List of Equations

Step 1: $CH_4 + H_2O \rightarrow CO + 3H_2$	(2.1)	4
Step 2: $CO + H_2O \rightarrow CO_2 + H_2$	(2.2)	4
$NaBH_4 + 2H_2O \rightarrow NaBO_2 + 4H_2$	(2.3)	7
$NaH + H_2O \rightarrow NaOH + H_2$	(2.4)	7
$MgH_2 + 2H_2O \rightarrow Mg(OH)_2 + 2H_2$	(2.5)	7
$Na + H_2O \rightarrow NaOH + H_2$	(2.6)	7
$K + H_2O \rightarrow KOH + H_2$	(2.7)	7
$2Al + 3H_2O + \text{additive} \rightarrow 3H_2 + Al_2O_3 + \text{heat}$	(2.8)	8
$2Al + 6H_2O \rightarrow 3H_2 + 2Al(OH)_3$	(2.9)	9
$Al[O_x(OH)_y(H2O)_z] \rightarrow (AlOOH)_4 \cdot H_2O \rightarrow AlOOH \rightarrow Al(OH)_3$	(2.10)	13
$Al(OH)_3 + OH^- \rightarrow Al(OH)_4^-$	(2.11)	17
$Al_2O_3 + 3H_2O + 2\ OH^- \rightarrow 2\ Al\ (OH)_4^-$	(2.12)	17
$Al(OH)_3 + 3H_3O^+ \rightarrow Al^{3+} + 6H_2O$	(2.13)	17
$Al_2O_3 + 6H_3O^+ \rightarrow 2Al^{3+} + 9H_2O$	(2.14)	17
$Al + 3H_2O \rightarrow 1.5H_2 + Al(OH)_3$	(3.1)	34
$Al + 2H_2O \rightarrow 1.5H_2 + AlOOH$	(3.2)	34
$\beta = A_P / H_P$	(3.3)	38
$D = k\lambda/\beta\cos\theta$	(3.4)	38
$(\beta)^2 = (1/D)^2 + (2\varepsilon\ d^*)^2$	(3.5)	39
$Al + 3H_2O \rightarrow 3/2H_2 + Al(OH)_3$	(3.6)	40
$Al + 2H_2O \rightarrow 3/2H_2 + AlOOH$	(3.7)	41
$2Al + 3H_2O \rightarrow 3H_2 + Al_2O_3$	(3.8)	41
$\Delta H^\circ_{rxn} = \Delta H^\circ_{f\ \text{Bayerite, Boehmite or } \alpha\text{-alumina}} - n\ \Delta H^\circ_{f\ \text{Water}}$	(3.9)	41

$pH = -\log[H_3O^+]$	(3.10)	41
$pOH = -\log[OH^-]$	(3.11)	41
$K_w = [H_3O^+]\,[OH^-] = 1 \times 10^{-14}$	(3.12)	41
$2Al + 6H_2O \rightarrow 3H_2 + 2Al(OH)_3$	(4.1)	66
$2Al + 4H_2O \rightarrow 3H_2 + 2AlOOH$	(4.2)	66
$Al + 3H_2O \rightarrow 1.5H_2 + Al(OH)_3$	(4.3)	77
$Mg + 2H_2O \rightarrow H_2 + Mg(OH)_2$	(4.4)	77
$2Al + 6H_2O \rightarrow 3H_2 + 2Al(OH)_3$	(4.5)	96
$2Al + 4H_2O \rightarrow 3H_2 + 2AlOOH$	(4.6)	96

To my Mother

Acknowledgements

I would like to express my sincerest gratitude to my supervisor Professor Tom Troczynski for his guidance and continuous support throughout this program. Thanks are also extended to other faculty and staff members, and to fellow graduate students in the Materials Engineering Department.

In particular, I would like to acknowledge the assistance offered by Mary Mager with the SEM and EDS analyses, Babak Raeisinia with the DSC, Alex Tswetkov with annealing experiments and Mati Raudsepp of Earth and Ocean Sciences Department with XRD analyses.

I greatly appreciate the financial support of Global Hydrofuel Technologies Inc. (GHTI), Hydrogen Power Inc. (HPI) and Natural Science and Engineering Research Council of Canada (NSERC).

Last but not least, I would like to thank most profoundly my spouse Serhat Beyenir for his understanding, love and invaluable support in my personal and professional life.

1. Introduction and Objectives

Since the industrial revolution, fossil fuels have powered the technology and transportation networks. The worldwide increased demand for more energy on one side and massive depletion of fossil fuels on the other side has prompted researchers to look for alternative fuel sources. Pollution and enormous environmental problems caused by conventional fuels as well as stricter green house emission controls in some countries are other reasons for increased search for fuel alternatives. A variety of alternative fuels have been proposed. Out of these, hydrogen offers the greatest environmental benefits. However, appropriate and safe storage, both for stationary and mobile applications, is complicated, mainly because of the very low boiling point of hydrogen (20.28 K at 1 atm) and low density in its gaseous state (0.0899 g/L at 273 K) [3]. Metal hydrides are a safe alternative for hydrogen storage but the total amount of hydrogen stored in the hydride is low (generally 1 to 2 wt. % and when heated to temperatures higher then 250°C max. 8 wt. %) [4]. Another sound alternative, which eliminates the need for storage, is the on-board on-demand hydrogen generation. In this method H_2 gas after being released from a chemical compound through chemical reaction, powers directly a fuel cell or internal combustion engine. A suitable chemical system is characterized by high gravimetric hydrogen storage capacity, safe and reliable hydrogen release mechanism, controllable reaction kinetics, reaction constituents' availability and affordability, as well as the reaction products regeneration possibility.

One of the non-fossil, natural, abundant and safe chemical carriers of hydrogen is water and most commonly water electrolysis is used to split water in its components: H_2 and O_2. A novel method of hydrogen generation through aluminum-assisted water split reaction was investigated in this thesis. It has been found previously [1, 2] that the passivation of aluminum

can be prevented in neutral (pH 7) or near neutral pH conditions in water by grinding aluminum with an additive, such as alumina (Al_2O_3) or boehmite (AlOOH). By doing so, aluminum metal reacts continuously with water and produces appreciable amounts of hydrogen. Generally, aluminum has a very high affinity to oxygen and rapidly forms an oxide film on its surface [3, 5, 6]. This film prevents aluminum from reacting with water because the dissolution rate of the oxide in solutions of neutral pH range (pH 4 to pH 9) is very low. Reaction of aluminum at high rates with water is only possible in highly alkaline or highly acidic aqueous solutions in which the oxide film can be dissolved and hydrogen produced.

This research is a continuation of experimental work performed in the Ceramics Group of UBC in the last several years. The research was initiated by Prof. Asok Chaklader and led to two US patents "Hydrogen Generation from Water Split Reaction" [1, 2]. The present work also resulted in US patent application [7].

Specific objectives of this project are as follows:

1. Investigate the new Al-WIS (Water-soluble Inorganic Salts)-Water system and compare it to the previously studied Al-Alumina-Water system for H_2 generation,
2. Evaluate the influence of various processing and reaction parameters on water split reaction,
3. Study the role of ball-milling and the role of additives to the Al-H_2O system,
4. Optimize the parameters and maximize the H_2 generation yield and reaction rate,
5. Use SEM, EDX, XPS, BET and XRD to characterize the powders and reaction products,
6. Advance understanding of the process mechanisms and effects of the process parameters on the reaction.

2. Literature Review

2.1. Hydrogen as Fuel

Hydrogen has the highest energy content per unit weight of any known fuels (energy of combustion (LHV): 120.7 kJ/g for H_2, 42.5 kJ/g for gasoline) and it can be used with very high efficiency and zero or near-zero emissions at the point of use [8, 9, 11]. Through its reaction with oxygen, hydrogen may release energy explosively e.g. in heat engines or "quietly" e.g. in fuel cells, to produce water as its only reaction by-product. With progress in development of fuel cells and hydrogen-fuelled combustion engines hydrogen will become the most significant energy carrier of clean energy.

Hydrogen gas does not occur naturally in large quantities on Earth. It occurs in a variety of chemical compounds like water or hydrocarbons, which must be chemically transformed from a primary source to extract H_2 fuel. Steam reforming of natural gas is currently the most widely used method of hydrogen production. Close to 96% of the hydrogen produced worldwide is presently generated from fossil fuels such as natural gas, oil and coal. Most of the produced hydrogen is used as a chemical, rather than a fuel, in a variety of commercial applications. The refinery sector (diesel fuel desulphurization, gasoline de-aromatization) and the chemical industry (production of ammonia-based fertilizers, methanol and hydrochloric production) account for most of the world hydrogen consumption. Hydrogen produced from fossil fuels, when purified and free from carbon monoxide, has the potential to be used for powering vehicles, running turbines or fuel cells to generate heat and electricity. However, the ultimate goal is to find inexpensive and efficient routes to create hydrogen in sufficient quantities using non-fossil natural resources and renewable energy sources.

2.2. Hydrogen Generation Methods

2.2.1. Steam Reforming

Steam reforming of natural gas is currently the most common commercial form of hydrogen production worldwide. In this process, gases such as methane (CH_4), propane, or ethane (also liquid hydrocarbons or methanol) are combined with high temperature steam (700°C to 1000°C and pressures in the order of 2.5 MPa) where they react in presence of a catalyst to hydrogen and carbon monoxide [3, 11]. A subsequent water-gas shift reaction treats the carbon monoxide with more steam and oxidizes it catalytically into carbon dioxide thereby producing even more hydrogen. The following reactions represent the methane steam reforming process:

Step 1: $CH_4 + H_2O \rightarrow CO + 3H_2$ (2.1)

Step 2: $CO + H_2O \rightarrow CO_2 + H_2$ (2.2)

Heavy hydrocarbons are converted to hydrogen by using a similar reaction called partial oxidation method where oxygen, steam and fuel are fed into the system in a controlled manner and oxidized. Steam reformation of natural gas is one of the best understood and least expensive method today. It currently accounts for approximately 80% of global hydrogen production [8]. The disadvantage of this hydrogen production method is its dependence on the potentially limited and volatile natural gas or fossil fuels supply and the emission of CO_2 into the atmosphere [10, 11].

2.2.2. Coal Gasification

Coal gasification is the second most used method for hydrogen production. In the coal gasification process pulverized coal is converted into gas by rapid oxidation of the coal with steam and oxygen (air) at temperatures up to 2000 K [11]. Significant emissions of carbon

dioxide and also other pollutants such as sulphur and carbon monoxide are associated with coal gasification [11]. Coal gasification is the oldest method of hydrogen production..

2.2.3. Water Electrolysis

Water electrolysis is a well-established industrial process in which electricity is used to split water into hydrogen and oxygen, generating hydrogen in a 1:1 molar ratio ($2\ H_2O \rightarrow 2H_2 + O_2$) with cell efficiencies in the order of 75 to 85%. In order to keep the produced gases isolated, the two reaction areas are separated by an ion conducting separator (diaphragm) [3].

Even though electrolysis is the most common and very well understood method of hydrogen production from non-fossil resources, hydrogen generation by water electrolysis is the most energy intensive and therefore costly method. However, hydrogen produced using electrolysis has the potential to be completely emissions free if the electricity used is generated from clean, renewable sources such as wind and solar [9, 10]. As aluminum smelting is also electrical energy-intensive, hydrogen generation through Al-assisted water split may be compared to water electrolysis (Appendix A).

2.2.4. Biomass Gasification

Biomass gasification is currently one of the most advanced methods of producing hydrogen from renewable resources [12]. A wide variety of agricultural wastes and other biomass sources can be used to produce hydrogen. In the biomass gasification process, biomass such as forestry by-products, straw, municipal solid waste or sewage is heated at high temperatures in a reactor and transformed to mainly hydrogen, carbon monoxide, and methane (CH_4). Using steam reformation processes, methane is converted into hydrogen and carbon dioxide. The hydrogen content of the gas is determined by the process parameters: pressure and temperature [11].

2.2.5. Other Methods

A variety of novel approaches to H_2 generation are being investigated on the laboratory scale. These include innovations in deriving hydrogen thermochemically from hydrocarbons; thermochemical, photoelectric or photocatalytic split of water and other chemical compounds such as HBr, as well as the biological hydrogen generation by algae and bacteria. However, for most of these methods, hydrogen storage and delivery to the user remain a major challenge.

2.3. Hydrogen Storage

Very large quantities of gaseous hydrogen can be stored underground in depleted oil or gas fields, and salt or rock caverns [10]. Intermediate to small quantities of H_2 gas are stored stationary in fuel vessels or tanks in either compressed (pressures up to 8000 psi) or liquidized form (at -253°C). Hydrogen can also be stored in a hydrogen compound such as a metal hydride, from which the hydrogen is removed by applying heat. For use in transportation, the on-board storage of hydrogen must be realized. Limited gas reservoirs, increased risks of a pressurized gas container or expensive and technologically challenging cooling solutions for cryogenic hydrogen are the major disadvantages of on-board hydrogen storage. An alternative, the on-board on-demand hydrogen generation is an elegant solution as it produces as much H_2 fuel as needed close to the site where it is consumed [9, 10] .

2.3.1. On-demand Hydrogen Generation by Water Splitting

The most promising route to produce hydrogen from non-fossil natural resources is by splitting water, which is a natural carrier of hydrogen. There are several systems - either in

development or already in commercial use - that are able to produce hydrogen on-demand by generation of hydrogen gas from water using chemical reactions.

In one of the methods, used by *Millennium Cell* [13], pure hydrogen is generated by the catalytic decomposition of sodium borohydride in aqueous solutions:

$$NaBH_4 + 2H_2O \rightarrow NaBO_2 + 4H_2 \quad (2.3)$$

Even though aqueous solutions of $NaBH_4$ have won more interest as a large scale high-purity hydrogen gas generator system in the last few years, the system is generally difficult to control as the reaction is highly exothermic and the hydrogen yield is temperature sensitive. Additionally, the reaction must take place at a high alkaline pH and requires an expensive catalyst (Ru, Rh or Pt) [14, 15]. Further disadvantage is the high cost (~ 60 to 80 US$/kg) and limited availability of the $NaBH_4$ compound.

Other potential sources for hydrogen are chemically decomposable metal hydrides. NaH, MgH_2 and CaH_2 after reacting with water provide acceptable hydrogen production rates and good yields to supply small fuel cells with hydrogen [16].

$$NaH + H_2O \rightarrow NaOH + H_2 \quad \text{or} \quad (2.4)$$

$$MgH_2 + 2H_2O \rightarrow Mg(OH)_2 + 2H_2 \quad (2.5)$$

These reactions are used in technologies developed by *Powerball Technologies* [17] and *Safe Hydrogen* [18] to generate high-purity hydrogen gas on-demand.

Alkaline metals, such as sodium (Na) or potassium (K) react spontaneously and violently in presence of water.

$$Na + H_2O \rightarrow NaOH + H_2 \quad \text{or} \quad (2.6)$$

$$K + H_2O \rightarrow KOH + H_2 \quad (2.7)$$

These reactions are highly exothermic, continue until metals are fully reacted and are therefore not easy to control. Additionally, the reaction products are strongly alkaline and thus corrosive, dangerous to handle and potentially polluting to the environment [3].

A few methods of hydrogen generation are based on aluminum-water reaction. Andersen et al. [19] patented a process of producing hydrogen by reacting aluminum with water in the presence of sodium hydroxide, NaOH, as a catalyst.

$$2Al + 3H_2O + \text{catalyst} \rightarrow 3H_2 + Al_2O_3 + \text{heat} \qquad (2.8)$$

The reaction rates in the highly alkaline NaOH solutions are high as long as the metal is physically separated from the solid reaction products. The reaction is complete and yields 100% of H_2 gas. However, the authors state that any chemical reaction that progresses in the presence of sodium hydroxide does not represent an attractive source of hydrogen for use by the general public as elevated safety procedures must be applied.

Watanabe et al. [20] patented a method for producing hydrogen gas utilizing a so called mechano-corrosive reaction of metals in water. Aluminum or Al alloys are turned into fine particles by applying friction movement to the surface under water. The reactivity of the metal is increased because continuously fresh aluminum surfaces are created by removing or destroying of the protective oxide layer. Additionally, numerous cracks and lattice defects which are formed during friction movements enhance further the chemical reactivity of the surface. H_2 gas is produced as long as the metal can be oxidized. The authors claim that this method is safe, of low cost and suitable especially for industrial waste metals.

A novel and unique method of generating hydrogen from water is through aluminum assisted water-split reaction using mechanical mixtures of metal-ceramic composites. This method was proposed in two patents by A. Chaklader [1, 2]. The water split reaction by aluminum takes place in water at neutral or near neutral pH ($4 < pH < 10$). The pure hydrogen is

released as gas and the oxygen combines with the aluminum to form aluminum hydroxide compounds.

$$2Al + 6H_2O \rightarrow 3H_2 + 2Al(OH)_3 \qquad (2.9)$$

The process requires that Al and the promoter are fine grained and intimately blended together. The addition of a promoter (alumina or boehmite) prevents the passivation of the aluminum metal during H_2 generation at a mild pH. The on demand hydrogen generation is simple, safe and pollution-free, and the high hydrogen storage capacity of 11 wt % is promising (see Appendix B). The amount of H_2 generated from an Al-calcined boehmite B700-H_2O system was reported to be 515 cc H_2 /1 g of Al at 50 °C after one hour of reaction. This thesis builds on this discovery by investigating alternative (e.g. water soluble) promoters of this reaction.

2.4. Aluminum and its Production

Aluminum is the most abundant metal, and the third most abundant element in the Earth's crust (about 8 % by weight); however, elemental aluminum does not occur in nature. The main source of aluminum is bauxite ore. On average 4 to 5 tonnes of bauxite are needed to produce two tonnes of alumina, from which one tonne of aluminum can be produced. Aluminum is a silvery-white, light metal with a specific density of 2.70 g/cm^3 and a melting point of 660°C. Pure aluminum is soft and highly ductile so that it can be easily formed, machined, or cast; is nonmagnetic and a good conductor of heat and electricity; has excellent corrosion resistance due to a protective coating of aluminum oxide formed on the surface. Al alloys are repeatedly recyclable for environmental sustainability. Its low mechanical strength can be significantly increased by alloying. Aluminum alloys may contain as much as fifteen percent of metals such as silicon, chromium, copper, iron, magnesium, manganese, nickel, titanium and zinc. Aluminum and aluminum alloys found many engineering applications from food packaging, to

construction and aircraft industry especially because of their combination of lightness with strength, their non-toxic qualities, as well as their high corrosion resistance.

Two industrial processes are applied to produce aluminum from bauxite. The first one, the Bayer process, is used to obtain aluminum oxide from bauxite; the second one, the Hall-Héroult process, is used to produce aluminum from alumina by electrolytic reduction. Figure 2.1 illustrates schematically the primary aluminum production process. Most smelters produce aluminum of 99.6-99.9% purity. High purity Al (99.99%) is used for special applications where high ductility or conductivity are required.

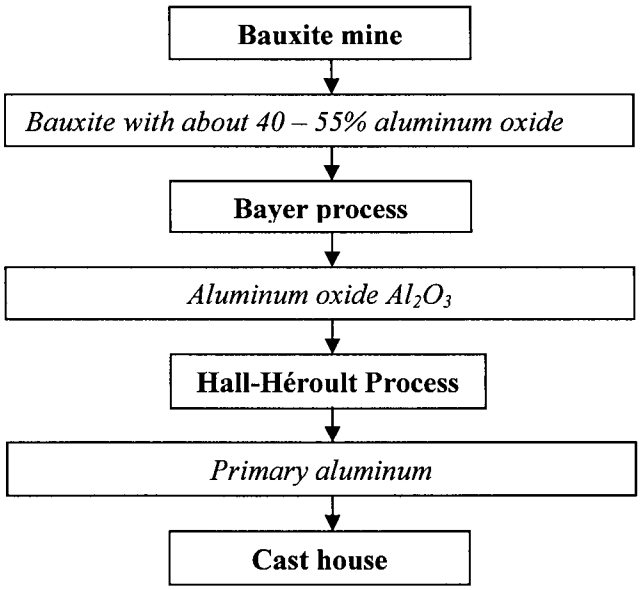

Figure 2.1 *Primary aluminum production (schematically).*

The aluminum smelting process is energy intensive, with electricity accounting for 25 to 35 percent of the total production costs. Only paper, gasoline, steel, and ethylene manufacturing consume more energy [12]. To reduce costs, aluminum smelters are often located in areas which have access to abundant power resources. Canadian aluminum smelters operate entirely on hydropower [12]. On average, it takes approximately 15 kWh of electricity to produce one

kilogram of primary aluminum from alumina. Design and process improvements have progressively reduced this figure from about 21 kWh in the 1950's.

The world trade price for 1 tonne of primary aluminum is currently US $1,850 or US $ 0.90/lb (September 2005) comparing to US $1,575 in December 2003 [21].

Secondary aluminum production (from Al scrap) accounts for roughly one-quarter of the total aluminum production worldwide. The melting and purification of scrap to produce secondary aluminum consumes less than 6 percent of the energy required to produce primary aluminum [12]. Depending on quality, the price for secondary aluminum is currently US $0.60 to 0.70/lb (September 2005).

2.5. Reaction of Aluminum with Water - Corrosion of Aluminum

Generally, "Corrosion is an irreversible interfacial reaction of a material (metal, ceramic, polymer) with its environment which results in consumption of the material or in dissolution into the material of a component of the environment. Often, but not necessarily, corrosion results in effects detrimental to the usage of the material considered." *(Definition by International Union of Pure and Applied Chemistry (IUPAC))* [101].

The corrosion of a metal covered with a thin film of condensed moisture or a metal immersed in an aqueous solution is determined by complex chemical and electrochemical corrosion reactions at the metal/electrolyte interface. An electrochemical reaction is a reaction involving the transfer of charges as part of a chemical reaction as different areas of the surface act as anode and cathode. At the anodic areas the metal is oxidized while at the cathodic areas the dissolved oxygen is simultaneously reduced or hydrogen is evolved. Typical electrochemical reactions in corrosion are metal dissolution ($Al \rightarrow Al^{3+} + 3e^-$) at the anode and oxygen reduction ($O_2 + 2H_2O + 4e^- \rightarrow 4OH^-$) and the H_2 evolution reaction (in acidic environment common is: $2\ H_3O^+ + 2e^- = H_2 + 2H_2O$) at the cathode. A typical chemical reaction, which does not involve a transfer of charge, is the precipitation of metal hydroxides ($Al^{3+} + 3OH^- \rightarrow Al(OH)_3$). An

insulating or semiconductive oxide film on the metal forms a barrier for electronic and ionic charges protecting the metal from oxidation and dissolution. Consequently, the properties of the oxide layer will determine the reactivity and corrosion behaviour of the metal.

2.5.1. Surface Oxide Film on Aluminum and its Formation

Aluminum is one of the most reactive metals, surpassed only by magnesium and beryllium. However, aluminum shows an excellent resistance to corrosion in air, water, many soils and chemicals, and most foods. The high corrosion resistance exhibited by aluminum and aluminum alloys is attributed to the formation of a highly protective oxide film which, if damaged, reforms almost immediately in most environments. The inert film attains a thickness of about 10 Å within seconds on the freshly exposed metal surface [22, 24]; continuation of growth is noticeably influenced by the environment, being accelerated by increasing temperature and humidity. Impurities and alloying metals will alter the formation and behaviour of the film. The barrier film formed on Al and Al-alloys is of duplex nature. It consists of an amorphous, compact and stable inner layer of oxide covered with a porous, less stable outer layer which is more susceptible to corrosion [22, 25, 26]. The outer layer of the air-formed oxide films is assumed to consist of bayerite, $Al(OH)_3$. However, the entire oxide is often referred to as amorphous aluminum oxide films because electron diffraction fails to disclose the true structure of the very thin films [27, 28]. An air-formed oxide film has a temperature-dependent limiting thickness and is about 2 to 5 nm thick when grown at room temperature and ~ 100 nm when grown at temperatures as high as 500°C [22, 29, 30]. Immersion in water results in oxide film thickening since the thin air-formed oxide film transforms in water to solid gel-like hydroxo-complexes of undefined structure and idealized formula of $Al[O_x(OH)_y(H2O)_z]$ [23, 33]. In the

process of aging, the gelatinous alumina transforms in aqueous solutions into pseudo-boehmite and finally bayerite according to [32, 34]:

$$Al[O_x(OH)_y(H2O)_z] \rightarrow (AlOOH)_4 \cdot H_2O \rightarrow Al(OH)_3 \qquad (2.10)$$

The structure as well as the chemical and physical properties of the oxide film can be very different as they depend on the growth conditions and environment. Besides spontaneous oxide formation in air, oxides can be grown anodically or thermally. Anodic films, for example, that were grown by anodization in borate and tartaric acid solutions are thin, dense, coherent and amorphous, whereas films grown in sulphuric and phosphoric acids are thick, porous and crystalline [29, 35]. Thermally grown oxide films which are formed during heating in oxygen or air at temperatures up to 425°C are amorphous, whereas films grown above 425°C show γ-Al_2O_3 crystals which form locally under the amorphous layer [36]. The composition and quality of oxide films grown in water depend primarily on the reaction temperature as well as the water constituents. At lower temperatures (up to 80°C) predominantly bayerite, $Al(OH)_3$ (expressed also as $Al_2O_3 \cdot 3H_2O$) and pseudoboehmite are formed, while at higher temperatures boehmite, AlOOH (expressed also as $Al_2O_3 \cdot H_2O$) grows on the Al surface [35, 37].

2.5.2. Kinetics of Oxide Film Formation

The Mott-Cabrera model is one of the models describing the formation and growth kinetics of the passive film. This model assumes that the film growth is due to the transport of metal cations Al^{3+} across the oxide film to the film/solution interface where they react with the electrolyte. The migration of the cations through the film is assumed to be assisted by the high electric field created by oxygen atoms on the outer amorphous oxide layer [36]. Oxide growth occurs simultaneously at the oxide/electrolyte interface by Al^{3+} metal ion migration outwards, and at the metal/oxide interface by O^{2-} ions migration inward [38, 39]. The rate-limiting step for the

film growth is the emission of metal cations from metal into the film at the metal/oxide interface [40, 41].

The initial stages of oxide film formation on monocrystalline Al in air were studied by Brune et al. [43]. The (111)Al surface with a very low defect density was investigated at 300 K and in an atmosphere where oxygen concentration was well controlled. The chemisorbed oxygen atoms nucleate preferentially at step edges forming islands up to 20 Å in diameter. Upon further oxidation these islands fill up the entire (111) aluminum surface and form ultimately a full monolayer of chemisorbed oxygen on the metal substrate [43, 44]. Jennison et al. predicts that in the next 2 to 3 O-layers (5 to 7 Å), Al ions will prefer distorted tetrahedral sites over the normal octahedral sites formed by oxygen [44].

2.5.3. Anomalies in the Oxide Film on Aluminum

"Easy Paths"

The microscopic surface roughness of the substrate plays a crucial role in the diffusion of oxygen through the amorphous oxide layer and the formation of the so called "easy paths" [36, 45]. The inwards diffusion of molecular oxygen through the amorphous aluminum oxide layer and the formation of γ-Al_2O_3 nuclei under the film during the process of thermal oxidation at temperatures in the range 300 - 425°C in air or oxygen is not random over the surface. The inward diffusion of oxygen follows "easy paths" that are located in the oxide film above and along metal ridges. Ridges on the Al substrate surface are associated with metal treatment prior to native oxide growth. The nature of "easy paths" and oxygen transport mechanism is still in discussion. The formation of cracks due to the development of tensile stresses above ridges (i.e. due to the difference in thermal expansion coefficient between the oxide and aluminum) or the less dense amorphous oxide film in the ridge region are the two possible explanations that were offered in literature [36, 45].

Locally enhanced oxidation on pre-existing ridges was also observed during anodic oxidation of aluminum in acidic solutions in which porous oxide films are formed [46]. Higher local conductivity, higher concentration of point defects and accumulation of impurities especially on ridges are some of the assumptions for the enhanced oxide growth at ridges.

Flaws

The morphology of the aluminum surface influences the growth and the morphology of the coating deposited on the metal in aqueous acidic solutions at room temperature [47, 48]. Preferential deposition was observed where grain boundaries or cellular boundaries intersect the surface forming ridges on the substrate and flaw sites in the protective oxide film. Grain boundaries are sites where an increased segregation of impurities occurs. These local impurities build-ups serve as cathodic sites during corrosion whereby flaws provide easy paths for electronic conduction through the otherwise insulating oxide. The geometry of the network of cathodic and anodic cells seems to be determined by the crystallographic orientation of grains at the surface, whereas their dimension is primarily dependent on the purity of the metal [47]. The presence of metallic impurities, even at concentrations that are in ppm range, affects the overall topography of the oxide by local film dissolution and pits nucleation. [49, 50, 51]

2.5.4. Surface Oxide Charge

The surface charge on the oxide film is important for the interaction with charged species such as dissolved anions or dipole present in the solution. The isoelectric point of the air-formed oxide film on aluminum when immersed in aqueous solutions has been determined to be a pH of 9.5 [52]. Because the outermost surface of an Al oxide film is terminated with a layer of hydroxyl groups, in neutral to acidic solutions the oxide film will have a positive surface charge; the surface will acquire a negative charge in solutions of pH > 9.5.

2.5.5. Dissolution of the Aluminum Oxide Film

The theoretical thermodynamic stability of the protective oxide and the corrosion behaviour of aluminum in aqueous solutions of varying pH may be expressed using the potential-pH or Pourbaix diagram, shown in Figure 2.2. Aluminum, which was passivated at lower temperatures (T = 25°C) with a film of bayerite, remains passive over a wide pH range - from about pH 4 to pH 8.5, indicating that the solubility of the protective oxide film on aluminum in neutral aqueous solutions at T = 25°C is very low. The solubility increases and is high in strong acidic and alkaline solutions, some exceptions apply (e.g. for concentrated nitric acid and ammonium hydroxide).

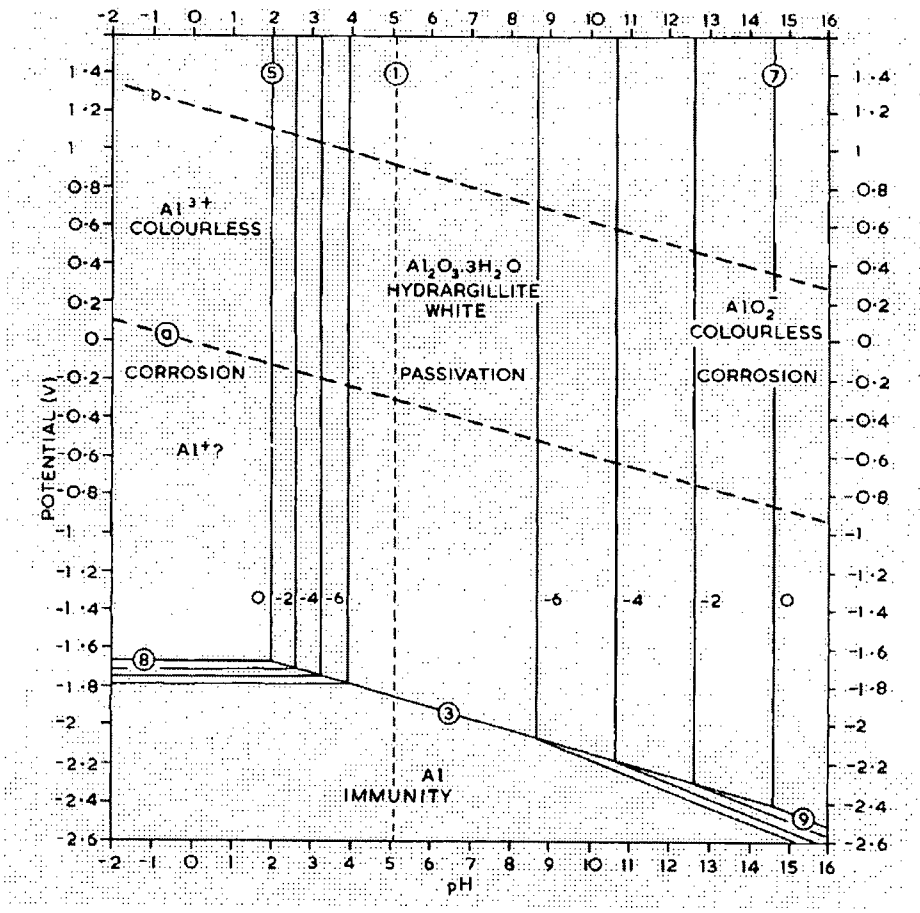

Figure 2.2 *Potential versus pH diagram for Al-H_2O system at 25°C* [53].
(Copyright permission has been granted by the publisher (NACE International)).

In strong alkaline environments aluminum oxide or hydroxide dissolves to produce aluminate ions $Al(OH)_4^-$, sometimes also expressed as AlO_2^-:

$$Al(OH)_3 + OH^- \rightarrow Al(OH)_4^- \quad (2.10)$$

$$Al_2O_3 + 3H_2O + 2\ OH^- \rightarrow 2\ Al\ (OH)_4^- \quad (2.11)$$

In strong acidic environments Al^{3+} ions are formed:

$$Al(OH)_3 + 3H_3O^+ \rightarrow Al^{3+} + 6H_2O \quad (2.12)$$

$$Al_2O_3 + 6H_3O^+ \rightarrow 2Al^{3+} + 9H_2O \quad (2.13)$$

Because of the small radius and high charge of the aluminum cation, water molecules bind to Al^{3+} forming the stable hexahydrated aluminum ions $[Al(H_2O)_6]^{3+}$ in acidic solutions (pH < 4) [54, 55]. In neutral and near-neutral solutions (4 < pH < 9) the dissolved product varies from $[Al(OH)]^{2+}$ to many different de-protonated hydroxo-complexes such as: $[Al(OH)(H_2O)_5]^{2+}$ $[Al(OH)_2(H_2O)_4]^+$, $[Al(OH)_3(H_2O)_3]$ or $[Al(OH)_4(H_2O)_2]^-$ [32].

The behaviour of Al in aqueous solutions of different pH is described in Chapter 2.5.7 and all essential reactions are presented in Table 2.5. The boundaries of passivity and the reaction product species that will be found in the solution depend on the temperature, pH, oxygen concentration, nature of the anionic species present in the solution and the form of the oxide or hydroxide present as their solubility varies [56]. Pseudoboehmite is more soluble than bayerite, and bayerite more soluble than corundum.

2.5.6. Precipitates in Al-O-H System and their Thermal Decomposition

The precipitates of aluminium after reaction with water are monomeric and polymeric hydroxy species, colloidal polymeric solutions and gels, as well as the crystallized solids, such as $Al(OH)_3$, AlOOH and the poorly crystallized pseudoboehmite. All the precipitates are based on

hydrated positive ions or hydroxylated aluminates. Table 2.1 lists some of the aluminum oxide and aluminum hydroxides properties.

Table 2.1 *Aluminum oxides and hydroxides.*

Name	**Formula**	**Crystal System**	**Density [g/cm^3]**	**ΔH_f [kJ/mol]**
Corundum	Al_2O_3	trigonal	3.98	-1654
Bayerite	Al(OH)3	monoclinic	2.53	-1277
Boehmite	AlOOH	orthorhombic	3.01	-988
Pseudoboehmite	$Al(OH)_3 \cdot nH_2O$ $(n \geq 3)$			

The crystal structure of the solids differs greatly from each other. Bayerite has a hydroxyl lattice structure that approximates hexagonal close-packing. The Al atoms occupy 2/3 of the available octahedral sites so that the basic structure can be described as a sandwich of aluminium atoms between a double layer AB of hydroxyl groups. Within the sandwich, the $Al(OH)_6$ octahedra are joined along edges forming hydroxyl sheets. Slight distortion of the octahedra lowers the symmetry of the structure to monoclinic. The stacking order of the hydroxyl group double layer is AB-AB-AB.

Boehmite has a layered structure comprising oxygen and hydroxyl ions with interstitial aluminum ions, held together by hydrogen bonding between the hydroxyl groups of adjacent layers. The orthorhombic boehmite is characterized by a more open, channel-like structure.

The crystal structure of corundum, α-Al_2O_3, consists of hexagonal close packed arrangement of oxygen anions (O^{2-}) and Al^{3+} cations that occupy 2/3 of the octahedral interstices. All oxygen octahedra share one face and three edges. The layer sequence is ABABAB. The hexagonal corundum has the highest density (3.98g/cm^3) of all the aluminas.

When aluminum hydroxides such as bayerite, boehmite or pseudoboehmite are heated at ambient pressure and at low water vapour pressure, they will be thermally dehydrated and different transition aluminas will be formed. The transformation and recrystallization sequence is affected by the starting material, particle size, heating rate, purity and partial pressure of water in the heating atmosphere. The dehydration of alumina species during the heating process leads up to 33% mass loss, increase in density from 2.42 to maximum 3.98g/cm^3 (density of corundum (α-Al_2O_3)), and development of large internal porosity [34].

2.5.7. Localized Corrosion of Aluminum in Solutions of Neutral and Near-Neutral pH

In environments in which the surface film is insoluble, corrosion of aluminum and aluminum alloys occurs usually locally at weak spots in the oxide film. There are two main causes for localized corrosion. The first one has an electrochemical mechanism and is caused by a difference in corrosion potentials in local cells formed in or on the metal surface. This difference is caused by the presence of cathodic microconstituents in form of insoluble intermetallic compounds or metal particles. The second one is caused by the presence of ions, such as chlorides or sulphates, in the neutral aqueous solution.

2.5.7.1. Localized Corrosion in the Presence of Metallic Impurities

Metallic impurities or alloying metals added to aluminum dramatically decrease the corrosion resistance of aluminum in water [35]. All the common metallic impurities found in aluminum, except magnesium, have much less negative standard electrode potentials than aluminum and are therefore able to induce a local galvanic corrosion in the aluminum matrix. The standard electrode potentials of some typical impurities in Al are listed in Table 2.2. Alloying elements incorporated in the passive film may influence the electronic behaviour of the oxide.

Table 2.2 *Standard electrode potentials vs. SHE (Standard Hydrogen Electrode) at 25°C for some metals.*

Metal	Mg^{2+}	Al^{3+}	Mn^{2+}	Fe^{2+}	Cu^{2+}	Cr^{2+}
Standard Electrode Potential [V]	-2.37	-1.664	-1.18	-0.440	0.337	0.91

The most common form of corrosion induced by impurities is pitting and intergranular corrosion. Pits, which result from the local pitting corrosion, are predominantly found in the vicinity of small metal particles/intermetallic compounds that were deposited or embedded on or in the aluminum surface. Weak passivity and/or the creation of local galvanic cells are named as the reasons for pit initiation [35]. Localized pitting corrosion depends on the composition of aluminum, concentration of impurities and the composition of the solution. Pitting is diminished when aluminum of high purity grade is exposed to water. Intergranular or intercrystalline corrosion proceeds along grain boundaries in heterogeneous aluminum. Local electrochemical cells are created between the intermetallic compound or trace elements, the aluminum matrix and the precipitate at the grain boundary. Potential differences lead to corrosion.

The formation of alkaline pits around the intermetallic compounds (or cathodic precipitates such as $AlFe_3$) was observed by Aballe et al. [57, 58]. A possible cause for the formation of these pits and for the local Al dissolution is the local pH increase (alkalinization) which is produced as a consequence of the oxygen reduction reaction in aerated NaCl solutions.

2.5.7.2. Localized Corrosion in Presence of Ions in the Aqueous Solution

Pitting corrosion and electrochemical behaviour of aluminum and aluminum alloys in the presence of various ions in neutral, weakly acidic and weakly alkaline aqueous solutions (pH ranging from pH 4 to pH 9.9) have been widely investigated [25, 56, 59, 60]. Particular attention has been given to pitting corrosion in the presence of chloride ions. Chloride ions, Cl^-, seem to

be the most aggressive anions that accelerate corrosion, increase the corrosion rates and lead to film breakdown [60, 61, 62]. Other ions such as perchlorates and phosphates have a reduced but also an enhancing effect on corrosion, whereas ions such as sulphates, molybdates or dichromates have an inhibiting effect on Al corrosion [25, 56, 63]. The nature of anions, their adsorption and incorporation at surface oxide film affects the growth and the dissolution behaviour of the oxide, the degree of hydration and its surface charge [64, 65].

Different pitting corrosion mechanisms in chloride solutions have been proposed but the exact detailed mechanism of pit initiation is still uncertain. In one of the models Cl^- ions breach the oxide film by film thinning, i.e. local dissolution of the oxide film [64]. Another model takes into account adsorption of chloride ions on the oxide surface, penetration of chloride ions through the oxide film via oxygen vacancy transport [64] or via faults and microfissures [63], and localized dissolution of aluminum at the metal/oxide interface in three consecutive single electron transfer steps [57, 64]. By using radiotracer techniques, it was shown that Cl^- ions get incorporated into the oxide film [32, 67] and that Cl^- ions migrate through the growing oxide film inwards, however, at rates slower than O^{2-} ions [38]. The Cl^- migration is not independent of the migration of Al^{3+} and O^{2-} ions. Generally, the transport of the anionic species depends not only upon their sizes and charges, but also on the electric field and the structure of the oxides.

The adsorption of chloride on aluminum is highly localized and coincides often with oxide imperfections or grain boundaries and corresponds with the location of pit sites [67]. The amount of chloride taken up by the passive film is smallest at a pH of about 9.5 and increases with decreasing pH [52]. The adsorption of Cl^- increases also at more anodic potentials and with the increase of temperature [61]. Tomcsanyi et al. observed that the amount of adsorbed chloride decreased after the onset of pitting [32]. Anionic ions once adsorbed at the surface or accumulated in the oxide film may affect the corrosion reaction in several ways [62]. Firstly, Cl^-

ions adsorbed at the oxide/solution interface make it negatively charged and thus charge transfer of oxygen ions from water into the oxide is inhibited. Secondly, Cl^- may react with aluminum oxide and form oxo-, hydroxo- and chlorocomplexes; and lastly, adsorbed Cl^- ions which penetrated into the oxide, will drastically change the properties of the oxide film from poorly conducting into a well conducting hydrated oxy-chloride.

McCafferty observed that pitting is initiated under the oxide film. According to this finding, the author states that there is no necessity to dissolve the oxide film down to the underlying metal substrate in order for a corrosion pit to initiate [64]. Chloride ions and water molecules have to be present at the metal/oxide interface so that a local chloride-assisted dissolution reaction beneath the film can start and hydrogen blisters can develop, grow and finally rupture due to the build-up of hydrogen pressure [52]. The pH within the internal pit electrolyte was calculated as pH 2.28 [52]. The acidic environment in the pit is produced by locally dissolved and hydrolyzed aluminum ions whereas Cl^- ions prevent repassivation by maintaining charge neutrality in the blister. An acidic environment in pits (pH 1 to pH 3) was also reported by other authors [35]. Szklarska-Smialowska states that pits can develop in chloride solutions only when acidic conditions are established within the pits. The time necessary for the attainment of a critical pH is seen as the induction time [35]. $AlCl_3$, $Al(OH)_2Cl$ and $Al(OH)Cl_2$ salts were found within Al pits as reaction products [61]. These salts precipitating directly on the bare Al surface may prevent locally the metal from passivation [68].

Slight pitting corrosion occurs also when increasing the pH of the solution and moving towards more alkaline conditions. However, in alkaline solutions pitting may have a different origin. Silva et al. who studied the morphology of pits in Al 2024 alloy in chloride solution at pH 8.2 implies that pitting is influenced by sub-surface microstructure. Pits nucleate from

microstructural defects such as grain boundaries or second phase particles as well as from recrystallized and deformed interfaces [69].

The dissolution process of pure aluminum in near neutral pH solutions is very slow. The corrosion rates of the Al-6061 alloy in aqueous solutions with various NaCl concentrations are presented in Table 2.3. The corrosion of > 99.5% pure Al samples in NaCl solutions of different pH is presented in Table 2.4. Al-6061 alloy, which shows an increased corrosion, has been added for comparison purpose. The evolution of H_2 in the pH range from 4 to 8 is difficult to detect due to its insignificant amount; H_2 evolves slowly above pH 8 and vigorously above pH 12 [70].

Table 2.3 *Corrosion rates of Al-6061 alloy in NaCl aqueous solutions [71].*

		NaCl solution 0%	NaCl solution 0.05%	NaCl solution 1%	NaCl solution 3%
pH 2	Corrosion rate [mm/year]	0.20	0.78	1.36	2.35
pH 6.92	Corrosion rate [mm/year]	0.02	0.11	0.16	0.22
pH 12	Corrosion rate [mm/year]	2.29	3.03	5.76	6.55

Table 2.4 *Corrosion of > 99.9% pure Al specimen and Al-6061 alloy in NaCl solutions of different pH.*

Al purity	**[NaCl]**	**pH**	**Al loss**	**Reference**
99.99	0.5M	5.7	No corrosion	[63]
99.99	0.5N	pH 4.2 pH 7 pH 8.6 pH 9.6	0.0009 g/cm^2 in 68 hrs 0.0009 g/cm^2 in 25 hrs 0.0036 g/cm^2 in 26.5hrs 0.0147 g/cm^2 in 45hrs	[70]
Al-6061 alloy	1%	pH 2 pH 6.92 pH 12	0.0032 mg/cm^2 in 48hrs 0.0012 mg/cm^2 in 48hrs 0.0135 mg/cm^2 in 48hrs	[71]

Corrosion and passivation processes of aluminum were predominantly studied in non-equilibrium or at conditions at which corrosion is accelerated: when the metal is anodically or cathodically polarized and different potentials are applied; when the solution is oxygenated and additional ions are introduced; when the solution is of alkaline or acidic pH and when the temperature is increased, or when other metals are dispersed in aluminum.

The reactions that govern the corrosion of aluminum in solutions of different pH are the anodic, the cathodic and the oxide dissolution reaction, see Table 2.5. The anodic Al dissolution reaction in alkaline solutions in the presence of native oxide is the direct metal dissolution reaction by migration of Al ions through the film ($Al + 4OH^- = Al(OH)_4^- + 3e^-$) and an indirect metal dissolution reaction by consecutive oxide film formation ($Al + 3OH^- = Al(OH)_3 + 3e^-$) and dissolution ($Al(OH)_3 + OH^- = Al(OH)_4^-$). The rate of corrosion in alkaline solutions is determined by the anodic reaction; the formation of $Al(OH)_4^-$ at the metal/oxide interface is the slow step of the reaction [72, 73, 74]. The cathodic reaction for Al corrosion in weakly alkaline solutions is primarily the reduction of water to hydrogen ($2 H_2O + 2e^- = H_2 + OH^-$). The reaction rate is strongly potential dependent [73] but pH and film thickness independent [74]. The electrons e^- react with water at the metal/film interface. The cathodic reaction, in which hydrogen gas is produced, dominates when high negative potentials are applied. OH^- ions which are formed at the same time increase the alkalinity at the film/solution interface causing hydration, dissolution or film structure changes [73].

Table 2.5 *The anodic, cathodic and oxide dissolution reactions of aluminum in acidic and alkaline environments.*

	Anodic reaction	Cathodic reaction	Film dissolution reaction
Acidic	$Al = Al^{3+} + 3e^-$	$2\,H_3O^+ + 2e^- = H_2 + 2H_2O$ (H_2 evolution reaction) $O_2 + 4H^+ + 4e^- = 2H_2O$ (O_2 reduction) $O_2 + 2H_2O + 4e^- = 4OH^-$ (O_2 reduction)	$Al(OH)_3 + 3H_3O^+ = Al^{3+} + 6H_2O$ $Al_2O_3 + 6H_3O^+ \rightarrow 2Al^{3+} + 9H_2O$
Alkaline	$Al + 3OH^- = Al(OH)_3 + 3e^-$ $Al + 4OH^- = Al(OH)_4^- + 3e^-$ (in weak alkaline solutions)	$3H_2O + 3e^- = 3/2H_2 + 3OH^-$ (H_2 evolution reaction) $O_2 + 2H_2O + 4e^- = 4OH^-$ (O_2 reduction)	$Al(OH)_3 + OH^- = Al(OH)_4^-$ $Al_2O_3 + 3H_2O + 2OH^- \rightarrow 2Al(OH)_4^-$

2.5.7.3. Corrosion of Aluminum in Presence of Alumina Particles and Chloride Ions in the Aqueous Solution

The corrosion behaviour of aluminum metal composites (AMCs) in neutral sodium chloride solutions was investigated by De Salzar et al. [75]. AMCs are Al alloys that are reinforced by alumina (Al_2O_3) particles. Studied were the possible reactions between the matrix components (Al, Si, Mg, Fe, Cu) and the matrix components with Al_2O_3 particles during annealing at 560°C as well as the influence of the reaction products and the reinforcement particles on corrosion. Due to heat treatment new intermetallic phases such as Mg_2Si or Al_3Fe precipitated and were found in the Al matrix. Additionally, the formation of spinel ($MgAl_2O_4$) on the outskirts of the Al_2O_3 particles and an Mg depleted zone around the Al_2O_3 particles was identified. Matrix dissolution was observed predominantly around spinel coated alumina particles and intermetallic compounds. As these newly created compounds behave either anodic or cathodic in relation to the adjacent zone, local potential differences between these zones were the proposed reason for the pitting corrosion in aluminum based composites reinforced with alumina.

2.5.8. Influence of Microstructure and Deformation on Aluminum Corrosion

Generally, the number and type of constituents, grain size and grain orientation, defect concentration and type, as well as the metallurgical treatment, affect the corrosion behaviour of aluminum and its alloys. Cold work and thermal treatment determine predominantly the distribution of the constituents and the magnitude of residual stresses in the metal. Leth-Olsen et al. and Afseth et al. showed that plastically deformed aluminum corrodes faster in water solutions, as compared to strain-free aluminum [76-80]. Cold and hot rolled Al alloys show an increased susceptibility to corrosion especially in the most upper surface layer of the rolled sheet. The drastic loss of corrosion resistance was first attributed to enhanced surface shear deformation and higher density of fine intermetallic precipitates in the upper, 1 μm thick, layer after thermo-mechanical processing as oppose to the underlying bulk. However, in later publications and after the microstructural analysis the authors state that the presence of a strong grain refined surface layer to which high local strains have been introduced during rolling, is not the reason for corrosion [78, 79]. As the surface layer was more active after annealing and the content of impurities or alloying elements was higher, the proposed reason for the increased electrochemical reactivity at the surface after thermo-mechanical treatment of the Al alloys was mainly the enhanced secondary precipitation of intermetallic particles, such as Mn or Fe, on grain boundaries during annealing. The finer the dispersion of intermetallic particles, the higher the number of potential corrosion initiation sites on the metal surface.

Huang et al. studied the role of oxide film debris on the aluminum microstructure during rolling. The presence of oxide debris or a second phase in cold rolled aluminum enhances the rate and changes the nature of the development of the overall microstructure [81]. With relatively low load the structure was rapidly refined and the fraction of high angle boundaries was increased. To obtain a similar structure in pure aluminum, much higher loads and severe

plastic deformations are required. The formation of an ultrafine microstructure (mixture of small cells and subgrains) is caused mainly by the changed slip pattern of the matrix when small alumina particles are present [81]. The influence on corrosion was not presented.

2.6. *High Energy Ball-Milling*

In this work, high energy ball-milling is used for the fabrication of Al-additive powder composites. High energy ball-milling is a mechanical processing technique used usually for the synthesis of various intermetallic compounds, amorphous phases and nanocomposite powders. High energy ball-milling of solid powders involves repeated impacts between balls, balls and powder, and between balls and the vial walls. These impacts cause plastic deformation, fracture and cold welding of powder particles trapped at the collision points, and thus lead to formation of composite particles (if two or more solid phases are involved). This composite structure becomes increasingly finer with continued milling. The rate of refinement of the internal structure (particle size, crystallite size, lamellar spacing) is roughly logarithmic with processing time [82]. Mechanical alloying will start during further milling when solid state reactions between the starting phases are activated and the component particles are converted into an alloy. Mechanical alloying is favoured in the early stage of the milling process when one of the components present in the powder is a ductile metal [82]. Generally, three different system combinations are possible: ductile-ductile, ductile-brittle and brittle-brittle. The ductile-brittle system is the most applicable to this work. Aluminum, a ductile metal, acts as host or binder, whereas brittle metals, intermetallic compounds, non-metals or ceramics can be chosen as the second phase.

The refinement mechanism during mechanical alloying and the final microstructure of the powders greatly depend on the constituents present in the system. Using a ductile-brittle material

combination (mixture) the ductile metal powder particles get flattened in the first minutes of milling by the ball-powder-ball collisions, while the brittle phase or intermetallic particles get fragmented. These fragmented brittle particles tend to become occluded by the ductile constituents and trapped in the ductile particles along the interlamellar spacings. With further milling the lamellae get refined, the interlamellar spacing decreases and the brittle particles – assuming they are insoluble - get uniformly dispersed in the ductile matrix [82].

Repeated plastic deformation of powder particles during ball-milling increases the grain boundaries density and induces a large number of defects in the crystalline structure, such as dislocation, vacancies, and stacking faults. Structural defects increase the interatomic diffusion and allow a solid-state reaction to proceed. In addition, severe plastic deformation as well as continuous breaking up the crystal into smaller pieces is the cause for microstrain formation [83].

2.6.1. Factors Affecting Mechanical Milling

The high energy ball milling process is complex and affected by many factors. These factors include:

- Type of mill (Attrition Mill, Planetary Ball Mill, Rod Mill, Shaker)
- The materials of milling tool (e.g., ceramics, stainless steel, and tungsten carbide)
- Types, size and number of milling media (e.g., balls or rods)
- Milling atmosphere (e.g., air, nitrogen, and an inert gas)
- Milling environment (e.g., dry milling or wet milling)
- Milling media-to-powder weight ratio
- Milling temperature

- Milling time
- Powder properties and its characteristics.

The optimization and control of the milling conditions is important as many powder properties such as the final stoichiometry, particle size distribution, the degree of disorder and homogenization, will be affected. For that reason some of the factors need to be explained in more detail.

Milling media, including balls and container, may abrade a substantial amount of milling material into the milled powder. This will contaminate the powder and alter its chemistry. Contamination can be minimized by using same materials for vial and balls and by choosing high density and high abrasion resistant grinding materials. Additionally, it is favorable when the density of the balls is high enough to create enough impact force on the powder.

The size of the balls determines the milling efficiency. The larger and denser the balls, the higher the impact energy to the powder particles will be. However, best results were obtained when balls with different diameters are used [82].

Milling atmosphere is a potential source of contamination during ball milling. For reactive metals such as aluminum when milled in air, oxygen contamination is the most severe. The presence of air in the vial has been shown to produce oxides in the powders [82]. Inert gases, typically argon or helium, are widely used to prevent oxidation or contamination of the powder.

Ball-to-powder weight (W_b:W_p) ratio has a significant effect on the size of particles obtained and on the time required to achieve a particular phase in the powder. Increasing the W_b:W_p ratio accelerates the process of alloying since the number of opportunities for the powder particles to be reacted and interdiffused increases with the weight and/or number of balls. The disadvantage of using too high weight ratios is the high concentration of contaminants found in the final

product [84]. Best results were obtained when W_b:W_p ratios in the range between 10:1 and 20:1 were used [85].

The time of milling is one of the most important parameters. Milling times required to achieve a specific condition in the powder vary depending on the type of mill used, the intensity of milling, the ball-to-powder ratio, and the temperature of milling. Milling times have to be decided for each combination of the above parameters and for the particular powder system. For mechanical alloying milling times of up to few hundred hours have been applied [86]. However, too long milling times will increase the level of contamination and lead to the formation of some undesirable phases.

Regarding the particle size, the longer the milling is the smaller the particles are. The particle size decreases exponentially with time and reaches for some systems a small value of only few microns after a few minutes of milling. For other systems, the powders first coarsen to a size as large as several hundred microns due to cold welding and agglomeration and then disintegrate exponentially to few microns [84].

2.6.2. High Energy Ball-Milling with SPEX 8000

SPEX 8000 mill was used primarily in the course of this work. SPEX 8000 is a high-energy shaker mill most suitable to produce mechanically alloyed powders (see Figures 3.1 and 3.2 in Chapter 3). The vial which contains the sample and grinding balls is secured in the clamp and swung energetically not only back-and-forth but also laterally several thousand times a minute. With each swing of the vial the balls impact against the powder and the end of the vial, both milling and mixing the sample. The balls develop velocities in the order of 5 m/s making the impact unusually high [82]. Ball milling is usually performed on dry powder mixtures at ambient temperature. However, the temperature rises during milling and depends on the kinetic

energy of the balls and exothermic processes during milling. At the time of impact, the local temperature may raise up to 350°C [86].

Applications:

Mechanical alloying using high energy ball-milling has been successfully used in laboratories and industry to produce versatile equilibrium and non-equilibrium alloy phases with enhanced material properties, such as higher strength and fracture toughness, higher electrical or thermal conductivity or higher chemical stability. Jangg et al. [87] used mechanical alloying to synthesize novel aluminum alloys with fine dispersions of oxides and carbides in the aluminum matrix for applications in the aerospace industry. The dispersion of carbides (Al_4C_3) was achieved by adding graphite during milling to aluminum, whereas the in-situ oxide formation (Al_2O_3) was controlled by adjusting the oxygen content in the milling atmosphere. Manna I. et al. and Shaw L. et al. report about a number of amorphous and nanocrystalline aluminum alloys, such as $Al_{40}Zr_{40}Si_{20}$, $Al_{65}Cu_{35}Zr_5$ and $Al_{93}Fe_3Cr_2Ti_2$, that were produced by mechanical alloying as they are technologically relevant due to low density and high strength [88, 89, 90]. Recently, mechanical alloying was applied for the synthesis of nanosized crystalline magnesium alloys and magnesium hydrides as well as aluminum hydrides ($LiAlH_4$, $NaAlH_4$) [91, 92]. These alloys are promising as novel hydrogen storage materials. Chaklader A. used for the first time ball-milled aluminum-boehmite (AlOOH) composite powders for hydrogen generation from water split reaction at neutral and near neutral pH [1, 2].

3. Experimental Procedures

3.1. Materials

Atomized aluminum powder from Alcoa, 101 common grade (99.7% Al, main impurities: Fe (max 0.25%) and Si (max 0.15%) as well as 0.6% Al_2O_3 on the surface of powder particles, with average particle size of 35 μm, was used as received without any pre-treatment for all experiments. Aluminum oxide, Al_2O_3 A16 SG (Alcoa), was used as reference additive. For the most part water-soluble inorganic salts (WIS) such as potassium chloride, KCl (technical grade, McArthur Chemical), sodium chloride, NaCl (99.9%, Fisher Chemicals) and sodium nitrite $NaNO_3$ (99.9%, Fisher Chemicals) were applied as additives. Several other additives were used for testing and comparison purposes. As inorganic water-insoluble additives predetermined were quartz (SiO_2), silicon carbide (SiC 600RA) and kaolin ($(Al,Fe,Mg)_n[(OH)_4/SiO_5]$ (white diamond)); whereas the water-insoluble Polyaethylene Glycol 2000, PAG, from Fluka AG and the water-soluble Poly(vinyl alcohol), PVA, 88-89%, hydrolyzed, from J.T. Baker Chemicals were selected as organic additives.

The term "additive" is used to describe the material milled with Al when preparing the powders.

3.2. Powder preparation

Aluminum-additive powder mixtures were prepared by high-energy ball-milling in a SPEX 8000 shaker mill. The balls and vial inner lining were made of alumina. The grinding vial had an internal diameter of 38 mm and a length of 44 mm, corresponding to a capacity of about 55 ml. Up to 2.5 g of aluminum-additive powder mixtures were introduced into the vial. The duration of milling was varied from 7.5 minutes to 4 hours. In a typical experiment, a 50/50 wt% mixture of an additive and aluminum powders were loaded together with 70 alumina balls (5 ±

0.15mm diameter each), and ball-milled in air atmosphere for either 10 minutes (optimized ball-milling time for non-salt additives) or 15 minutes (standard time for salts). The ball-to-powder mass ratio corresponded to 13:1 when using 2.2 g of powders. The water-soluble inorganic salts were pre-ball-milled separately for 5 minutes to reduce their initial particle size. Other additives were used as-received. The mill and milling media are depicted in Figures 3.1 and 3.2.

Figure 3.1 *Ball mill SPEX 8000.*

After ball-milling, 2 g of the mechanically alloyed powder mixture consisting of aluminum and additive was placed into a teabag-like confined filter container and exposed to a relatively large amount of tap water (water/solids ≈ 1000, by mass). The tap water temperatures were varied between 20 and 70°C. Most of the experiments were performed at the standard water temperature of 55°C. The pH of the tap water fluctuated slightly between pH 6.5 to pH 7.1. The progress of the water split reaction was monitored through the measurement of released

H_2 that was captured by water displacement in an inverted cylinder. The volume of hydrogen produced was compared to the volume of H_2 gas stored at 25°C. Theoretically, according to the reaction (3.1) and (3.2), a volume of maximum 1359 cc hydrogen gas can be produced from 1g of Al during a complete corrosion reaction of aluminum metal with water at 25°C.

$$Al + 3H_2O \rightarrow 1.5H_2 + Al(OH)_3 \quad (3.1)$$

$$Al + 2H_2O \rightarrow 1.5H_2 + AlOOH \quad (3.2)$$

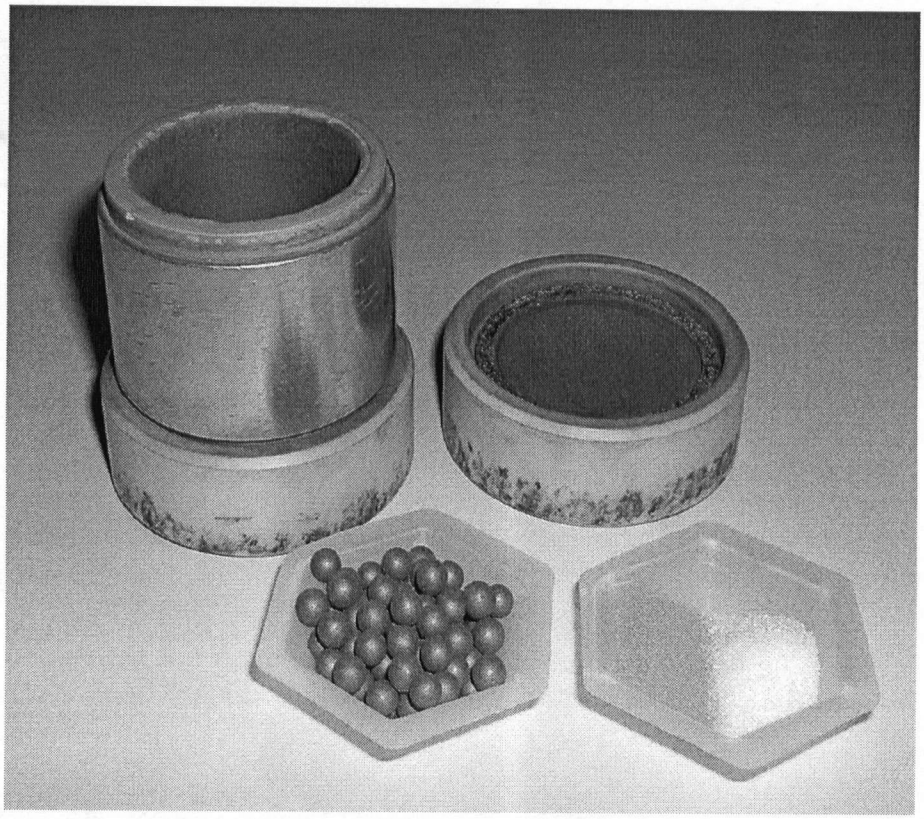

Figure 3.2 *Vial, grinding media and Al-additive powders.*

Table 3.1 lists the experimental ball-milling conditions under which Al-additive powder mixtures were fabricated. For hydrogen generation experiments freshly prepared powders were used. Table 3.2 lists the ball-milling and experimental conditions under which the hydrogen generation reactions of Al-additive-H_2O systems were carried out.

Table 3.1 *Ball-milling parameters for Al-additive systems.*

Additive	Al/Additive Ratio [wt%]	Total Amount of BM Powders [g]	Ball-to-Powder Mass Ratio	Ball-Milling time [min]	Ball-Milling Atmosphere
ORGANIC:					
PVA	50/50	2	14	10	Air
PAG	50/50	2	14	10	Air
INORGANIC:					
SiC	50/50	2	14	10	Air
SiO_2	50/50	2	14	10	Air
Kaolin	50/50	2	14	10	Air
Al_2O_3 (A16)	50/50	2	14	10	Air
SALTS:					
NaCl	50/50	2.2	13	15*	Air
KCl	50/50	2.2	13	15*	Air

*In addition pre-ballmilling of salts for 5 min

Table 3.2 *Ball-milling parameters and experimental conditions for hydrogen generation reaction of Al-additive-H_2O systems.*

Additive	Al/Additive Ratio [wt%]	Ball-Milling time [min]	Amount of Powder /Amount of Water [g/ml]	Reaction Temperature T_{Water} [°C]
Al-KCl	50/50	7.5, 15, 30, 60, 120, 240*	2/2000	55
Al-KCl	95/5,90/10, 85/15, 80/20, 70/30, 60/40, 50/50, 30/70, 10/90	15*	2/2000	55
Al-KCl	50/50	15*	2/2000	22, 40, 55, 70, 100

*In addition pre-ballmilling of salts for 5 min

To study the influence of additives many organic and inorganic additives were applied. They were listed in Section 3.1.

To study the influence of additive concentration on hydrogen generation, Al-KCl powder mixtures with various compositions were alloyed (BM = 15 min) and reacted in tap water at 55°C. The investigated Al-KCl concentration ratios in weight per cent were: 95-5, 90-10, 85-15, 80-20, 70-30, 60-40, 50-50, 30-70 and 10-90.

The milling time was varied from 7.5 min to 4 hrs (7.5, 15, 30, 60, 120, 240 min) for the Al-salt systems.

To investigate the influence of water quality on hydrogen generation from deformed Al powders, three types of water were tested: distilled water, sea water and a KCl-saturated aqueous solution. The vast majority of experiments were performed in tap water.

To study the influence of temperature, experiments were performed in water at 22, 40, 55, 70 and 100°C; most of the experiments were carried out in tap water at 55°C.

To test the effect of pH on the hydrogen generation reaction, experiments were conducted in solutions with a pH between pH 3.5 to pH 9. Slightly acidic solutions, such as pH 5, pH 4 and pH 3.5 were adjusted by addition of acetic acid ($C_2H_4O_2$), whereas the slightly alkaline solution, pH 9, by the addition of potassium hydroxide (KOH) to tap water.

3.2.1 Leaching of Ball-Milled Al-Salt Powder Mixtures

To study the influence of the additive on hydrogen generation kinetics, Al-additive and additive-free Al systems were compared. Additive-free Al powders were prepared from mechanically alloyed Al-salt powder mixtures by leaching-out the water-soluble system component. Al-NaCl(50wt%) and Al-KCl(50wt%) powder mixtures were washed for up to 3 hours in cold tap water (T = 12°C) using a magnetic stirrer. The remaining powder (i.e. predominantly Al) was filtered into a paper filter bag and used for hydrogen generation

experiments. The solution, which contained the dissolved salt and also the smallest Al particles that could not be captured by the filter, was placed in a dryer at 65°C. After the water has evaporated, the amount of the leached-out salt was determined by weighing.

3.2.2 Annealing of Ball-Milled Powders

To study the effect of defects and strain induced in aluminum during the process of high energy ball-milling on hydrogen generation, some of the Al-additive systems were annealed in Argon atmosphere (99.998%) and compared to the equivalent not-annealed powder systems. Al-NaCl(50wt.%) powder mixtures were annealed at 550°C for 30 minutes. Al-Al_2O_3(50wt%) powders, which were ball-milled for 10 minutes, were annealed at 600°C for 1 hour. Al-Al_2O_3(50wt%) was also heat-treated at 700°C and 800°C, which is above the melting point of aluminum ($T_{melt\ Al}$ = 660.37°C), for up to 1 hour. For better handling, some of the ball-milled powders were compacted to pellets at 3350 psi using a hydraulic press.

3.3. Microstructural Characterization

Following microstructural techniques were used for the physical and chemical characterization of the as-received powders, ball-milled powders and the reaction products.

3.3.1. Scanning Electron Microscopy (SEM / EDS)

Particle morphology, microstructures, elemental composition and the distribution of elements within the particles before and after ball-milling as well as after the reaction were examined using a Hitachi S-3500N scanning electron microscope equipped with energy dispersive x-ray spectrometry (EDS). The working distance for EDS was 15mm. Powder specimens were spread on conductive carbon tape and placed on aluminium stubs. To reduce

surface charging caused by non-conducting specimens some of the powder samples were gold- or carbon-coated.

3.3.2. X-Ray Powder Diffractometry (XRD)

Phase identification, crystallite size and microstrains were determined from x-ray diffractograms. X-ray diffraction patterns (XRD) were recorded with a Siemens D-5000 diffractometer using 40 kV/30 mA and Cu K_α radiation (λ = 1.5405 Å). The diffraction patterns were recorded at an angular speed of 1.2°(2θ)/min. The counting time was 2 s/step. Data accumulation and processing was performed using Diffrac^{plus} software from Bruker Analytical X-ray Systems. Phase identifications were performed with help of PDF database and EVA V4.0 software.

The mean crystallite size (D) of the ball-milled Al powder was determined from the broadening (β) of the strongest aluminum peak in the X-ray diffraction pattern, the (111) peak at 2θ = 38.47°. The analyzed (111) metal peak was corrected by subtracting the background noise as well as the $K\alpha_2$ contribution by employing the Rachinger correction. The broadening β of the profile is defined as:

$$\beta = A_P / H_P \qquad (3.3)$$

where, A_P is the total area under the peak and H_P is the peak height. The total area under the peak was calculated using the Trapezoidal Rule method and additionally corrected by the amount of instrumental broadening. The amount of the instrumental broadening was determined by using barium fluoride (BaF_2) as a standard. The determination of crystallite size (D) is based on the Scherrer equation:

$$D = k\lambda/\beta\cos\theta \qquad (3.4)$$

where λ is the radiation wavelength (for Cu K_α λ=1.5405 Å), k = 0.90 and θ is the Bragg angle. Because of repeated plastic deformation of the Al lattice during the process of high energy bal-

milling, it has to be assumed that microstrains have contributed to the Al (111) peak broadening. The separation of the microstrain contribution to peak broadening was determined by using the Aqua and Wagner method [94]:

$$(\beta)^2 = (1/D)^2 + (2\varepsilon\, d^*)^2 \qquad (3.5)$$

where $d^* = 1/d = 2\sin\theta / \lambda$ and ε is the crystalline strain.

3.3.3. X-Ray Photoelectron Spectroscopy (XPS)

The oxidation state and elemental composition of the surface were analyzed using x-ray photoelectron spectroscopy. The Leybold MAX 200 X-ray spectrometer equipped with an Al K_α x-ray source (1487 eV) was operated at 15 kV and emission current of 20 mA. The aperture was set for an area analysis of 4 x 7 mm^2. The binding energy scale of the spectrometer was calibrated using an Au 4f ($E_{binding}$ = 84.0 eV) substrate. The pass energy of the hemispherical analyzer was maintained at 48 eV for the narrow scan. The peaks were fitted using an asymmetric Gaussian/Lorentzian mixed function.

3.3.4. Surface Area Measurement by BET Analysis

Surface area measurements were performed with Quantachrome Autosorb-1 Surface Area Analyzer on as-received, ball-milled and additive-free aluminium powders as well as on reaction products. Powder samples (0.5 to 2 g) were out-gassed for at least 6 hrs (150°C, 5 mm Hg) prior to analysis. Adsorpion-desorption isotherms were measured at 77 K. The specific surface area was estimated using multi-point adsorption data from the linear segment of the N_2 adsorption isotherm in the relative pressure range of 0.05 to 0.2 using Brunauer-Emmett-Teller (BET) theory.

3.4. Reaction Characterization

3.4.1. Differential Scanning Calorimetry (DSC)

The quantity of reaction heat (reaction enthalpy) released during the corrosion reaction of mechanically alloyed Al-additive powders in water was measured by using a C80 Calvet differential scanning calorimeter from Setaram. The apparatus is designed as a twin calorimeter comprising two identical cells. The cells - a sample and a reference cell - are located at identical height in a shielded calorimetric block and maintained in an isotherm or temperature programmable (heating, cooling) mode. The caloric effect during an experiment is recorded by means of the thermal power difference between the thermopiles of the sample cell and the reference cell.

To activate the reaction the aqueous solution with ball-milled Al-additive powder was heated up to 50°C at a heating rate of 2°C/min and held at this isothermal condition for 3 hours before cooling down to room temperature at a rate of 100°C/min. No pressure increase during the reaction was assumed as the sample cell was not pressure-tight and as only very small amounts of reactive Al were used (10 mg). Equivalent weights of alumina-additive-water mixtures were used as reference system. In the reference sample aluminum and reacted aluminum (aluminum hydroxides) were replaced by alumina.

The measured DSC heat flow profile contains the heat generation rate of the chemical reaction. The integration of the baseline-corrected heat flow over time gives the reaction enthalpy for a particular system.

The Al-H_2O reactions (3.6) and (3.7) are exothermic. The standard enthalpies of reaction ΔH°_{rxn} have been calculated for reactions (3.6) and (3.7) using standard enthalpy of formation ΔH°_f data, which are included in Table 3.3 [3, 96].

$$Al + 3H_2O \rightarrow 3/2H_2 + Al(OH)_3 \qquad (3.6)$$

$$Al + 2H_2O \rightarrow 3/2H_2 + AlOOH \quad (3.7)$$

$$2Al + 3H_2O \rightarrow 3H_2 + Al_2O_3 \quad (3.8)$$

$$\Delta H^\circ_{rxn} = \Delta H^\circ_{f\ \text{Bayerite, Boehmite or } \alpha\text{-alumina}} - n\ \Delta H^\circ_{f\ \text{Water}} \quad (3.9)$$

Table 3.3: *Standard enthalpies of formation and standard enthalpies of reaction ΔH°_{rxn} for Al-H_2O as per reaction (3.6), (3.7) and (3.8).*

	ΔH°_f at 25°C, 1 atm [kcal/mol]	ΔH°_f at 25°C, 1 atm [kJ/mol]	ΔH°_{rxn} calc. at 25°C, 1 atm [kJ/mol]
Bayerite $Al(OH)_3$	-304.8[1)]	-1274[1)]	**-418**
Boehmite AlOOH		-988[2)]	**-417**
H_2O	68.3[1)]	285.6[1)]	
Alumina Al_2O_3		-1668[1)]	**-811.5**

[1)]Perry R.H. *Chem. Eng. Handbook* [2)]Holleman-Wiberg *Inorganic Chemistry*

3.4.2. pH Measurements

The pH of tap water and pH changes in aqueous solution before, during and after hydrogen generation reaction was monitored by using the Φ250 pH meter from Beckman. The instrument was equipped with a gel-filled combination electrode. To investigate pH changes during hydrogen generation, the volume of reaction water was significantly reduced from 2000 ml to 30 ml. The change in concentration of the H_3O^+ or OH^- ions in aqueous solutions is reflected as a pH shift. Using the relations below, the concentration of the hydronium and hydroxyl ions was determined.

$$pH = -\log[H_3O^+] \quad (3.10)$$

$$pOH = -\log[OH^-] \quad (3.11)$$

$$K_w = [H_3O^+]\,[OH^-] = 1 \times 10^{-14} \quad (3.12)$$

where K_w is the ion-product constant of water at 25°C.

4. Results and Discussion

4.1. Characterization of As-Received Materials

The powders from Alcoa (aluminum and alumina) and powders from Fisher Chemicals (KCl and NaCl salts) have been characterized with respect to the particle size, particle size distribution, and morphology. Figures 4.1 – 4.5 show SEM micrographs of the commercially available, as-received aluminum powder (Fig. 4.1), the additive potassium chloride, KCl as-received (Fig. 4.2) and after 5 minutes of milling (Fig. 4.3), as well as the additive aluminum oxide, Al_2O_3 A16 as-received (Fig. 4.4 and Fig. 4.5).

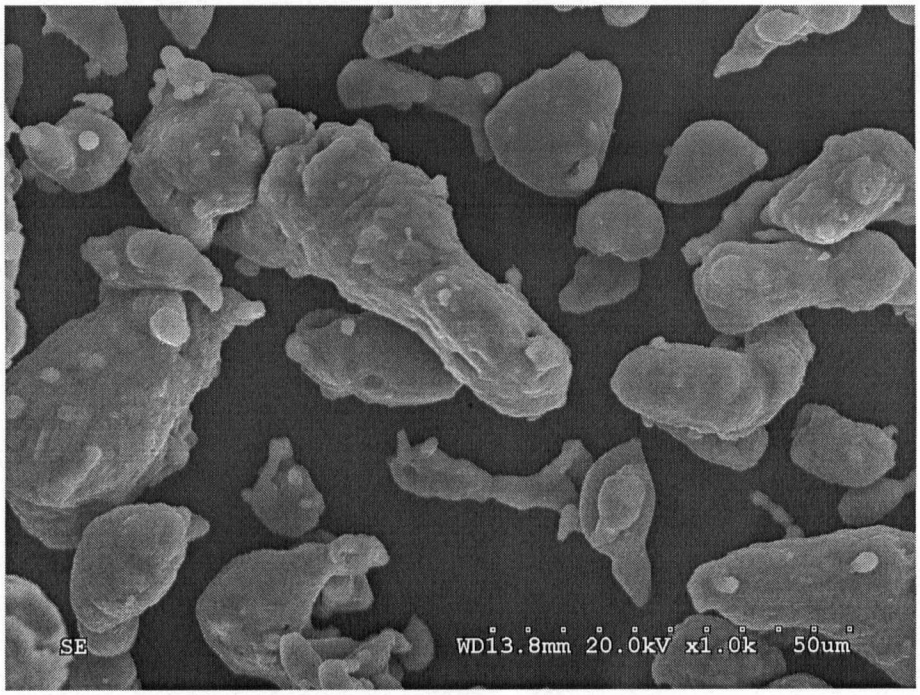

Figure 4.1 *SEM micrograph of as-received Al.*

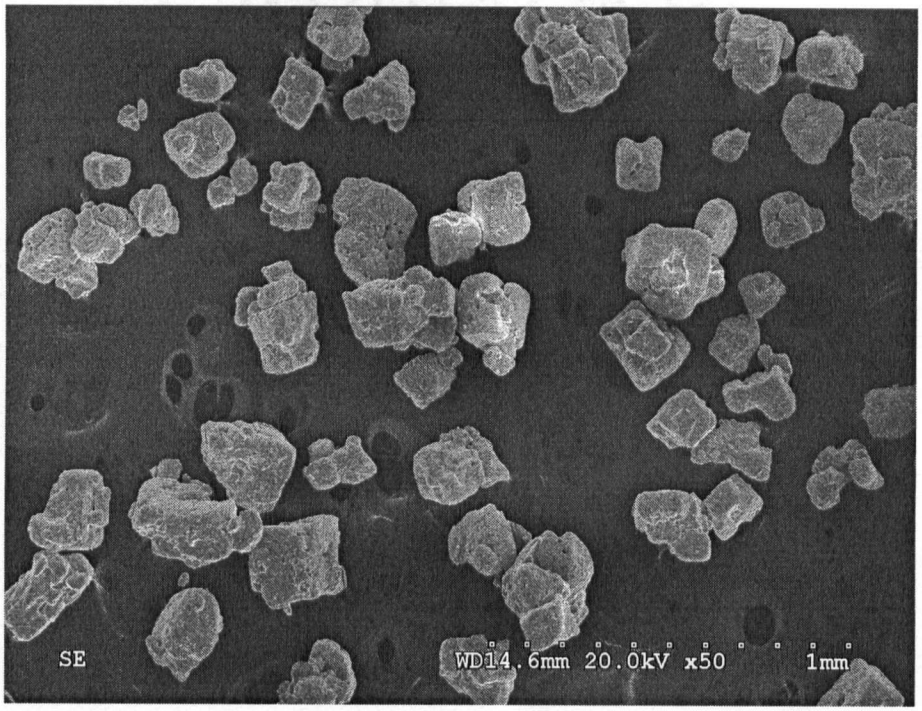

Figure 4.2 *SEM micrograph of as-received KCl.*

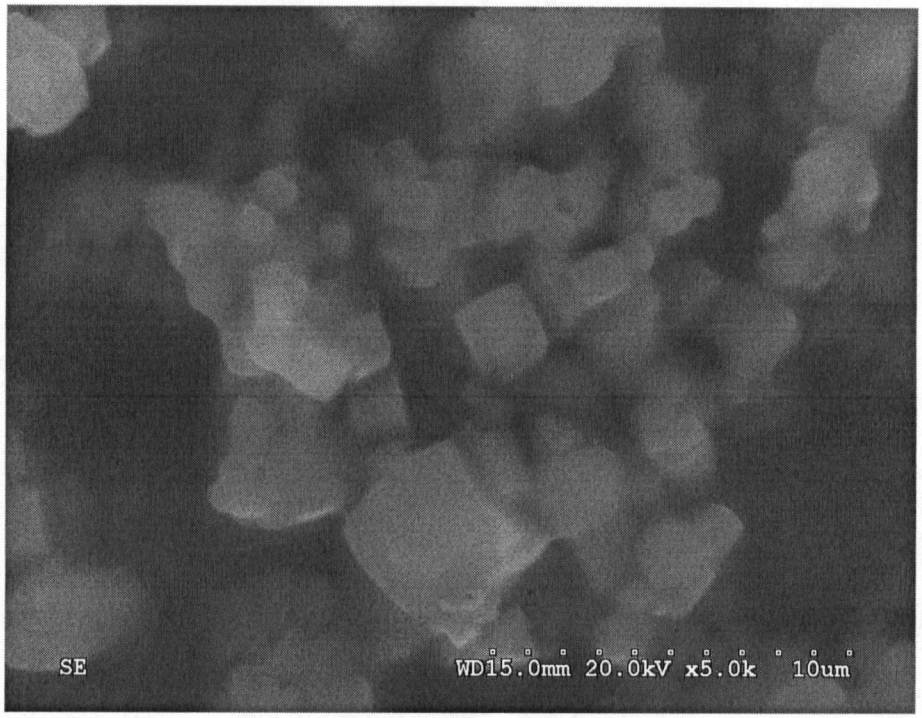

Figure 4.3 *SEM micrograph of KCl after ball-milling (BM = 5 min).*

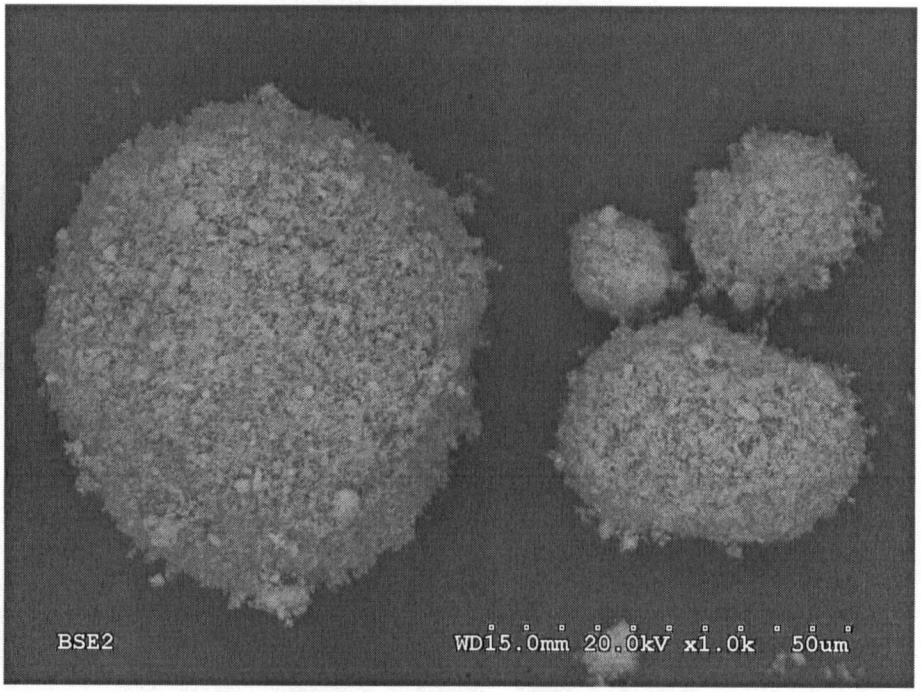

Figure 4.4 *SEM micrograph of as-received Al_2O_3 A16 (x1000).*

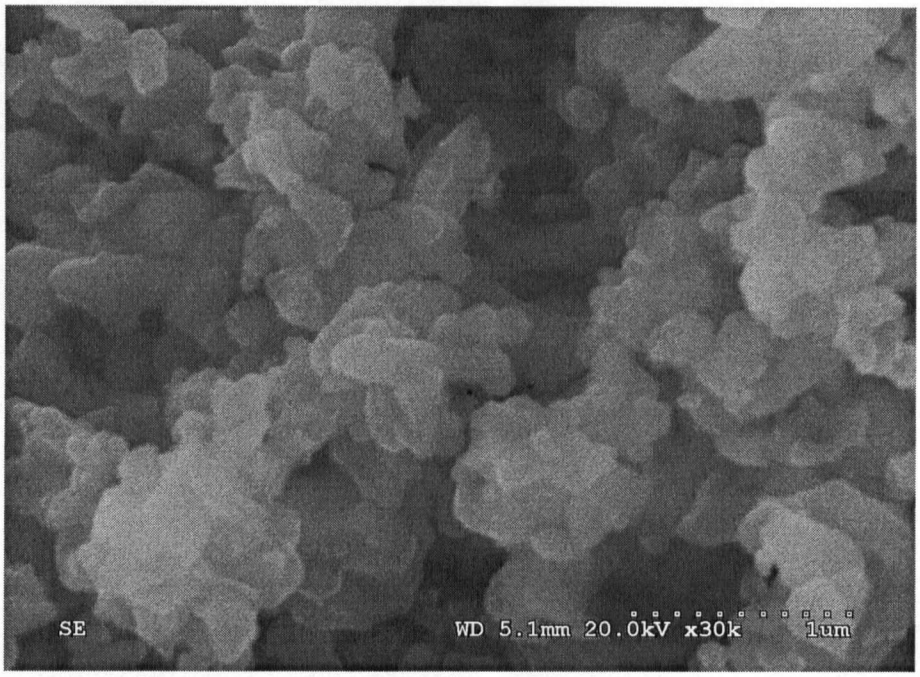

Figure 4.5 *SEM micrograph of as-received Al_2O_3 A16 (x30 000).*

The atomized Al powder particles have an irregular shape and range from 5 to 100 μm in size (meane size: 35 μm). KCl and NaCl powder particles are up to 400 μm large cubic crystals. Their size is substantially reduced after 5 minutes of ball-milling and ranges from 1 to 5 μm. Al_2O_3 A16 agglomerates form large spheres of up to 100 μm in diameter and consist of 300 to 400 nm small primary alumina particles. These obtained results correspond well with the manufactures specifications of the powders.

The as-received Al powders were further characterized by using BET, XPS and XRD methods. The specific surface area of as-received Al powders was 0.30 m^2/g. The Interfacial Analysis & Reactivity Laboratory (IARL) of UBC conducted the elemental surface analysis of the as-received Al powder by using XPS. Figure 4.6 presents the XPS survey scan and Figure 4.7 the high resolution Al 2p core–level scan of the upper 10 nm thick surface layer of the as-received Al powders. In the 0 to 1400 eV survey the following peaks for as-received Al powders were detected: the aluminum peaks (Al 2p at 75.0 eV and Al 2s at 119.8 eV); the oxygen peaks (O 1s at 532.6 eV and O Auger at 978.2 eV) and the carbon peaks (C 1s at 285.4 eV and C Auger at 1223 eV) which originate from surface contamination caused by the vapour residuals of the oil pump. The Al 2p core level peak consists of the elemental component, Al_{Metal}, at 72.8 eV and a broader oxide component, Al_{oxide}, at 75.3 eV. While the Al_{oxide} shoulder grows with oxide layer thickness, the Al_{Metal} peak reduces in size and disappears totally when the oxide layer exceeds the thickness of 10 nm. From Figure 4.7 and the intensity ratio of the oxidic to metallic components, the oxide film thickness of as-received Al powders was estimated between 3.2 to 9.6 nm. According to literature, an air–formed oxide film has a thickness of 2 to 5 nm; its thickness varies and depends mainly on formation temperature and environment conditions [22, 28, 29, 30, 31].

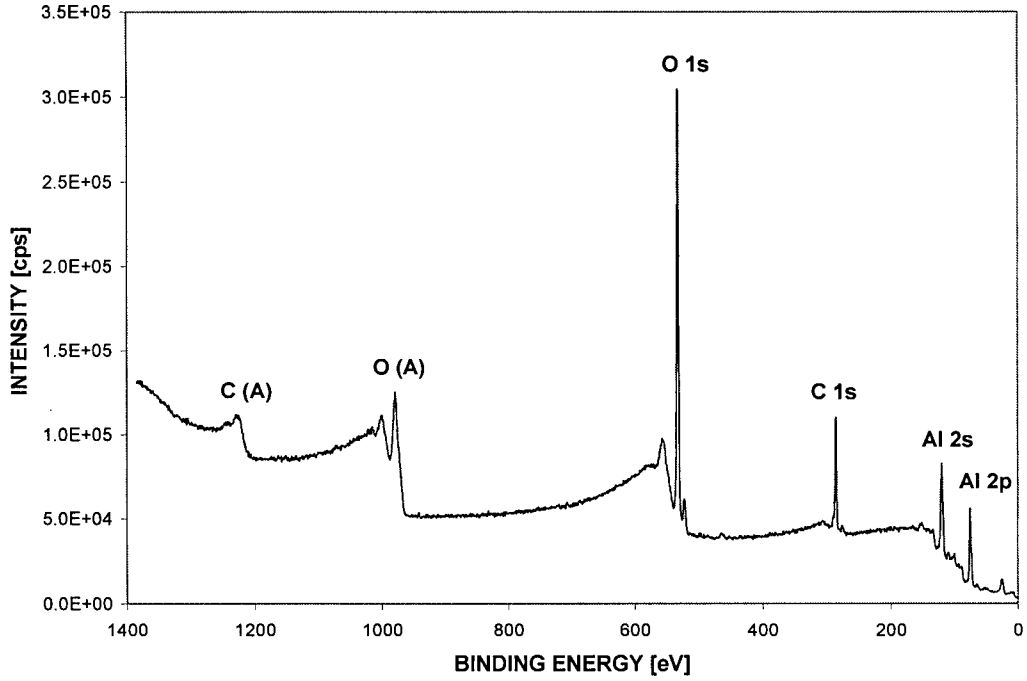

Figure 4.6 *XPS survey scan of as-received Al powders.*

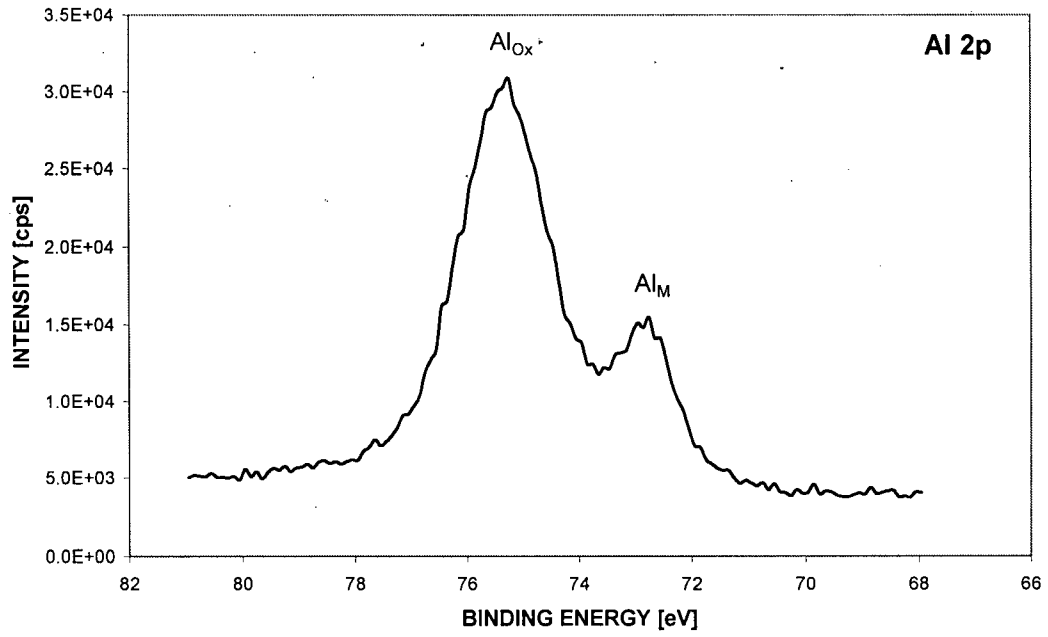

Figure 4.7 *High resolution Al 2p core–level XPS spectrum of as-received Al powders ($Al_M = Al_{Metal}$, $Al_{Ox} = Al_{oxide}$).*

The elemental composition of the surface obtained by XPS was compared with EDX bulk analysis, see Table 4.1. XPS data reveal that the 10 nm near-surface volume of Al particles

consists mainly of oxygen (48.4 at%) and aluminum (27.5 at%). Thin layer of carbon on the particle surface distorts the results. EDX data collected from bulk of the Al particles reveal that Al powders contain 3.8 wt% oxygen in their structure. No other impurities have been detected. The chemical analysis published by Alcoa [98], shows that the produced Al powders have only 0.6 wt% of aluminum oxide on the Al particle surface. The difference may be explained by the use of different analytical methods, the presence of adsorbed oxygen and by the limited information depth carried by the back-scattered electrons during EDX (the interaction depth of the electron beam with the specimen at 20 kV is around 4 μm for Al) [99].

The crystal structure of the as-received Al was determined from XRD data. The characteristic peak positions and intensities correspond perfectly to the synthetic aluminum found in ICPDS database [95]. The predominant peak is the (111) at $2\theta = 38.47°$. Other characteristic peaks are located at following 2θ: (200) at 44.74°, (220) at 65.13°, and (311) at 78.22°. Aluminum crystallizes with face-centred cubic (FCC) lattice structure ($a_o = 4.049Å$).

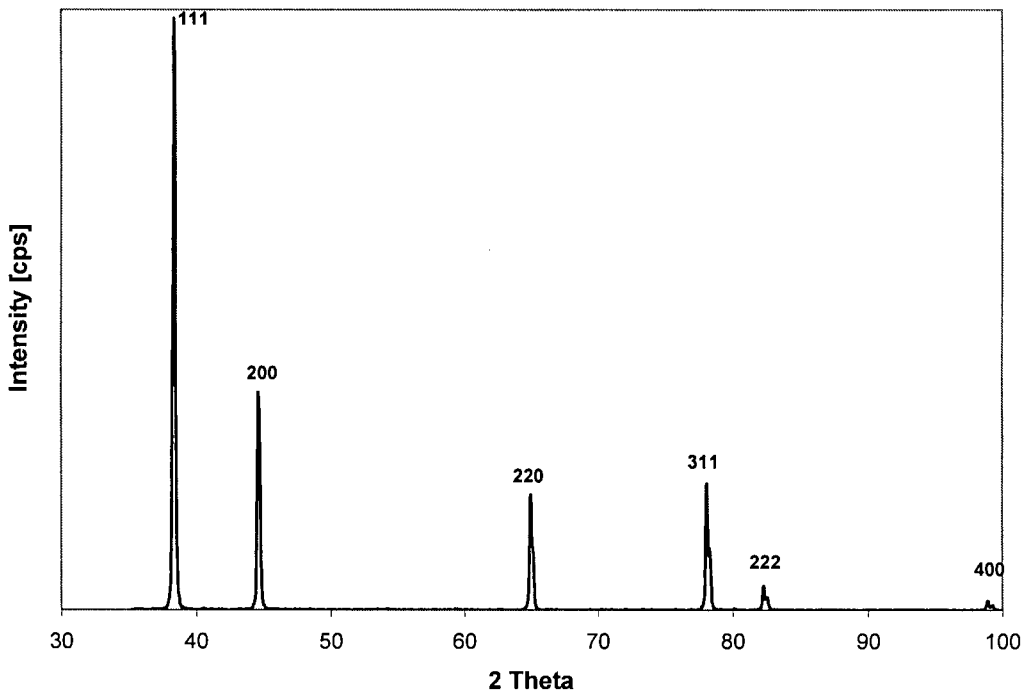

Figure 4.8 *XRD pattern of as-received Al powders.*

Table 4.1 *The elemental composition of the Al powder surface obtained by XPS and of Al bulk obtained by EDX.*

Composition / Sample: **As-received Al**	Al	O	C
XPS	27.5 at% (41.1 wt%)	48.4 at% (42.9 wt%)	24.1 at% (16 wt%)
EDX	96.2 wt%	3.8 wt%	-

4.2. Characterization of Ball-Milled Powders

Various aluminum-additive systems were produced using high energy ball-milling by varying the additive and milling time. Water-soluble inorganic salts (WIS), such as KCl and NaCl were used predominantly as additive, and for comparison purposes the chemically inert and water-insoluble alumina, Al_2O_3 A16 was also applied. The milling times were varied from 7.5 minutes to 4 hours, whereby the ball-milling time, BM = 15 min, was chosen as a standard and used in most of the experiments. The details to the Al-additive systems were given in Chapter 3. Because mechanical alloying of aluminum with an additive is a necessary processing step that changes the morphology of the Al powder in such a way that it loses its passivity in water, various analytical methods were applied to characterize the microstructure of the ball-milled powders.

4.2.1. Surface Morphology and Particle Size Analysis

Figures 4.9 and 4.10 show SEM micrographs of Al-KCl(50wt%) powder mixtures that were mechanically alloyed for 15 min. The particles are irregular, often agglomerated and their size varies from few to several tens of μm. The morphology of these particles changes drastically when the water-soluble salt was leached out from the powder mixture leaving only very thin and cold welded Al foils fragments behind. SEM micrographs of leached out Al are shown in Figures

4.11 and 4.12. These particles are highly porous and characterized by largely increased surface area. Specific surface area (SSA) measurements on leached out Al revealed that its SSA increases from 0.30 m^2/g for as-received Al powder to 9.68 m^2/g (~ 32-fold) for 15 min alloyed powders.

The incorporation and distribution of chemically inert and water insoluble additives, such as Al_2O_3 A16, on the mechanically alloyed powder particle surface is seen in Figures 4.13 and 4.14. The alumina crystals, that are fairly uniform in size (~400 nm small), are homogenously imbedded in the ductile aluminum matrix after 15 min of alloying, covering entirely the surface of the particles.

The change of particle size with ball-milling time is presented on the Al-KCl system in Figure 4.15. There is a clear decreasing trend in the particle size with increase of milling time. The average particle size reduces from 50-60 μm after 15min of milling to 5-10μm after 60 min of milling. Particle refinement is caused by repeated fracturing and cold welding during high energy ball-milling.

The distribution of Al, K, and Cl in Al-KCl(50wt%) powders after 15 and 60 min of milling was analyzed by EDS mapping, see Figure 4.16. It can be seen that the fine solid salt particles are distributed more homogenously in the Al matrix when milled for 60 min and are less homogenously distributed when milled for 15min. In the latter, Al and KCl dominant areas were detected. However, unlike alumina crystallites, salt crystallites cannot be identified. Salts have low hardness and cleave easily, especially parallel to their (100) planes. This accelerates their re-distribution in the Al metal during the process of high energy ball-milling.

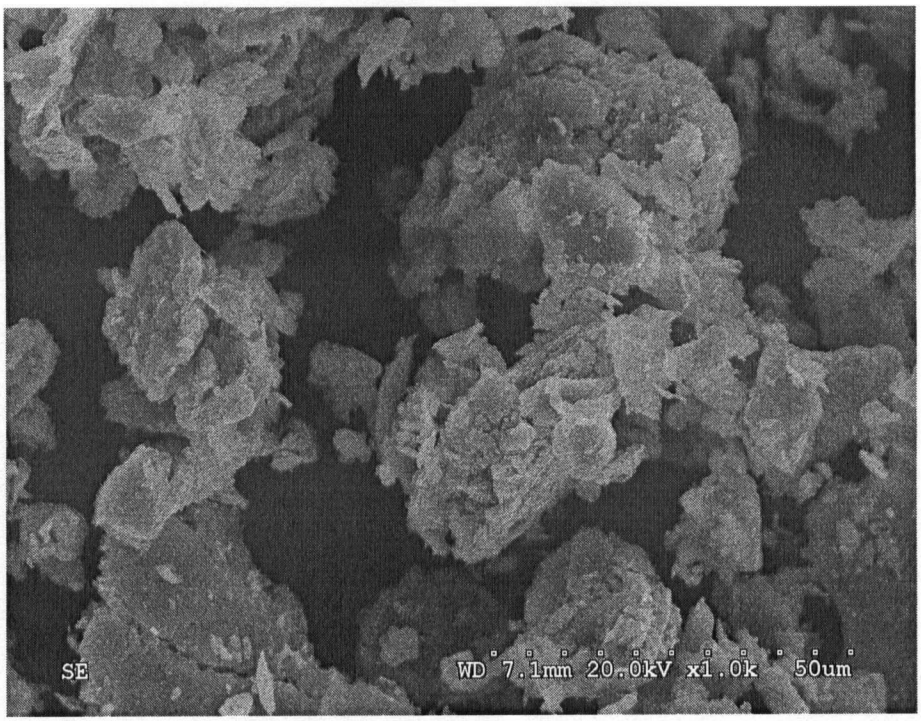

Figure 4.9 *SEM micrograph of Al-KCl (1:1) after 15 min ball-milling (x1000).*

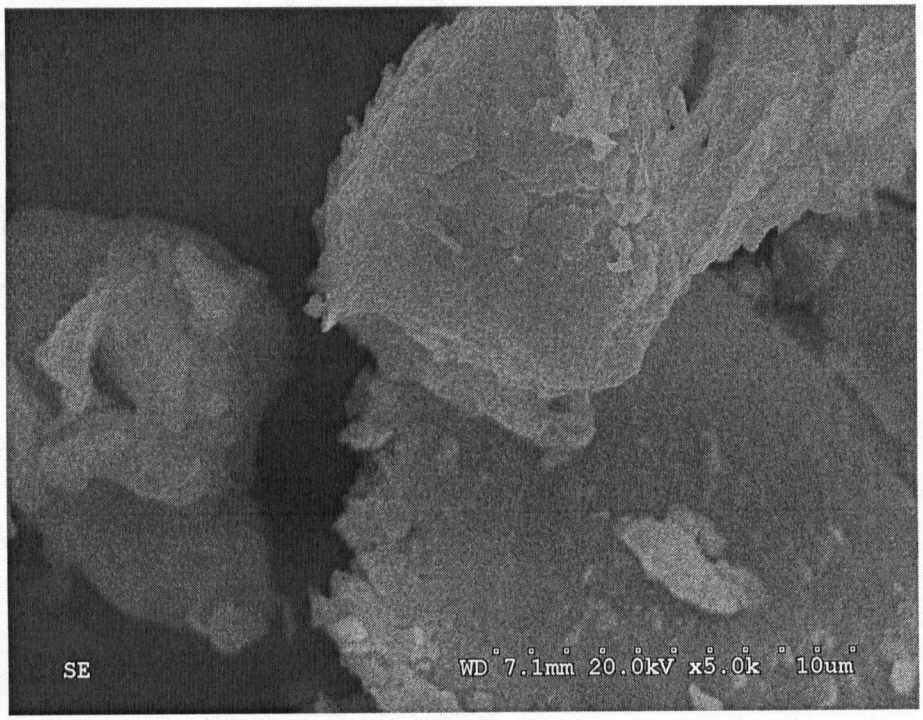

Figure 4.10 *SEM micrograph of Al-KCl (1:1) after 15min ball-milling (x5000).*

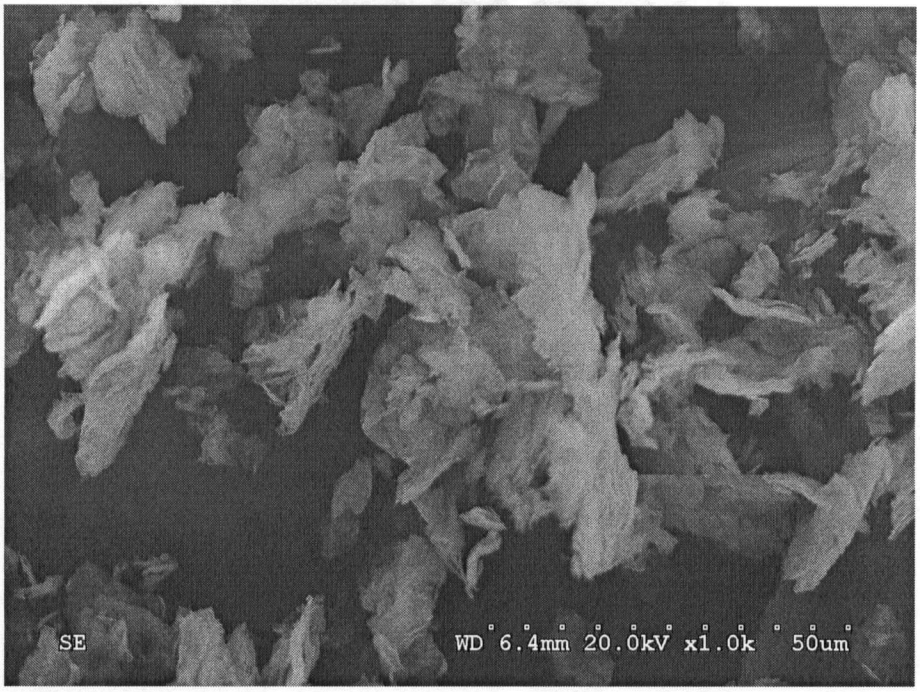

Figure 4.11 *SEM micrograph of 15 min ball-milled and leached-out Al (x1000).*

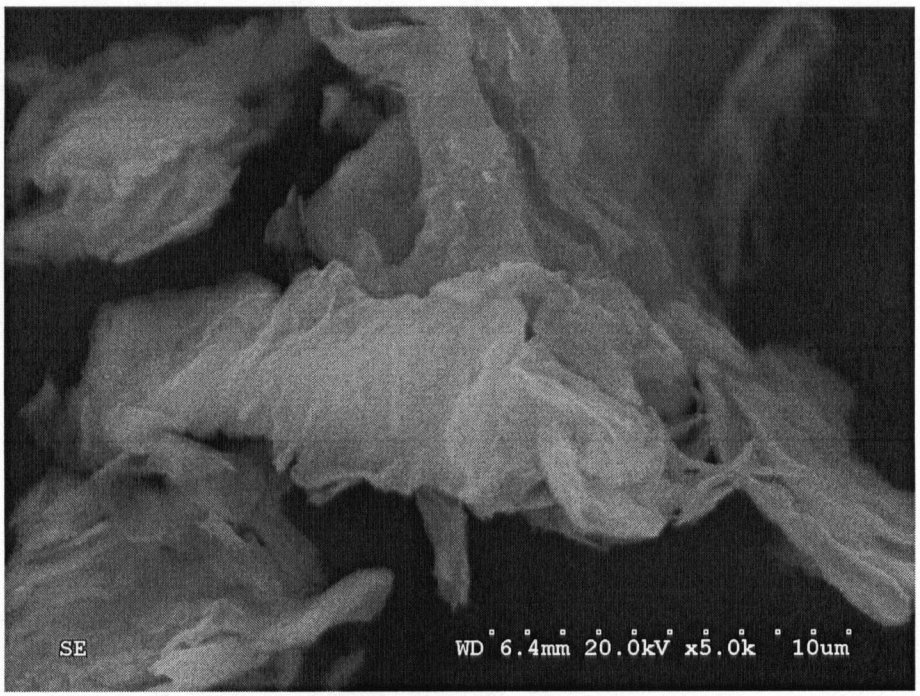

Figure 4.12 *SEM micrograph of 15 min ball-milled and leached-out Al (x5000).*

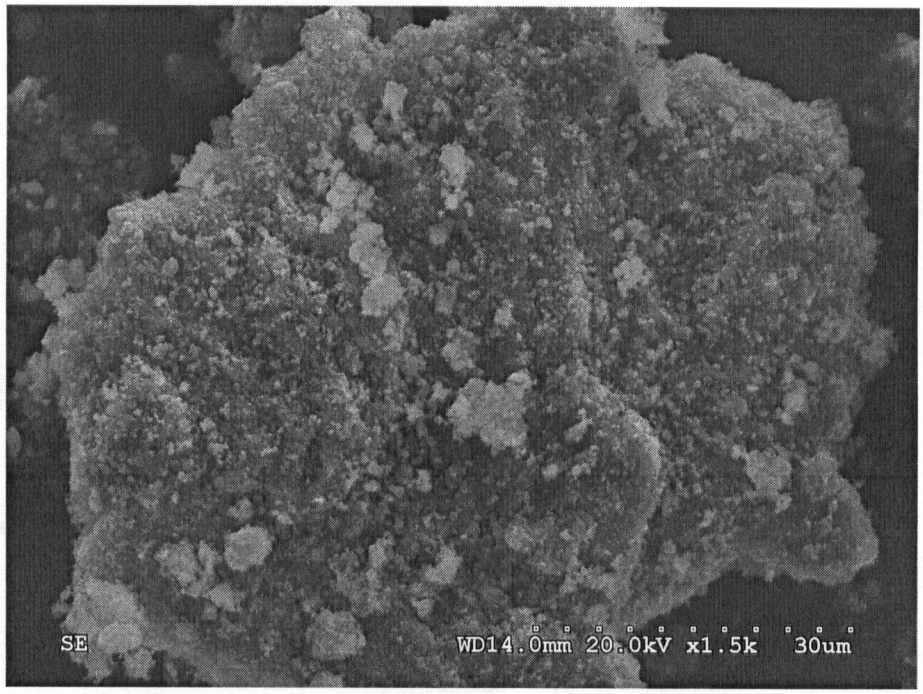

Figure 4.13 *SEM micrograph of Al–Al_2O_3 A16 powder mixture after ball-milling (BM = 15 min). (x 1500)*

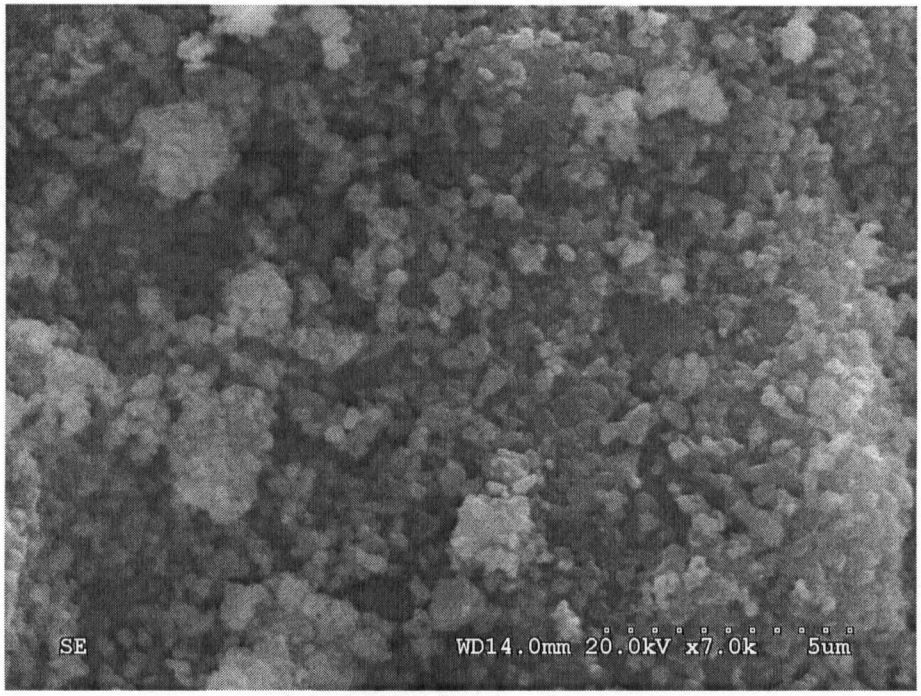

Figure 4.14 *SEM micrograph of Al–Al_2O_3 A16 powder mixture after ball-milling (BM = 15 min). (x 7000)*

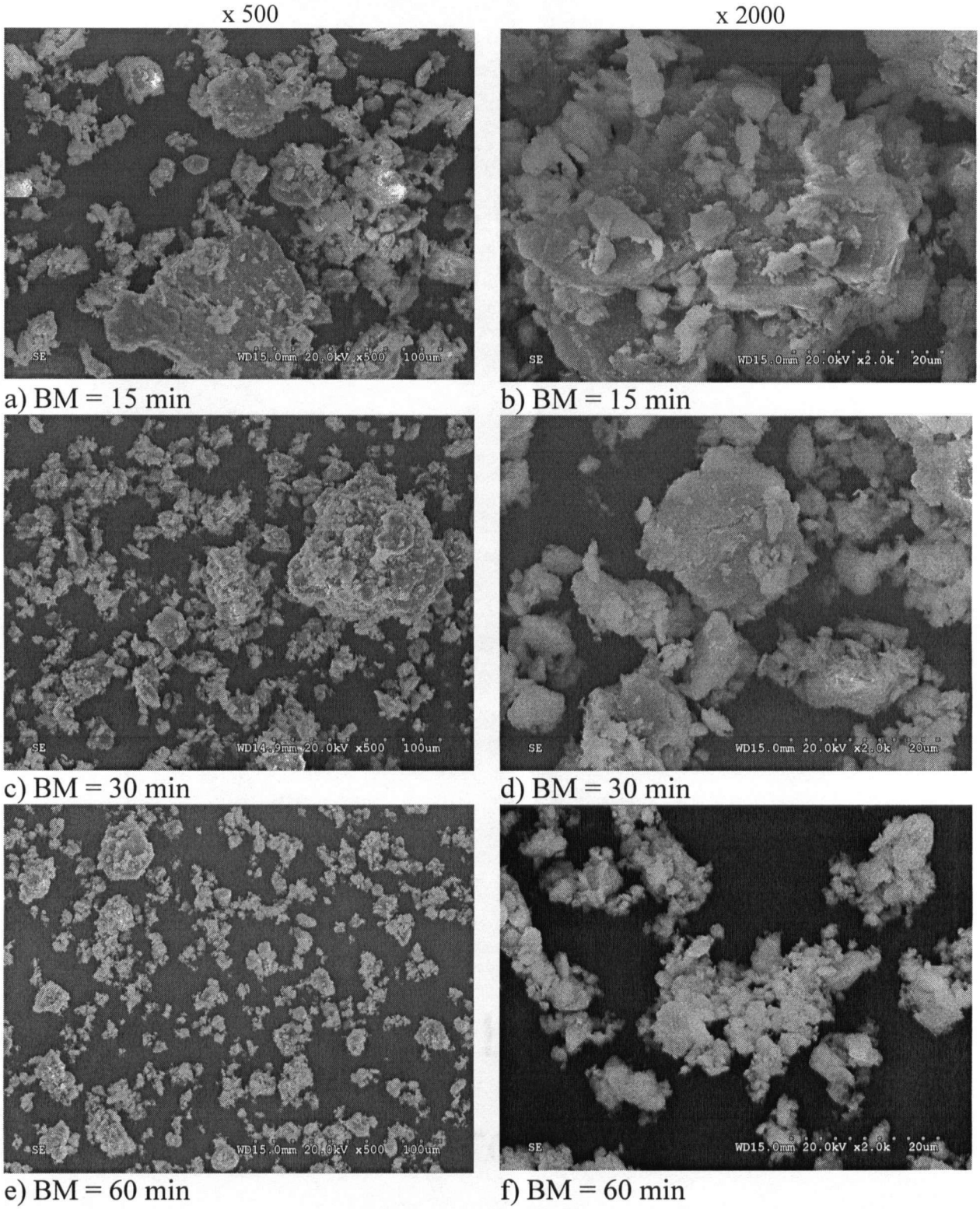

Figure 4.15 *SEM micrographs of Al-KCl(50wt%) powder mixtures after mechanical alloying a) and b) 15 min, c) and d) 30 min, e) and f) 60 min.*

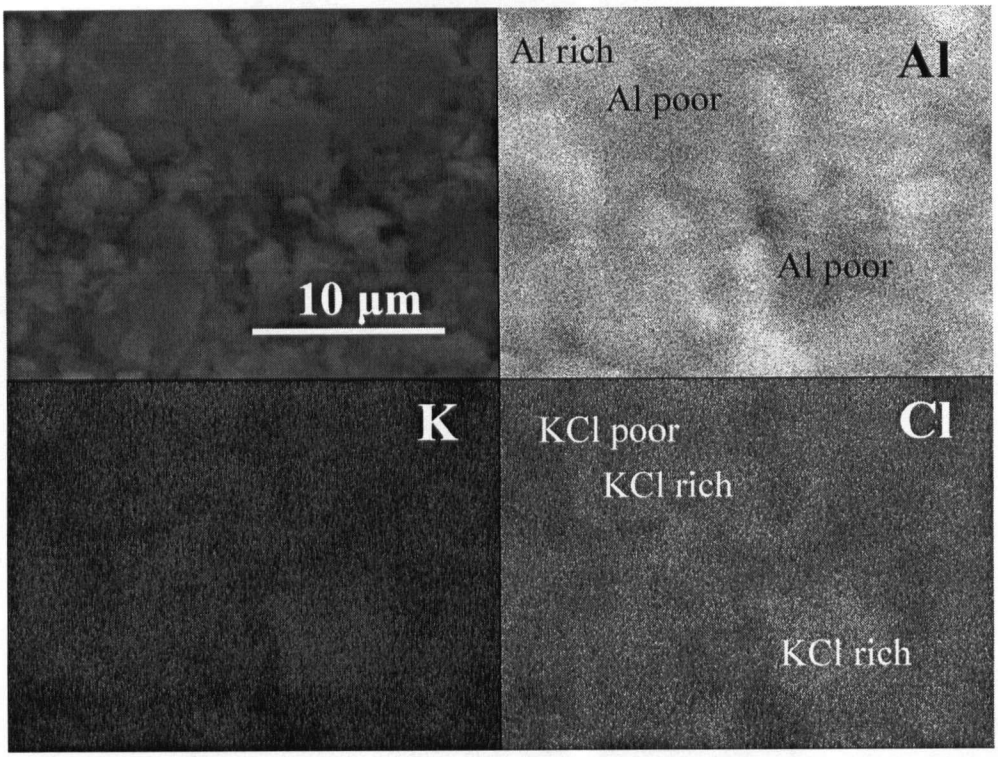

a) BM = 15 min

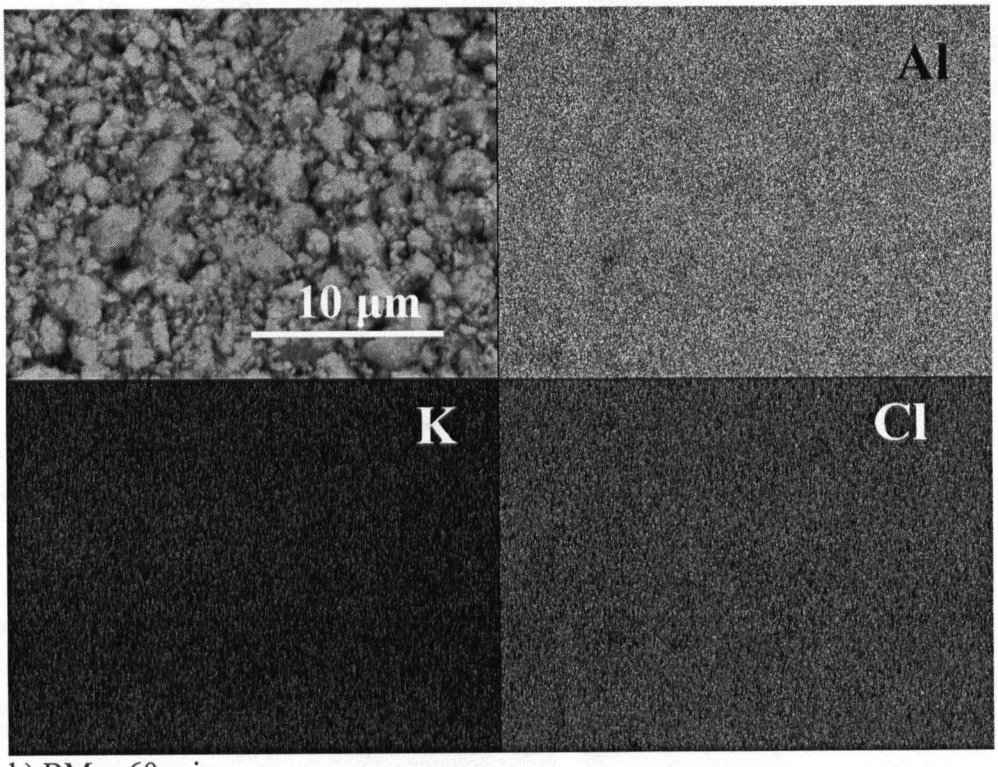

b) BM = 60 min

Figure 4.16 *Spatial element distribution in Al-KCl(50wt%) powders after mechanical alloying: a) BM = 15 min, b) BM = 60 min.*

Figure 4.17 shows XRD patterns of the Al-KCl(50wt%) powder mixtures ball-milled for 15 and 60 min that are compared to hand-mixed (not milled) Al-KCl(50wt%) powders. As milling time increases, the aluminum (111) and (200) peaks intensity at $2\Theta = 38.47°$ and 44.74° decreases and the peaks become broader. The decrease in peak intensity can be attributed to the distortion of the Al crystal structure due to cold working during milling. Peak broadening is ascribed to reduction in Al crystallite size and to changes in the lattice of Al during SPEX milling. Continuous Al lattice deformation induces microstrains and is the reason for increased concentration of defects and dislocations.

The XRD patterns in Figure 4.17 clearly show only two phases in the powder mixtures: that of Al and KCl. No other phases or solid solutions have been formed during the applied longer milling periods.

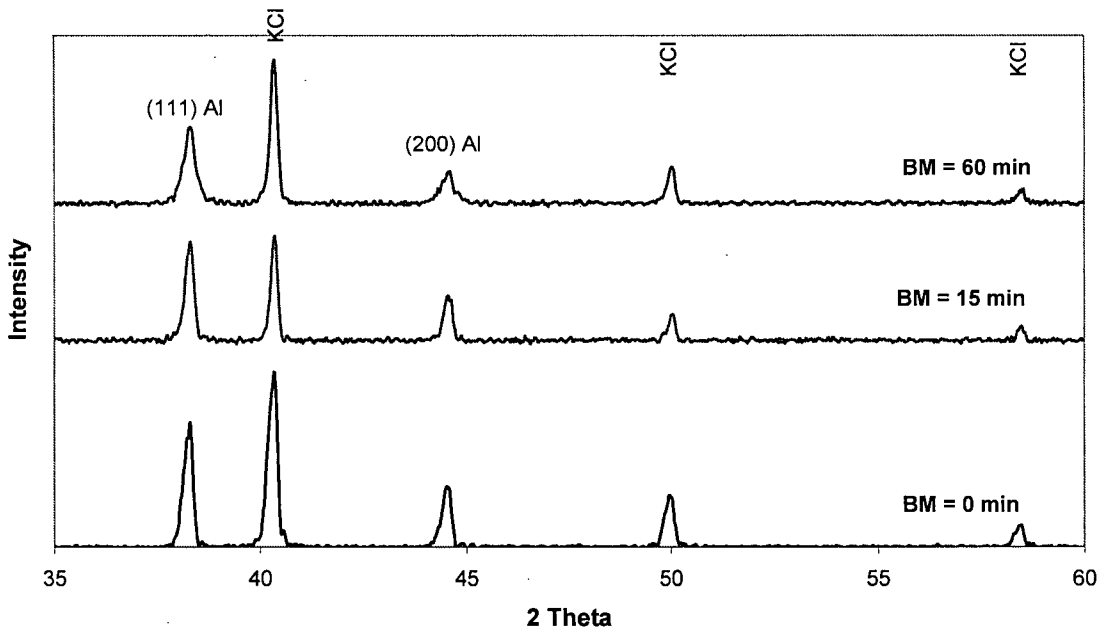

Figure 4.17 *XRD diffractograms of non-milled and mechanically alloyed Al-KCl(50wt%) powders after BM = 15 min and 60 min.*

The change in crystallite size with the increase of ball-milling time was determined as described in Section 3.3.2 by analyzing the peak broadening of the (111) Al reflex at $2\Theta =$

38.47°. As seen in Table 4.2 the average crystallite size of the Al in Al-KCl(50wt%) powder mixture reduces to 136 nm after 15 min of milling and reaches 60 nm after 2 hrs of milling. The microstrains induced in Al increase with ball-milling duration from 0.004 after 15 min of milling and reach a value of 0.01 after 2 hrs of milling.

Table 4.2 *Crystallite size and microstrain of ball-milled Al in Al-KCl(50wt%) powder mixtures obtained from XRD.*

Sample	Crystallite Size [nm]	Microstrain
Al as-received	211	
Al-KCl(50wt%) BM=15min	136	0.004
Al-KCl(50wt%) BM=1 hr	72	0.009
Al-KCl(50wt%) BM=2 hrs	60	0.010
Al-KCl(50wt%) BM=4 hrs	56	0.015

Generally, annealing of solids at elevated temperatures reduces the number of induced defects [31, 82]. The effect of annealing on Al in Al-NaCl(50wt%) powder mixtures after 15 min of ball-milling is presented in Figure 4.18. Annealing was performed on pressed powders (pellet) in argon atmosphere at 550°C for 30 min. The (111) diffraction peak of the annealed Al has a slightly higher intensity then the Al that was not annealed. Whether some of the defects and microstrains induced in the plastically deformed lattice of aluminum during the milling process recovered, cannot be decided on.

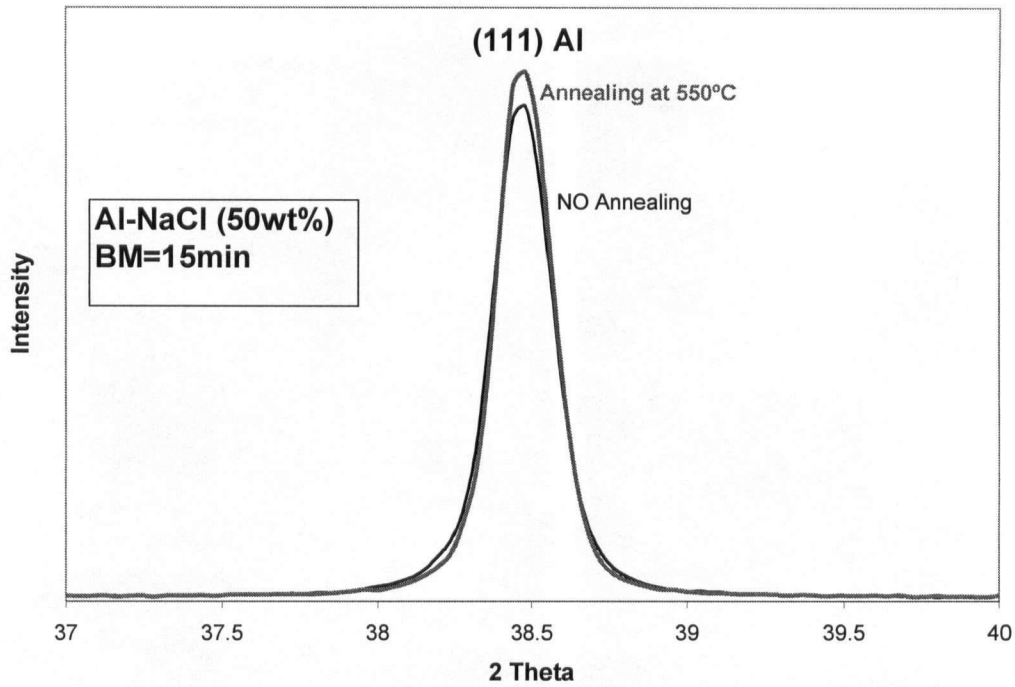

Figure 4.18 *(111) Al diffraction peak of annealed and non-annealed Al-NaCl(50wt%) powders (ball-milling time BM = 15 min) obtained by XRD.*

4.2.2. Elemental Analysis of Ball-Milled Composite Powders

4.2.2.1. X-Ray Photoelectron Spectroscopy (XPS) of Powder Surface

4.2.2.1.1. XPS Survey Scans

The elemental composition of the aluminum surface and chemical state of the near-surface atoms was studied using XPS. Figure 4.19 illustrates the XPS survey scan of Al-NaCl(50wt%) powder mixture after ball-milling for 15 min. Figure 4.20 shows the XPS survey scan of leached-out Al powder (this Al originates from Al-NaCl(50wt%) powder mixture that was ball-milled for 15 min). Figure 4.6 in Section 4.1 presented the XPS spectrum of as-received Al powders, for comparison purpose. All specimens were analyzed in the binding energy range from 0 to 1400 eV.

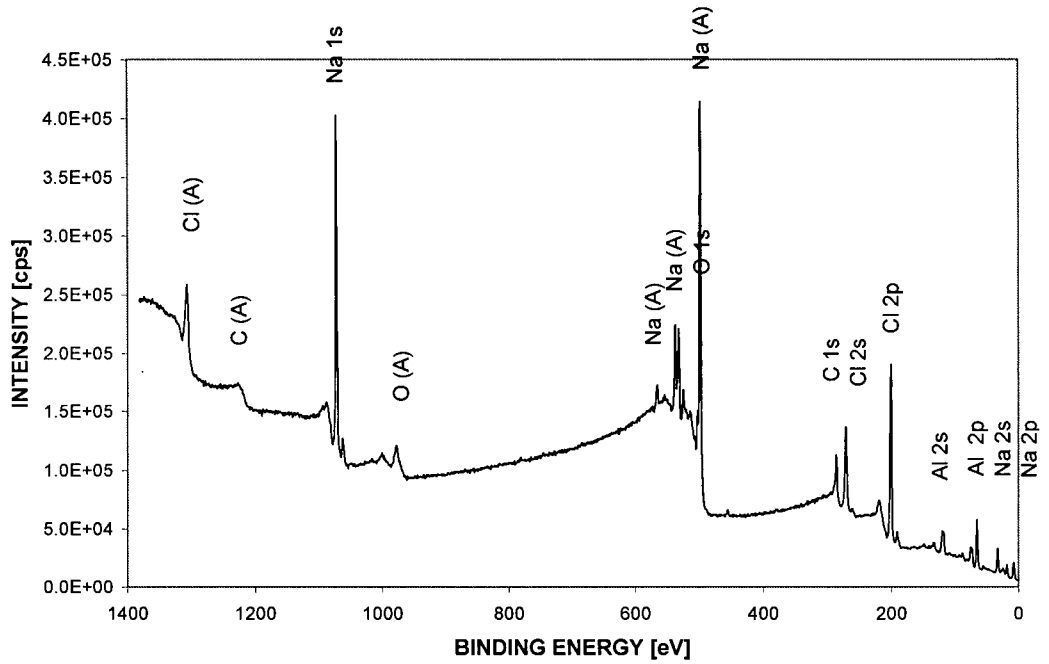

Figure 4.19 *XPS survey scan of Al-NaCl(50wt%) powder mixture, ball-milled for 15 min.*

The XPS spectrum of leached-out Al, see Fig. 4.20, is very similar to the spectrum of the as-received Al and consists of: the aluminum peaks (Al 2p at 75.0 eV and Al 2s at 119.8 eV); the oxygen peaks (O 1s at 532.6 eV and O Auger at 978.2 eV); as well as the carbon peaks (C 1s at 285.4 eV and C Auger at 1223 eV) which originate from surface contamination caused by the vapour residuals of the oil pump. Only one additional peak was found in the spectrum. It is the small peak of Cl 2p at 192.6 eV.

For freshly ball-milled aluminum-salt, Al-NaCl(50wt%), powder mixture with BM = 15 min, peaks of sodium (Na 2p at 23.72 eV, Na 2s at 65.52 eV, Na Auger at 498.32 eV, 531.92 eV and 564.92 eV as well as Na 1s at 1072.72 eV) and chlorine (Cl 2p at 200.72 eV, Cl 2s at 271.12 eV and Cl Auger at 1306.32 eV) were additionally detected and are visible in the XPS broad scan in Figure 4.19.

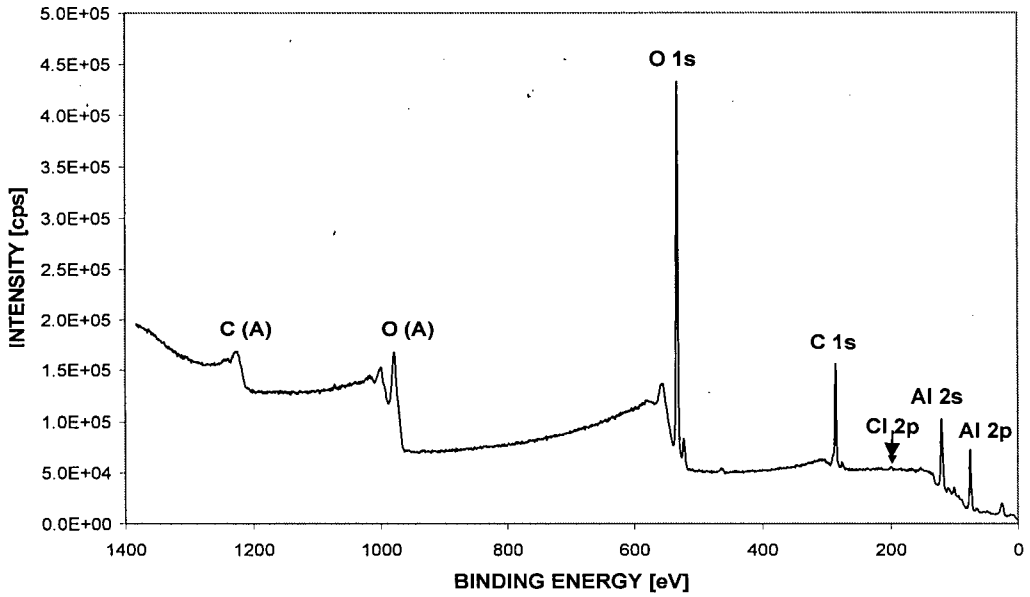

Figure 4.20 *XPS survey scan of 15 min ball-milled and leached-out Al powder.*

The elemental composition of the powder particles surface obtained by XPS is given in Table 4.3, where two processed samples are compared with as-received Al powder. Besides a thin carbon film, that impures the surface and contributes largely to the analysis values (~ 25 at%), the 10 nm of the near-surface predominantly consists of oxygen (48 at%), unless salts are present in the powder matrix. Salts, which were mixed into Al in weight ratio 1:1, are distributed relatively evenly and cover almost half of the surface (48.7 at%). Traces of NaCl (0.3 at%) were detected in the leached-out Al. Where these salts are, whether they are in the intergranular spacing or on the Al surface (as salt remnants from aqueous solution), can only be speculated.

Table 4.3 *The elemental composition of the Al and Al-NaCl powders obtained by XPS.*

Composition [at%] / Sample	Al	O	Na	Cl	C
As-received Al	27.5	48.4	-	-	24.1
Leached-out Al	24.1	48.6	0.1	0.2	26.9
Al-NaCl (BM=15min)	14.3	12.0	22.3	26.4	25.0

4.2.2.1.2. *High Resolution XPS of O 1s and Al 2p*

The structure, composition and thickness of the oxide layer influence largely the corrosion behaviour of aluminum in aqueous environments and dictate the surface reaction kinetics. To understand the rapid corrosion of ball-milled Al in water the collection of oxide related data is therefore crucial. The positions of characteristic XPS peaks give information to preferred bonding and oxidation state of the atoms. The XPS O 1s and Al 2p were therefore analysed in high resolution mode. Figure 21 a) represents the narrow scans of the O 1s and Figure 4.21 b) the narrow scans of the Al 2p core level peaks of the leached-out Al, Al-NaCl(50wt%) powder mixtures ball-milled for 15 min, and the as-received Al powders, for comparison purpose.

The XPS O 1s peak contains information about the bonding of oxygen and indicates the contribution of chemisorbed water, OH^- groups and the O^{2-} species (highest to lowest binding energy, respectively). The O 1s binding energy of pure O^{2-}, OH^- and H_2O species was found in literature and is used as reference to identify which species dominates in the surface of the measured powders [93, 100]. As seen in Table 4.4, the peak positions of the hydroxyl oxygen (OH^-) and the oxide species (O^{2-}) are 1.6 to 2.6 eV apart, whereas the water peak is shifted 0.6 to 1.6 eV away from the OH^- peak.

Table 4.4 *Reference binding energies for the O 1s core-level.*

O 1s species	O^{2-}	OH^-	H_2O
Binding Energy [eV]	529.5[1)] 531.3[2)]	532.1[1)] 532.9[2)]	533.7

[1)] *Chen C., 1997* [2)] *McCafferty E., 1998*

The O 1s peak of as-received and produced Al powders, see Figure 4.21 a), is located at 532.25 eV and is relatively broad (2.5 to 3 eV FWHM) for all the samples. According to Table

4.4, where the reference binding energies for the O 1s core-level peaks are listed, it can be concluded that all three peaks may overlap and that all of the species may be present. However, the clearly predominant species in the near-surface area of the analysed Al powders is the hydroxide or hydroxyl (OH^-) species. In Chapter 2, it has been indicated that the oxide film most likely consists of bayerite, $Al(OH)_3$ [32, 34, 37].

The XPS Al 2p peak belongs to the Al metal and is located at 75 eV on the broad scan. However, with increasing exposure to an oxidizing atmosphere the Al 2p peak splits and its oxidic shoulder drifts from the elemental peak and grows with the growth of oxide layer thickness [93, 100]. By measuring the intensity ratios of the oxidic to metallic components, the oxide film thickness may be calculated.

The Al 2p core level peaks acquired from three different powder samples contain the elemental component, Al_{Metal}, and a broader oxide component, Al_{Oxide}, to higher binding energy values in the upper 10nm thick surface layer (Figure 4.21 (b)). The Al 2p (Al_{Metal}) peak is located at 72.8 eV, whereas the Al 2p (Al_{Oxide}) at 75.3 eV. From the spectrum it is apparent that the oxide film thickness on the Al particles is the lowest for ball-milled Al-NaCl powders and highest for leached-out Al. The ball-milled Al-NaCl powders were freshly prepared and loaded to the XPS vacuum chamber no later than 30 minutes after ball-milling in air atmosphere. The leached-out Al powders were washed in water for approx. 3 hrs and were then air-dried for several days. Consequently, their surface was exposed to two different environments much longer and a thicker oxide film could develop. The oxide film thickness difference between leached-out and as-received Al may be attributed to different oxide growth kinetics in dry and wet atmosphere. It has been reported that thicker oxides are grown in wet environments [28, 32, 33, 67] and our results support it. Table 4.5 gives a rough estimation of the oxide film thickness on Al and composite powders.

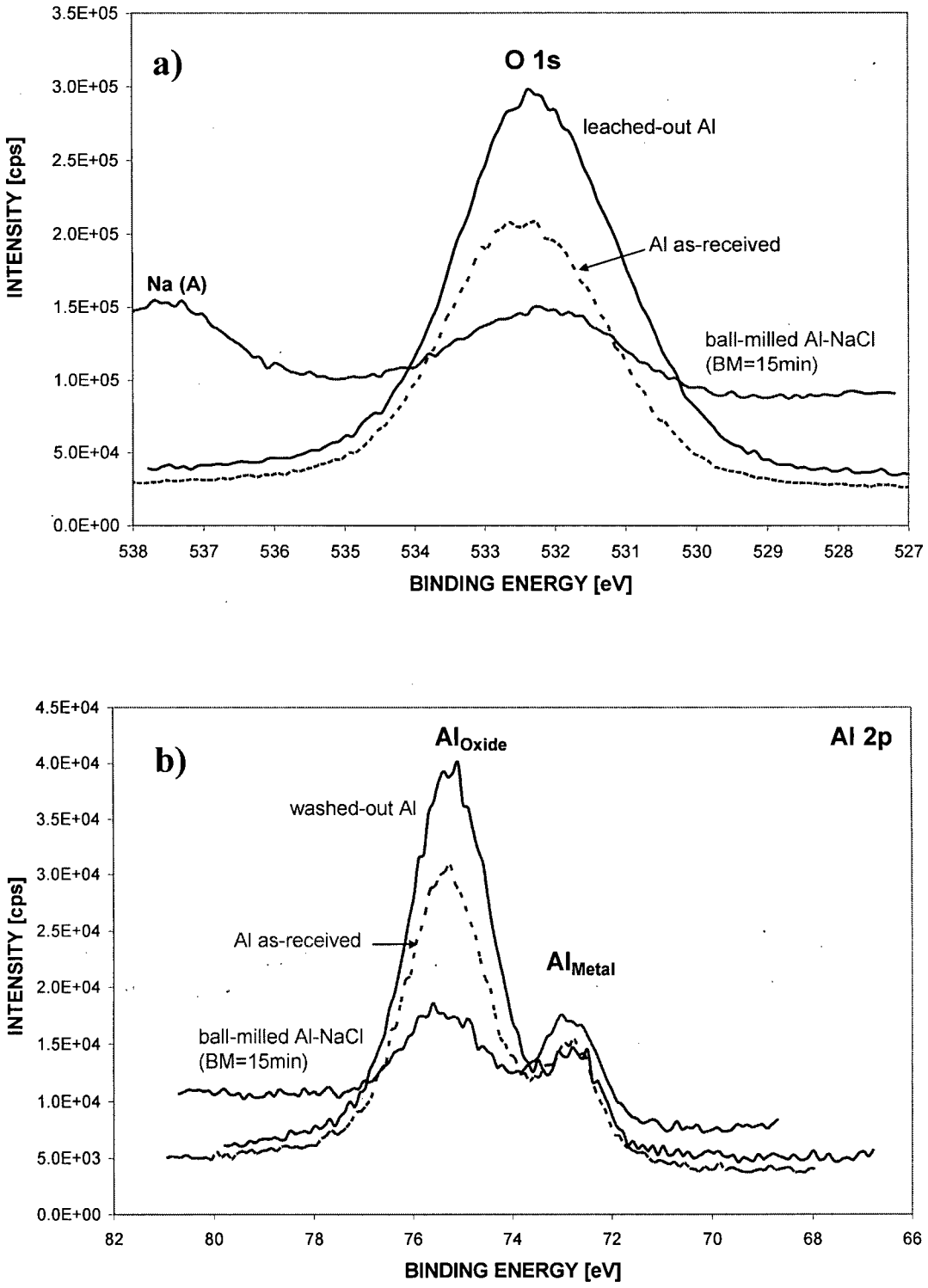

Figure 4.21 *High resolution (a) O 1s and (b) Al 2p core–level XPS spectra of leached-out Al and Al-NaCl(50wt%) powder mixtures, ball-milled for 15 min, compared to as-received Al powders.*

Table 4.5 *Aluminum oxide film thickness estimated from Al 2p peaks intensities.*

Sample	Al_{oxide} / Al_{Metal} [atomic ratio]	Al Oxide Thickness	Al Oxide Thickness [nm]
As-received Al	3.88/1	1.6 lambda*	3.2 – 9.6
Washed-out Al	8.88/1	2.3 lambda*	4.6 – 13.8
Al-NaCl (BM=15min)	1.15/1	0.8 lambda*	1.6 – 4.8

* lambda is the inelastic mean free path of Al_{oxide} (lambda may vary between 2 to 6 nm)

4.2.2.2. Energy Dispersive X-Ray Analysis (EDS) of Ball-Milled Composite Powders

Aluminum has very high affinity to oxygen so that oxidation or hydration of the metal surface proceeds instantaneously. The standard enthalpy of formation ΔH°_f is: -1668 kJ/mole for aluminum oxide (α-Al_2O_3), -1274 kJ/mole for bayerite ($Al(OH)_3$), and -988 kJ/mole for boehmite (AlOOH) [3, 96]. During ball-milling when fresh Al surfaces are continuously created and exposed to the milling atmosphere these fresh surfaces may react with oxygen in the very short time between ball collisions. As ball-milling takes place in air and also ball-milled powders are handled and stored in air, there is a high probability that additional aluminum oxide would be formed. Therefore, the variation in oxide concentration [O] was investigated. The oxygen concentration in fresh prepared and aged Al-KCl(50wt%) powders in function of ball-milling time was examined by using EDS. The results are summarized in Table 4.6. The [O] change was related to oxygen concentration measured in as-received Al powders. The net increase in oxygen concentration in fresh ground and 3 weeks aged Al-KCl powders is presented in Figure 4.22. The freshly ball-milled powders were exposed to air for a maximum of 15 minutes before they were loaded to the SEM vacuum chamber. After the measurement the powders were kept on specimen stubs in air and were characterized again 3 weeks later.

As seen in Table 4.6 the gross oxygen concentration in freshly milled powders increases steadily from 3.83 wt% for 15 min ball-milled powders to 13.67 wt% for 4 hours ball-milled powders. The powders include oxide debris from the original native oxide film that was present on the as-received Al powder particles (3.79 wt%). It was not attempted to determine the percentage of oxidation during or the percentage of oxidation right after ball-milling. After 3 weeks of aging the powders continued to oxidize and reached oxygen concentrations of 4.11 wt% for 15 min ball-milled powders and 20.26 wt% for 4 hours ball-milled powders. Even though the aging time was the same for all investigated powders, the increase in oxygen is the lowest for powders ball-milled for 15 min and highest for powders ball-milled for 4 hours (see Figure 4.22). The largely increased surface area which increases with ball-milling duration (due to particle refinement) and the higher surface reactivity which depends on the degree of deformation as well as on the defect concentration in Al and its oxide (that also increases with ball-milling duration), are the most probable reasons for oxide amount increase. The fraction of adsorbed oxygen and/or water on the particle surface could not be identified.

Table 4.6 *Gross oxygen concentration in fresh milled and 3 weeks aged Al-KCl(50wt%) powders, obtained by EDS.*

Sample	Oxygen concentration in fresh ground powder [wt%]	Oxygen concentration in 3 weeks old powders [wt%]
Al source, **no BM**	3.79	3.79
Al-KCl, **BM=15min**	3.83	4.11
Al-KCl, **BM=1hr**	7.94	9.48
Al-KCl, **BM=2hrs**	9.32	14.05
Al-KCl, **BM=4hrs**	13.67	20.26

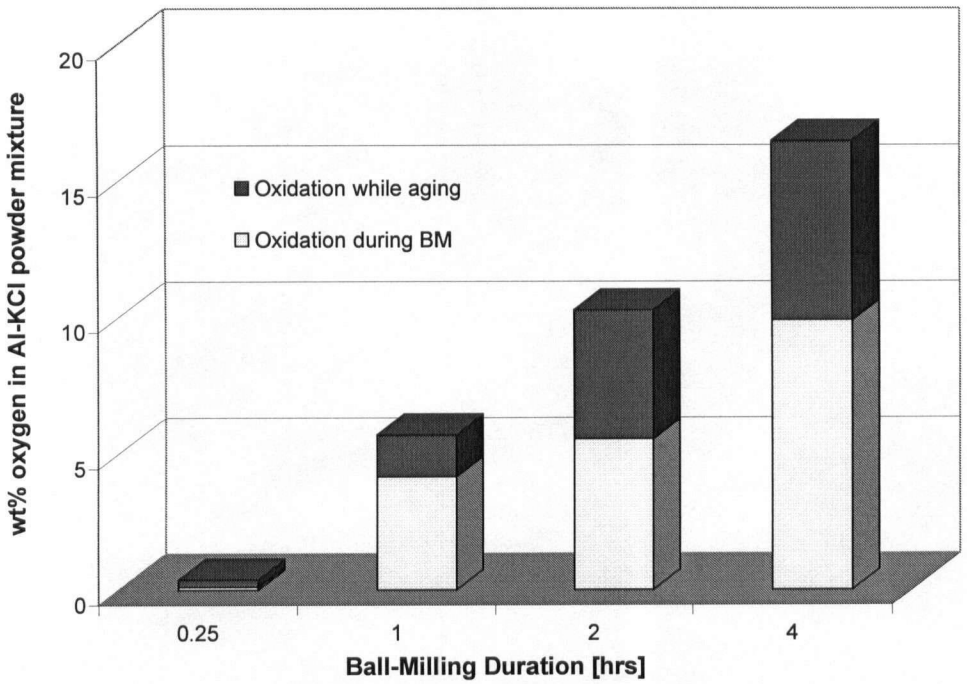

Figure 4.22 *Net increase in oxygen concentration in fresh ground and for three weeks aged Al-KCl(50wt%) powders.*

4.3. Hydrogen Generation through Al-assisted Water Split Reaction

As discussed in Chapter 2.5, the corrosion reaction of aluminum in water at near-neutral pH conditions at 25°C is generally very slow due to the nm-thin passive film of oxides and hydrated oxides preventing (or slowing down) access of the reactants to the metal surface. These oxide films on aluminum have very low solubility in neutral and near-neutral pH water solutions. Localized corrosion, such as pitting and intermetallic corrosion, has been observed in the presence of aggressive ions and metallic impurities or alloying metals respectively [25, 35, 56, 59, 60]. The oxide film solubility increases when the solution's pH is shifted into the alkaline or acidic region ($9 < pH < 4$). When the protective film is dissolved, a rapid corrosion of Al in water will proceed.

In this section the massive and "atypical" corrosion of Al in water at near-neutral pH accompanied with the development of exceptional high amounts of hydrogen gas will be

presented. The prerequisite for this rapid reaction, in which the re-passivation of the aluminum metal fails, is mechanical alloying of Al powders with an additive, as described in Chapter 3. The Al-assisted water split reaction is very complex not only because of a series of simultaneous partial cathodic and anodic reactions involved but also because of the surface oxide, the environment and the metal itself. When bayerite, $Al(OH)_3$, or boehmite, AlOOH, are the reaction products, the overall reactions can be written as:

$$2Al + 6H_2O \rightarrow 3H_2 + 2Al(OH)_3 \quad (4.1)$$

$$2Al + 4H_2O \rightarrow 3H_2 + 2AlOOH \quad (4.2)$$

There are several factors which influence the atypical Al corrosion reactions (4.1) and (4.2) leading to massive hydrogen gas generation. Some of the most significant parameters, which will be discussed below, are: the properties and concentration of the additive, powder particle size, alloying conditions, temperature, pH, and the chemistry of the solvent.

4.3.1. Influence of the Additive on Hydrogen Generation

4.3.1.1. Additive - free Aluminum-H_2O Systems

As-received Al powders and Al powders ball-milled for 15 min and 60 min without the addition of a second phase, were exposed to water (tap water, pH 6.5 to 7.1) or corrosion promoting aqueous solutions. The progress of the overall Al-assisted water split reactions (4.1) and (4.2) was measured by capturing the generated hydrogen gas. The complete corrosion of 1 g of Al metal at 25°C and 1 atm pressure, results in a maximum of 1359 cc generated hydrogen gas.

The H_2 generation results obtained from as-received and ball-milled additive-free aluminum powders in different environments are summarized in Table 4.7. No H_2 generation

was observed for as-received Al powders in cold water (T = 20 ± 2°C). The experiment was aborted after 14 days. Some H_2 generation was observed at increased water temperature (T = 55°C). Hydrogen evolution started after 15 min and after 1 hour of exposure ~ 90 cc hydrogen gas/1g of Al was collected. This amount corresponds to a corrosion of ~ 6.5 % of the Al to aluminum hydroxides. Comparable H_2 generation reaction progress was measured in 0.007 M KCl. Increased H_2 evolution reaction of Al powders was monitored in KCl saturated and pH 10 aqueous solutions at T_{Water} = 55°C (see Table 4.7). The progress of the H_2 generation reaction in the first 60 minutes is shown in Figure 4.23. The induction period, in which no H_2 generation is measured, decreased to 5 min for Al powder in pH10 solution; the highest H_2 yields from as-received Al powders were obtained in saturated KCl solutions (155 cc H_2/1g of Al after 60 min of reaction).

Table 4.7 *Hydrogen generation from as-received and ball-milled additive-free Al powders during corrosion in different environments. (T_{Water}= 55°C).*

Al - H_2O System	**Ball-milling duration [min]**	**Induction time [min]**	**H_2 yield after 60min of corrosion [cc H_2/1g Al]**
as-received Al	0	15	90
as-received Al hand mixed with KCl (1:1)	0	15	90
as-received Al in pH10 solution	0	5	110
as-received Al in saturated KCl solution (T_{sat} = 55°C)	0	8	155
ball-milled Al	15	10	10 to 50
ball-milled Al	60	5	125
ball-milled Al hand mixed with KCl (1:1)	15	15	12
ball-milled Al in saturated KCl solution (T_{sat} = 55°C)	15	5	18

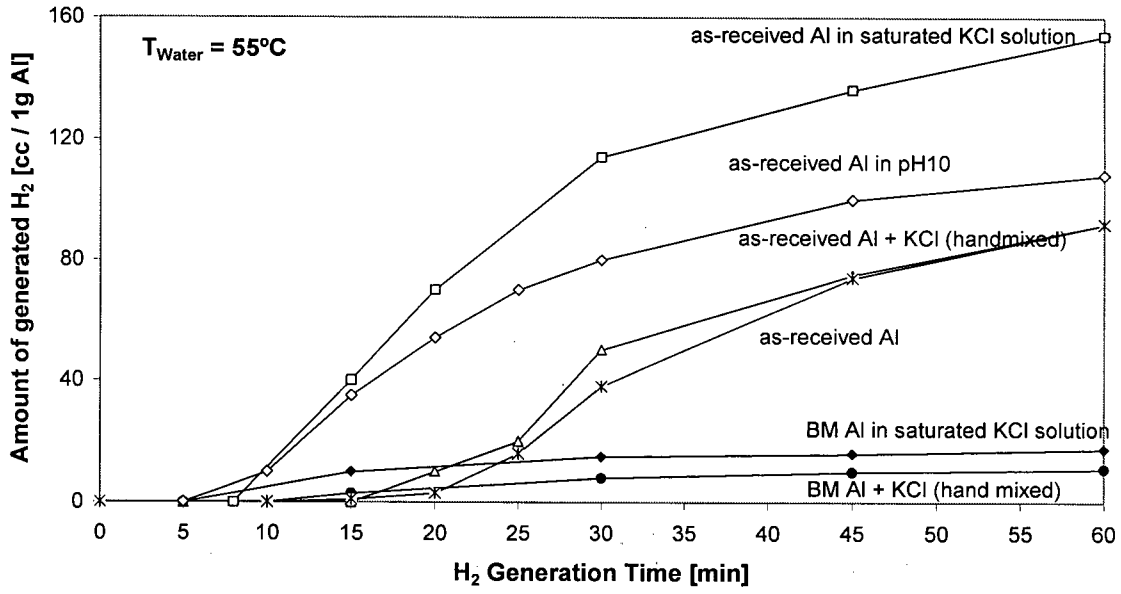

Figure 4.23 *Hydrogen generation from as-received and ball-milled Al-only powders in the first hour of corrosion in different environments. (T_{Water}= 55°C).*

As-received Al, mechanically alloyed for 15 min without any additives, shows only very limited reactivity even in aggressive environments. As shown in Figure 4.24, BM Al-only powders tend to form large metal flakes - up to a millimeter in size - due to cold welding during the high energy ball-milling process. The largely reduced surface area may be the reason for the reduced corrosion susceptibility when comparing to as-received Al powders with mean particle size of 35 μm. The amount of hydrogen collected from Al-only powders ball-milled for 15 min was not reproducible and fluctuated between 10 and 50 cc H_2/1g of Al. Al-only powders ball-milled for 60 min generated higher amounts of hydrogen (125 cc H_2/1g of Al), see Table 4.7. Because corundum (milling media materials) was confirmed in the powders - see XRD diffractograms in Figure 4.25 - the probable reason for H_2 fluctuation (when using short milling times) as well as the increased Al activity (when using longer milling times) is the incorporation of hard abrasives debris coming from balls and crucible walls particles and the formation of a two-phase matrix by amalgamation with the ductile and sticky Al.

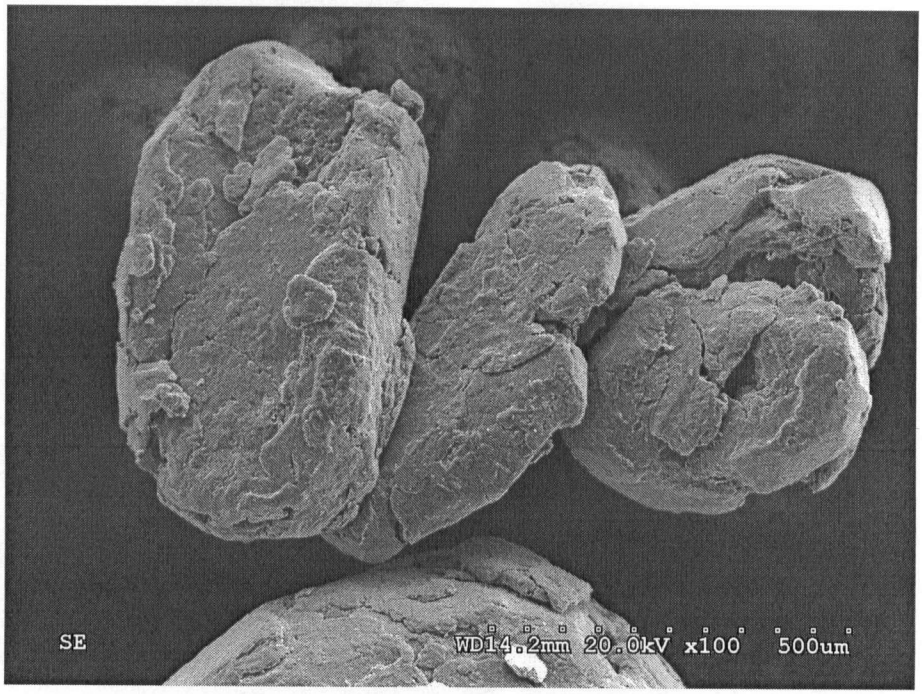

Figure 4.24 *SEM micrograph of ball-milled Al-only powders (ball-milling time BM = 15min).*

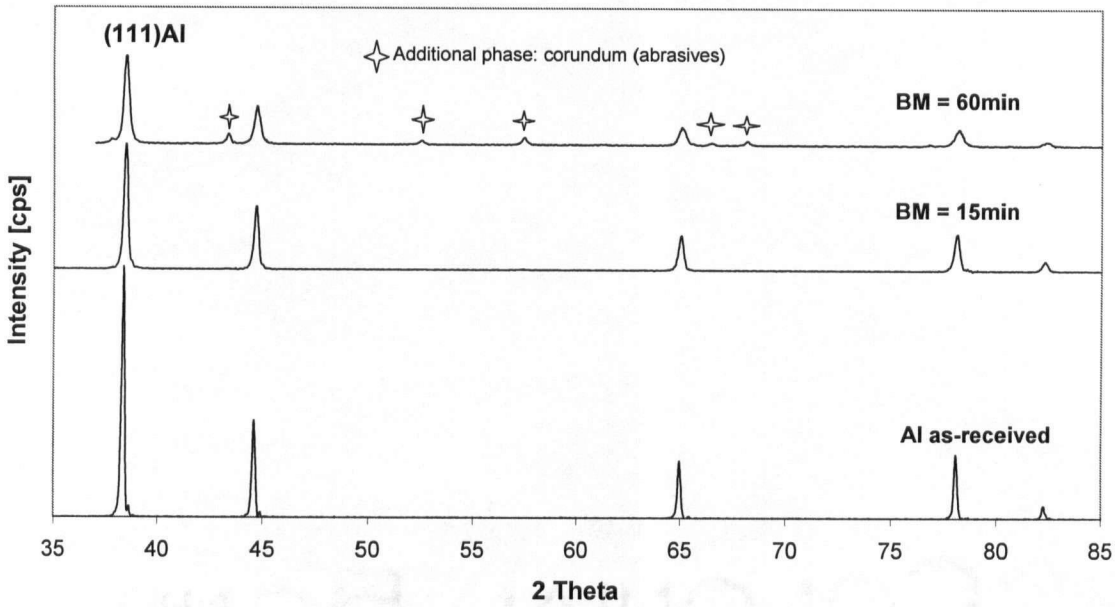

Figure 4.25 *XRD diffractograms of as-received and ball-milled Al-only powders.*

4.3.1.2. Aluminum-Additive-H_2O Systems

Different Al-additive systems (50/50wt%) have been explored and the amount of generated H_2 compared. As additives chosen were water-soluble and water-insoluble organic and inorganic materials. Potassium chloride (KCl) and sodium chloride (NaCl) were the most used system compounds. The chosen additives differ from each other significantly. Not only their chemical composition and chemical reactivity with Al and H_2O, but also their physical properties, such as initial particle size, hardness or mechanical strength, vary greatly.

As shown in Figures 4.26 and Table 4.8, all additives after being mechanically blended with Al in a comparable ball-milling process have an accelerating effect on the corrosion of Al regardless of their variation in chemistry and physical properties. Figure 4.26 presents graphically the effect of various additives on the hydrogen generation reaction of Al in water, whereas Table 4.8 gives the amount of hydrogen gas generated in 1 hr during corrosion reaction of Al in water, and lists the initial particle size of the used additives.

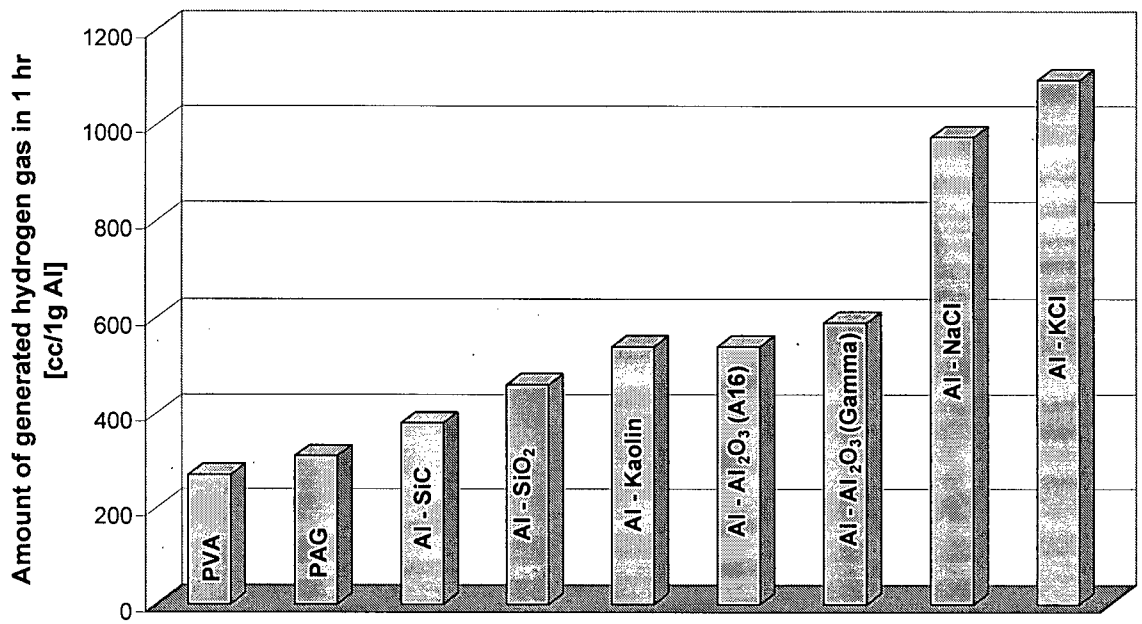

Figure 4.26 *Effect of various Al-additive systems on the amount of hydrogen gas generated in one hour during corrosion reaction of Al in water.* (T_{water} = 55°C)

The lowest H_2 yields were obtained from Al blended with organic additives and the highest when using common water-soluble inorganic salts (WIS), such as NaCl and KCl. In the first hour of the reaction, 270 cc H_2 for PVA and 1095 cc H_2 for KCl were released from 1g of Al, or 20% and 80% respectively from the aluminum present in the system was corroded to aluminum hydroxide. For the water insoluble additives, which were employed as-received, a correlation between particle size and H_2 generation rate was observed. The smaller the additive particle size the higher the hydrogen yield was. This result did not apply to salts. Water-soluble inorganic salts are characterized by very large initial particle size, yet the highest hydrogen yields were obtained by using them as an additive. The reason is that salt crystallites can be reduced in size much more efficiently than any other tested inorganic materials due to their low hardness and easy cleavage during the process of high energy ball-milling (in pre-ball-milling and subsequent mechanical alloying with Al).

Table 4.8 *Initial particle size of additives and the effect of various additives on hydrogen yield after 1 hr of Al corrosion in water.*

Additive	**Initial Particle Size** [μm]	**Amount of generated H_2** [cc/1g Al in 1hr] T_{Water}= 55°C
ORGANIC:		
PVA	≤ 1000	270
PAG	≤ 4000x500 (slab form)	310
INORGANIC:		
SiC	8 - 10	380
SiO_2	150	460
Kaolin	< 2	540
Al_2O_3 (A16)	0.4	540
Al_2O_3 (γ alumina)	0.04	590
SALTS:		
NaCl	< 300	970
KCl	< 350	1095

The H_2 yield obtained from Al in the Al-salt-water systems is 250% higher than the H_2 yield obtained from the Al-PAG system and 100% higher than the H_2 yield from the Al-Al_2O_3 or Al-AlOOH system found in literature [1,2]. Using KCl as additive, more than 80% of the aluminum have been corroded to $Al(OH)_3$ and/or AlOOH after 1 hour of reaction, and more than 70% using NaCl. In these reactions hydrogen yields of 1095 cc and 970 cc H_2 gas /1g Al respectively, were obtained. Multiple H_2 generation experiments using ball-milled Al-WIS and Al-Al_2O_3 powders and same conditions were performed to test the reproducibility of the experimental results. The mean hydrogen yield was determined to 1115 ± 4% cc /1 g Al for Al-KCl(<0.5wt%NaNO3)-H_2O system and 505 ± 7% cc /1 g Al for Al-Al_2O_3-H_2O system after one hour of water split reaction.

From all tested materials, Al-KCl powder mixtures form the most hydrogen efficient two-component systems, followed by Al-NaCl powder mixtures (~ 10% less efficient). The finest water-insoluble inorganic powders lay far behind the Al-salt systems.

The hydrogen generation reaction for Al-salt-H_2O systems as a function of time is presented in Figure 4.27. Typically three reaction stages can be distinguished. The first stage, in which no or very little hydrogen is generated, is called induction period. This stage lasts from a few seconds for salts and several hours for Al-only powders. The second stage is characterized by a very fast reaction during which hydrogen is produced at its highest generation rates of 60 to 450 cc H_2/min per 1g Al for Al-salt systems. The third and final stage shows considerably slowed down hydrogen generation rates of < 1 to 20 cc H_2/min per 1g Al. Hydrogen evolution continues in this slowed-down mode as long as the powders are in contact with water. The precipitated aluminum hydroxide most likely affects the reaction by hindering the water access to the remaining Al metal. Regrinding of the incomplete reacted powders usually reactivates the Al that is still contained in the sample, leading to a faster corrosion completion of the metal.

The induction period, reaction rate and total hydrogen yield depend not only on the additive but also on many other factors that will be presented and described in the following sections.

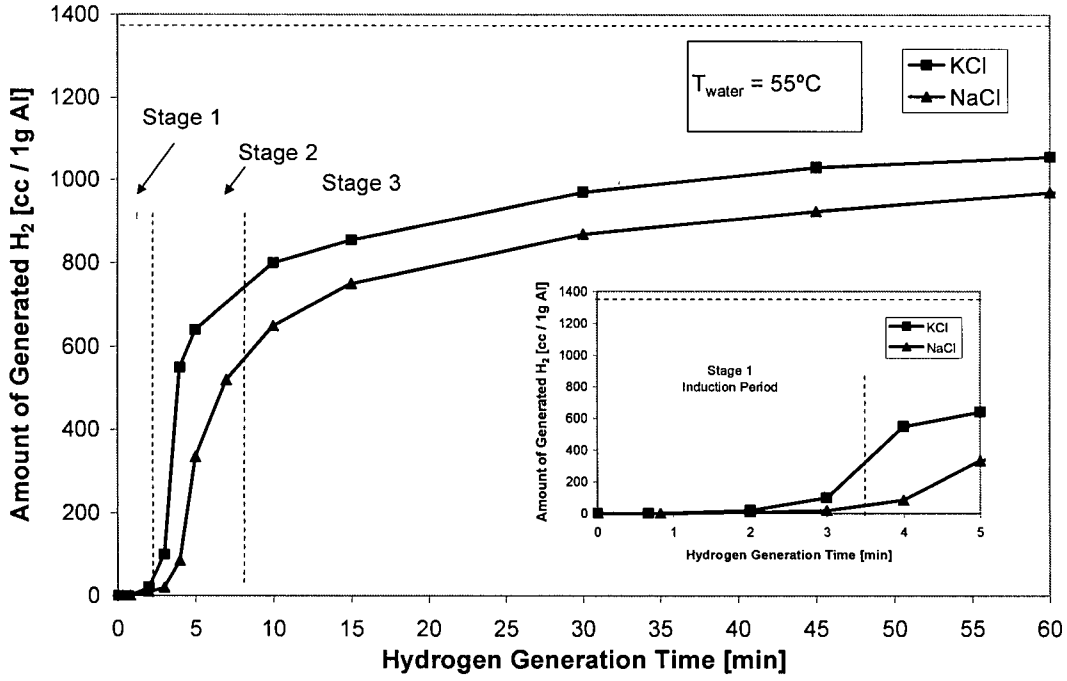

Figure 4.27 *Typical stages of hydrogen generation during the first hour of Al-H_2O reaction on the basis of Al-salt-H_2O systems. (T_{water} = 55°C)*

4.3.1.3. Aluminum-H_2O Systems with Leached-out Additive

In this section hydrogen generation from additive-free Al-H_2O systems will be demonstrated. Additive-free Al powders were prepared from mechanically alloyed Al-additive powder mixtures by removing (leaching-out) the water-soluble system component. Water-soluble inorganic salts, such as NaCl and KCl, are best suitable for these experiments due to their high solubility in water, including cold (< 20°C) water. According to EDS and XPS results presented in Section 4.2, essentially pure Al was obtained after a thoroughly washing process of the Al-salt powder mixtures. The remaining salt concentrations were found well below 1 wt%.

The amount of hydrogen gas generated from such leached-out Al-H_2O system during 2 hours of reaction is shown in Figure 4.28. The reactivity and hydrogen evolution from Al with leached-out KCl and leached-out NaCl, as well as standard Al-NaCl powder mixtures are compared. From Figure 4.28 it can be seen that ball-milled salt-free Al powders behave like Al-salt powder mixtures in water. They maintain the same water split reaction rate, have similar induction periods and comparable hydrogen yields. Leached-out Al-H_2O systems yielded between 900 and 950 cc H_2 gas in one hour and approximately 1000 cc in two hours of corrosion. The reaction efficiency is 65 to 70% and 74% respectively.

Two important conclusions can be drawn from obtained results. Firstly, because the water split reaction remains unchanged in the additive-free Al-H_2O systems, the presence of a salt or any other additive is not required for the rapid corrosion reaction of aluminum. However, structural changes in aluminum and its oxide formed during mechanical alloying, as well as the increased porosity and increased surface area may be some of the reasons for the increased corrosion of such "additive-free" aluminum powders. As reported earlier in Section 4.2.1, the specific surface area of leached-out Al increases more than 30 times from 0.30 m^2/g for as-received Al powder to 9.68 m^2/g after 15 min of ball-milling Al with a salt. Secondly, differences in H_2 yield and reaction kinetics when using Al-KCl and Al-NaCl systems were reported earlier (see Fig. 4.27). Because there is no H_2 yield difference between any of the leached-out Al powders, some chemical influence of the second phase is suggested. Besides the dominant mechanistic influence of additives during the process of mechanical alloying, there is a notable but limited chemical influence that affects the mechanism of the Al corrosion reaction. The absence of Na^+, K^+ and Cl^- ions in the aqueous solution or the absence of Na^+, K^+ and Cl^- ions at the corrosion site seems to be the reason for the corrosion setback.

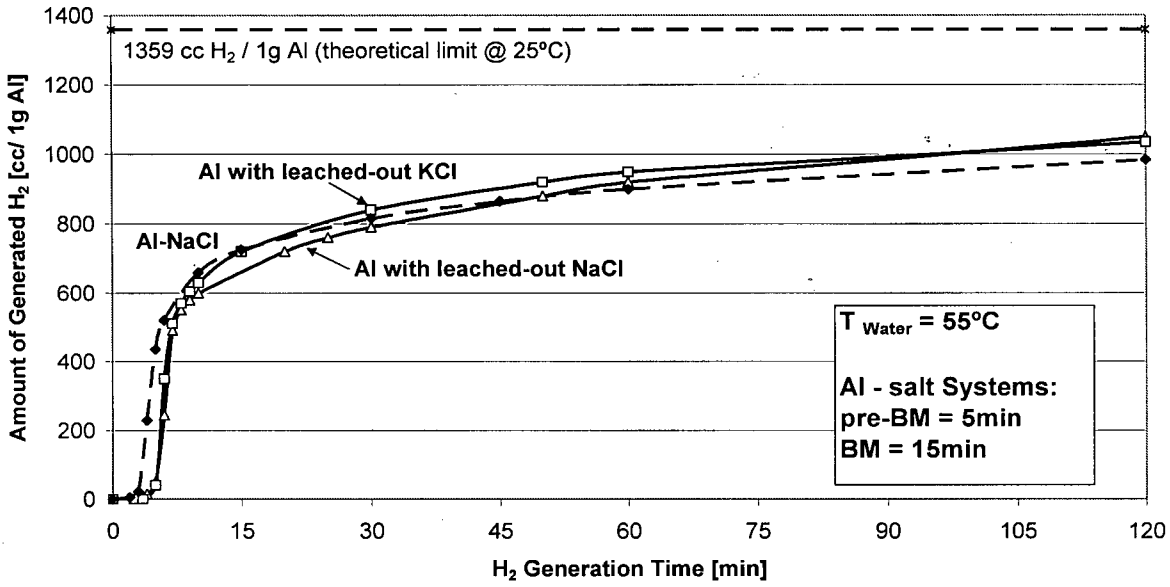

Figure 4.28 *Comparison of hydrogen generation from Al-NaCl-H_2O(♦) with leached-out Al-H_2O systems(KCl □; NaCl Δ) during 2 hours of corrosion reaction.*

4.3.2. Influence of Additive Concentration on Hydrogen Generation

Using potassium chloride, which is one of the most effective additives employed in this work for hydrogen generation through Al-assisted water split reaction, the influence of additive concentration on hydrogen generation was studied. The effect of the amount of KCl in Al-KCl powder mixture on the total amount of hydrogen produced in 1 hour per 1g of Al metal is presented in Figure 4.29. The data were normalized per gram of aluminum metal.

As seen in the plot, the higher the concentration of the KCl salt (or second phase) in the powder mixture, the more thoroughly the corrosion reaction of the Al contained in the sample is. The amount of H_2 generated from Al-KCl powders with [KCl] $\geq$ 90% equals nearly the theoretical limit for hydrogen generation (1359 cc per 1g of Al metal at 25°C), presented in the graph with broken line.

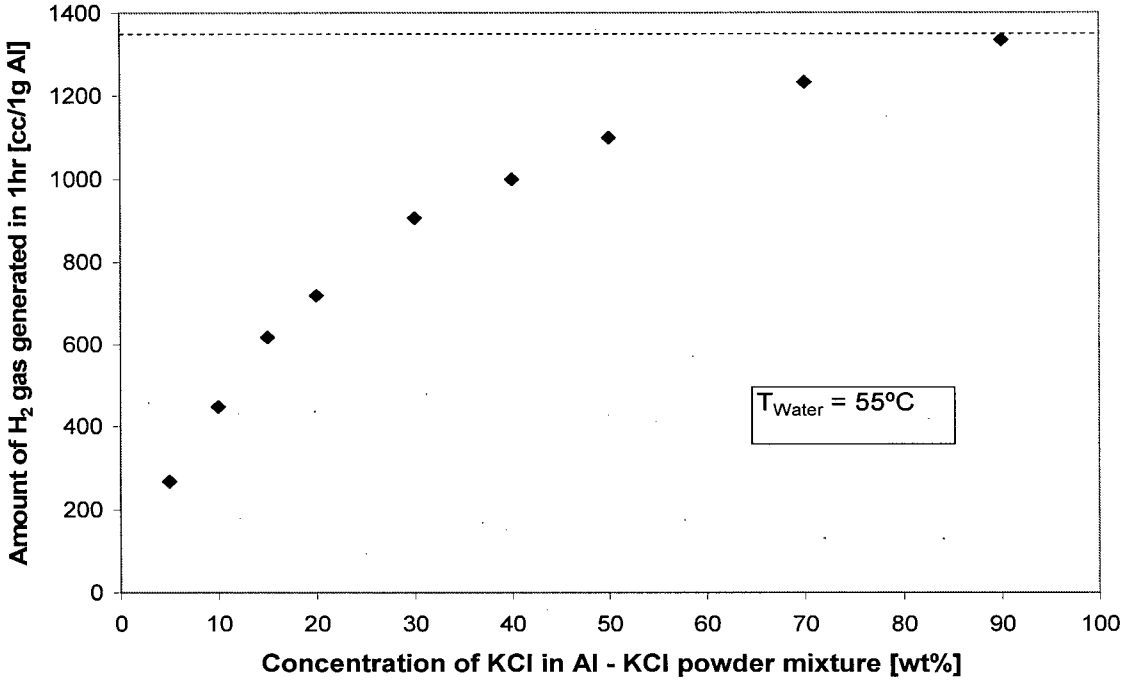

Figure 4.29 *Effect of the amount of KCl in Al-KCl powder mixture on the total amount of hydrogen produced in 1 hour. All data are normalized per gram of aluminum metal.*

4.3.3. Influence of Additives and Impurities on Hydrogen Generation

4.3.3.1. Influence of Other Additives on Hydrogen Generation

Additional additives, either other salts or inorganic materials added to a system, influence the corrosion kinetics of the Al-additive systems. Depending on their amount and chemistry they can either favor or hinder the aluminum corrosion reaction. Additives were added to the Al-additive system as the third component in relatively small quantities (up to 10 wt% of the additive).

Two additive types have been tested: elemental magnesium, Mg, and sodium nitrite, $NaNO_3$. Their effect on hydrogen generation reaction is shown in Figures 4.30 and 4.31. Figures 4.30-1 and 4.30-2 present the effect of Mg on the reaction kinetics and hydrogen yield of the Al-

KCl(50wt%, BM=15min) system in the first 15 min and 60 min, respectively. Magnesium metal, as seen in Fig. 4.30-1, shortens the induction period from 2 min for the Al-KCl system without additives to 45 sec when 1 wt% of the Al is replaced by Mg. Immediate reaction was observed when 5 wt% Mg or more were added. The addition of Mg also leads to an increase of the reaction rate in the first 5 min (up from 130 cc H_2/min for Al-KCl to average 170 cc H_2/min for Al-Mg-KCl). Hydrogen yield shows dependence from magnesium quantity, too. For the Al-Mg-KCl systems the H_2 amount is more than 10% higher after 15 minutes and less than 10% higher after 60 min of the reaction when comparing with bare Al-KCl system. The generated H_2 amount is expressed in cc H_2 per 1g of the metal alloy since Mg, like Al, reacts with water vigorously forming hydrogen. Even though the H_2 yield from the water-split reaction with Mg is lower, (theoretically, 1 g of Mg produces maximally 1006 cc H_2 gas at 25°C as oppose to 1359 cc H_2 obtained from 1 g Al, see stoichiometries below), the overall yield of the Al-Mg-KCl corrosion reaction is higher.

$$Al + 3H_2O \rightarrow 1.5H_2 + Al(OH)_3 \qquad (4.3)$$

$$Mg + 2H_2O \rightarrow H_2 + Mg(OH)_2 \qquad (4.4)$$

It can be concluded that the addition of Mg positively influences the reaction kinetics and accelerates the reaction of Al.

Sodium nitrate ($NaNO_3$), a water-soluble inorganic salt known for its oxidizing properties, is another additive that was applied. Figures 4.31-1 and 4.31-2 present the effect of $NaNO_3$ on the reaction kinetics and hydrogen yield of the Al-KCl(50wt%, BM=15 min) system in the first 15 min and 60 min, respectively.

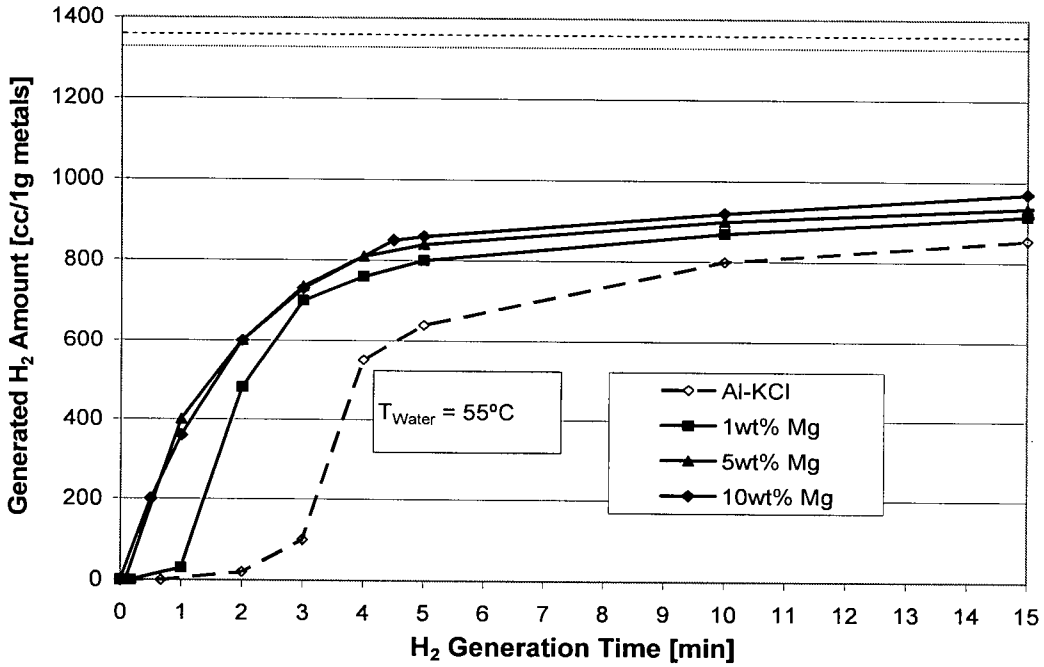

Figure 4.30 -1 *Effect of Mg on the induction time and reaction rate of the Al(Mg)-KCl-H_2O system in 15 min of water split reaction.*

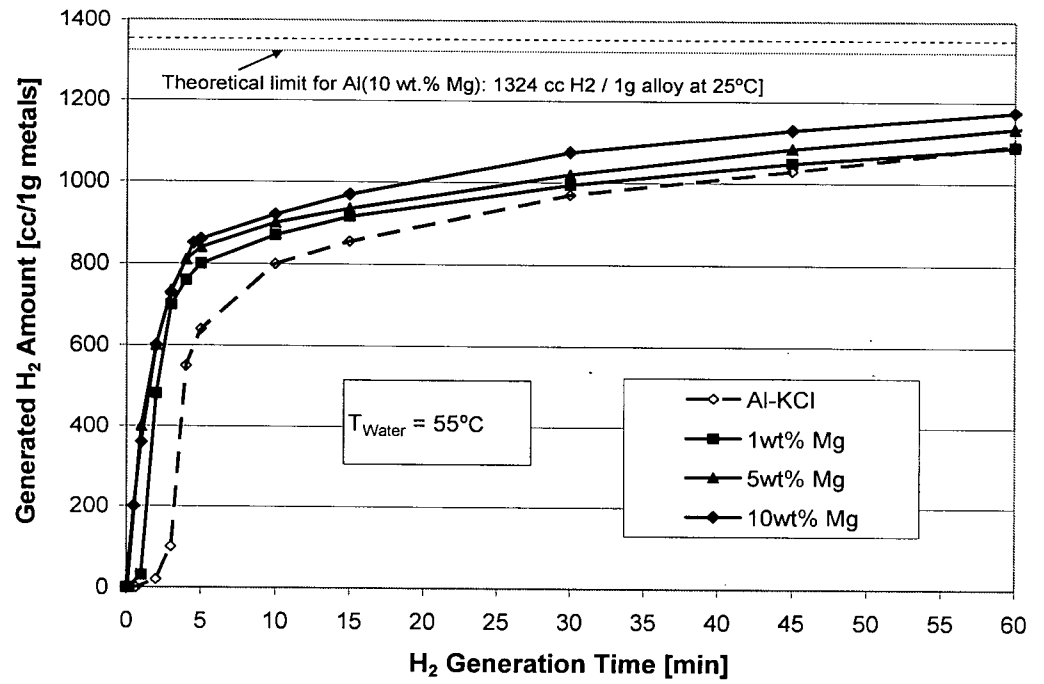

Figure 4.30-2: *Effect of Mg on hydrogen yield and reaction rate of the Al(Mg)-KCl-H_2O system in 60 min of water split reaction.*

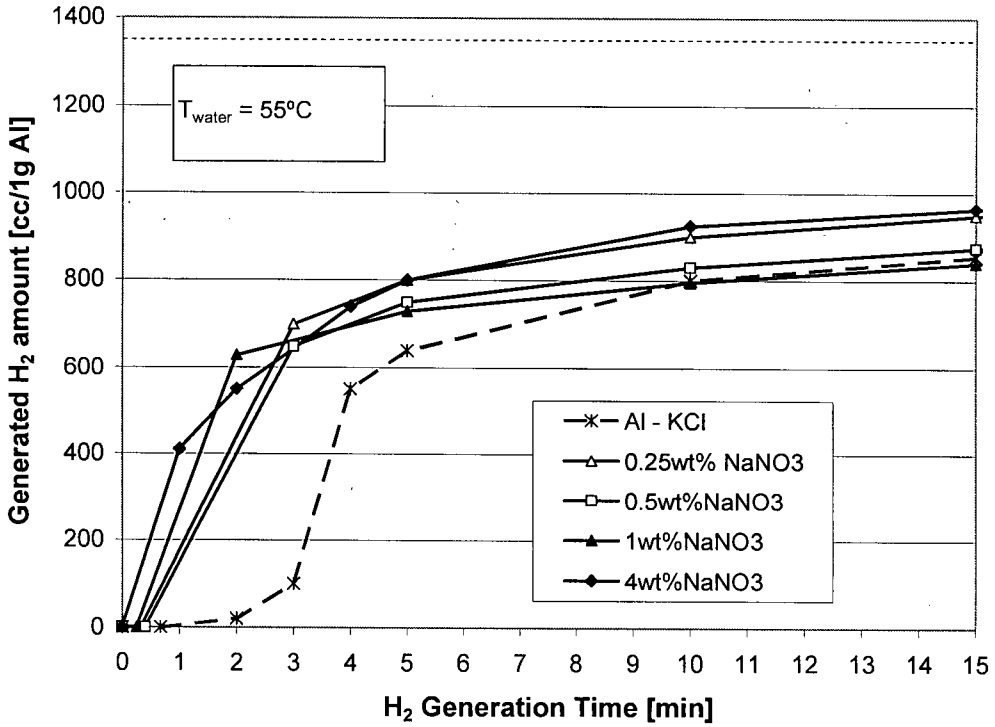

Figure 4.31-1 *Effect of $NaNO_3$ on the induction time and reaction rate of the Al-KCl($NaNO_3$) system in 15 min of the water split reaction.*

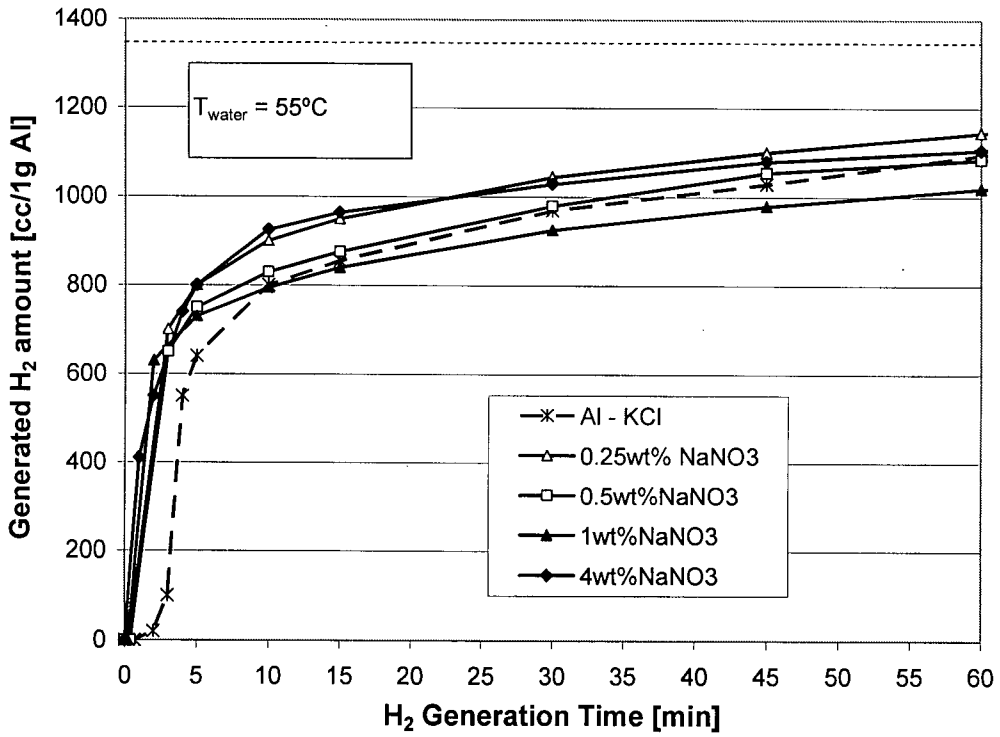

Figure 4.31-2: *Effect of $NaNO_3$ on hydrogen yield and reaction rate of the Al-KCl($NaNO_3$) system in 60 min of the water split reaction.*

Similar to Mg, $NaNO_3$ decreased the induction period of the Al-KCl system with the increase of $NaNO_3$ concentration in the powder mixtures from 2 min for the Al-KCl system without additives to 30 sec when 0.25wt% of $NaNO_3$ was added. Instant reaction was observed when 4wt% of $NaNO_3$ was blended into the Al-KCl powder. The reaction rate increased in the first 5 min from 130 cc H_2/min for Al-KCl to 160 cc H_2/min for Al-KCl(0.25wt%$NaNO_3$) and Al-KCl(4wt%$NaNO_3$). The reaction rates were slightly lower for Al-KCl(0.5wt%$NaNO_3$) and Al-KCl(1wt%NaNO3). The total H_2 yields after 15 min and 60 min of reaction also depended on the amount of $NaNO_3$ added. Best H_2 yields were obtained when 0.25wt% and 4wt% of $NaNO_3$ was added, 1145cc H_2 and 1105 cc H_2, respectively, after the first hour of reaction. This amounts to a corrosion of 85% of the Al enclosed in the system.

4.3.3.2. Influence of Water Quality on Hydrogen Generation

The majority of the Al corrosion experiments were performed with tap water at 55°C. To investigate the influence of water quality on corrosion of deformed Al, three additional types of water qualities were tested (distilled water, sea water and KCl-saturated aqueous solution) and the results compared to that of tap water.

Figure 4.32 shows the influence of water quality on hydrogen generation of the Al-KCl(50wt%, BM = 15 min) systems during the first 60 min of corrosion reaction. As seen in the plot, the hydrogen generation reaction progresses with similar kinetics, independent of the water used e.g. tap water, distilled water, or marine water. H_2 yields and hydrogen generation rates of the Al-KCl powder mixtures in tap water, distilled water and KCl-saturated aqueous solution are comparable. Consequently, the effect of impurities commonly found in tap water (e.g. salts of alkaline and alkaline earth elements), distilled water or even KCl-saturated aqueous solutions seems to have a minimal influence on the rapid corrosion phenomenon of Al. Surprisingly, the

strongly increased concentration of potassium and chlorine ions in the KCl-saturated aqueous solutions ($T_{saturation}$ = 55°C) does not accelerate or increase the corrosion as reported in many papers [25, 56, 59, 60]. However, reduced H_2 yields and reaction rates as well as extended induction times were measured for marine waters. It seems that some of the impurities present in sea water (other then chlorides) block the corrosion reaction so that a slowed down kinetics is observed. Sea water samples were taken from English Bay. Chemical water analysis was not performed; however slightly increased pH was measured (pH = 7.9).

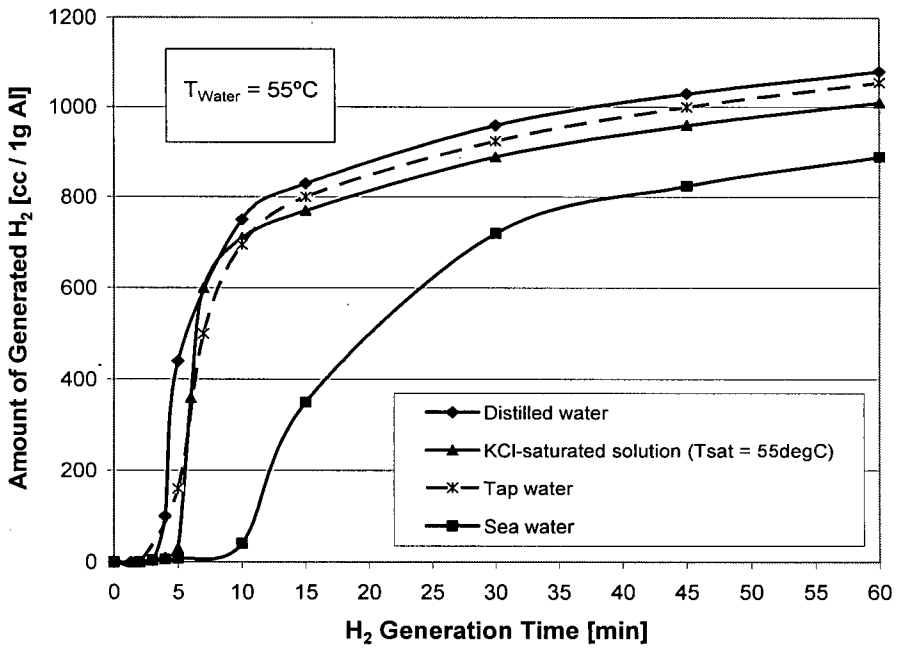

Figure 4.32 *Influence of water quality on hydrogen generation of the Al-KCl(50wt%) system during 60 min of water split reaction.*

4.3.4. Influence of Ball-Milling Time on Hydrogen Generation

One of the most significant process parameters during mechanical alloying is the milling time. For the Al-salt systems the milling time was varied from 7.5 min to 4 hrs. Figure 4.33 reflects the effect of ball-milling time on corrosion or the amount of hydrogen produced from 1g Al powder in the Al-KCl(50wt%) system after 15 min and 60 min of reaction.

The corrosion of Al in water increases steadily with ball-milling duration. The total H_2 yield increased from 900cc (when milled for 7.5min) to 1240cc H_2 (when milled for 1 hour) after 60 min of reaction time, increasing the efficiency from 67% to 92%, respectively. The induction period decreased from 2 min after 15 min of grinding to an immediate reaction start after 60 min of grinding. The reaction rate is the highest for powder mixtures that were mechanically alloyed for 60 min or longer. The H_2 yield from Al powder that was ball-milled for 1 hr was the highest and amounted to 1200 cc H_2/1g of Al. In this particular case more than 90% of the Al contained in the sample participated in the water split reaction forming aluminum hydroxide. The predominant part of the reaction (> 95%) occurred in the first 15 min. Al that was ball-milled for 4 hours had the highest recorded reaction rates in the first 5 min, but yielded less than 1000 cc hydrogen gas /1g of Al.

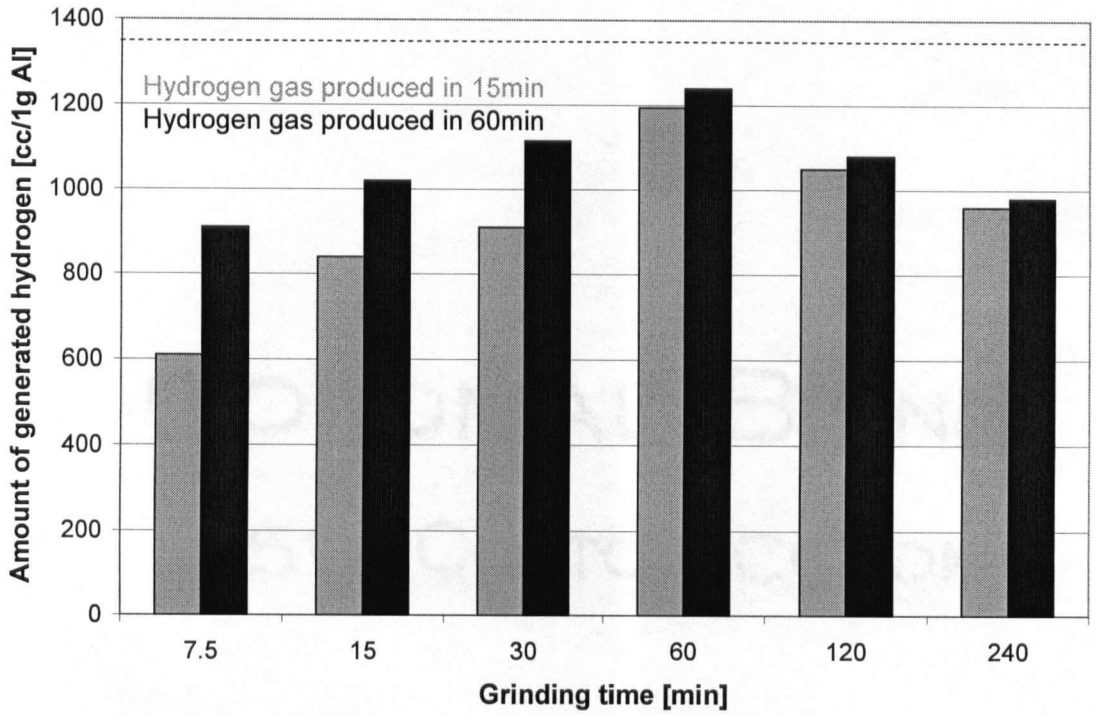

Figure 4.33 *Effect of grinding time on the amount of hydrogen produced from 1g Al powder after 15min and 60min of the Al-H_2O reaction. Al-KCl(50wt%) system. T_{water} = 55°C.*

Hydrogen generation from Al powders that were ball-milled for 15 min and 4 hours and re-ground after partial reaction is shown in Figure 4.34. Regrinding of partly corroded powders may re-activate the unreacted Al in the subsequent run, see Figure 4.34. Attempts to re-activate the spare Al by regrinding failed for the 4-hrs-milled and 60-min-reacted powders. Powders that were initially ball-milled for 15 min, produced additional 150 cc H_2 after regrinding them twice. Powders that were ball-milled for 4 hrs produced merely 25 cc more H_2. This result indicates that no unreacted Al metal was left in the powder – the corrosion was completed yielding a total of 1005cc H_2 /1g Al and a reduced efficiency of 74%. The reason for this H_2 deficiency most likely lies in Al oxidation during and just after ball-milling as milling and handling of powders takes place in atmospheric conditions. The longer the milling process the more Al will be sacrificed. Similar trend was also reported in Section 4.2.2.2 where increased oxygen concentration in extended time ball-milled Al powders was measured (EDS results). From the amount of generated H_2 it was estimated that in the case of Al that was ball-milled for 4 hrs around 25% of the Al was oxidized. This result matches well with results obtained by EDS (~ 27 wt%). Mechanical alloying in a protective/inert gas atmosphere and reduced/optimized milling times is therefore recommended.

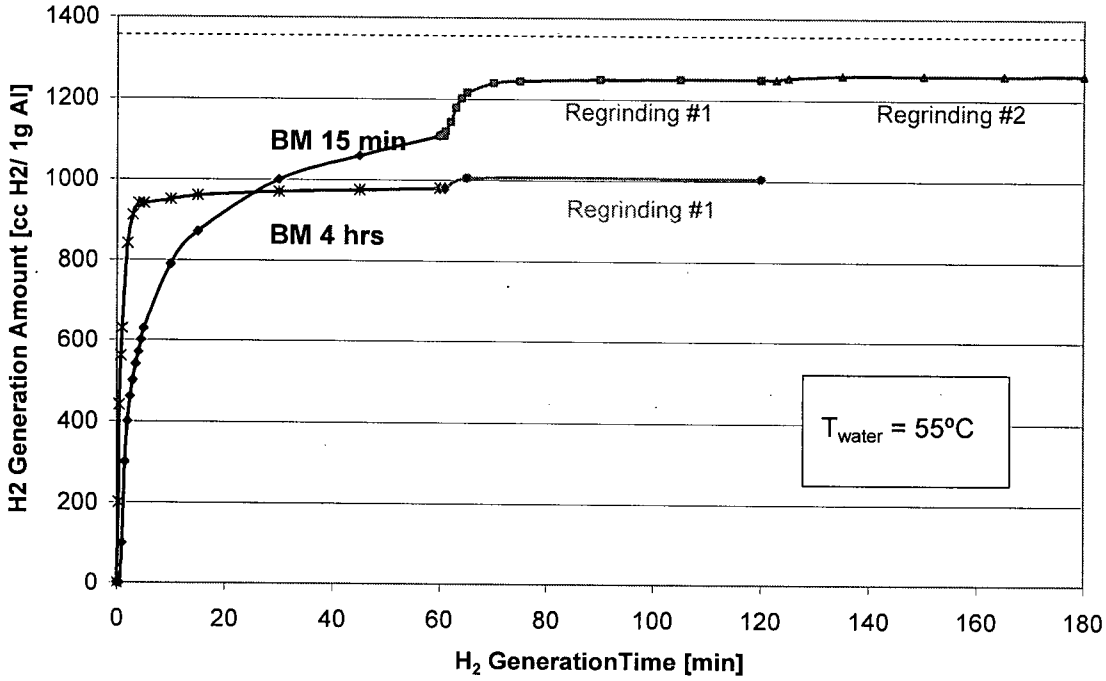

Figure 4.34 *Effect of regrinding of partly reacted powder mixtures that were initially ball-milled for 15 min and 4 hrs. Reaction time: 60 min for each run; Regrinding time: 15 min; Al-KCl(1wt%$NaNO_3$) system; T_{water} = 55°C.*

4.3.5. Influence of Aluminum Heat Treatment on Hydrogen Generation

Some of the important aspects of microstructure on aluminum corrosion are: the mechanical and thermal treatment history, grain size, as well as defects and their distribution.

The microstructure of the Al powders changes especially during the process of high energy ball-milling. The longer the milling time the more severe the damage is. Not only grain refinement and crystallite size reduction but also introduction of many defects and dislocations as well as induction of microstrains were indicated in Chapter 2. Heat treatment such as annealing is broadly applied to recover dislocations and reduce residual stresses present in metallic materials after cold-working.

Ball-milled Al-NaCl(50wt%) and Al-Al_2O_3(50wt%) powder mixtures were annealed at elevated temperatures for either 0.5 or 1 hour in Argon atmosphere (99.998 %) to prevent Al oxidation. Al-NaCl were annealed at 550°C, whereas Al-Al_2O_3 powders were heat-treated at temperatures as high as 700°C and 800°C which is above the melting point of Al (T_{Melt} = 660°C). Their reactivity in water was tested immediately after annealing. The amount of generated hydrogen from annealed Al-NaCl(50wt%) and Al-Al_2O_3(50wt%) powder mixtures was compared with the amount of hydrogen generated from equivalent not-annealed samples. The results are shown in Figures 4.35 and 4.36.

Annealed and not-annealed aluminum as well as aluminum that underwent melting and solidification transformation show similar kinetics and generate comparable amounts of hydrogen gas. Based on these experiments, it can be stated that in the process of melting-recrystallization all of the induced strains were eliminated from the Al structure. Consequently, lattice deformations, which are produced in Al during the process of high energy ball-milling, are not the reason for the massive corrosion reaction and they are also not a factor which influences the Al-assisted water split reaction.

The morphology of the single Al particles seems to be preserved during the heat treatments probably due to the oxide layer around them, compare Figures 4.37-1 and 4.37-2.

The longer induction period during the Al-H_2O reaction, when using annealed powders, indicates that some changes occurred in the oxide layer. Extended induction periods without loses in H_2 yield, were also observed for aged ball-milled powders. Loss of water and densification of the oxide may be valid for heat treated powders, while film thickening could be the explanation for aged powders (see XPS analysis in Section 4.2.2.1).

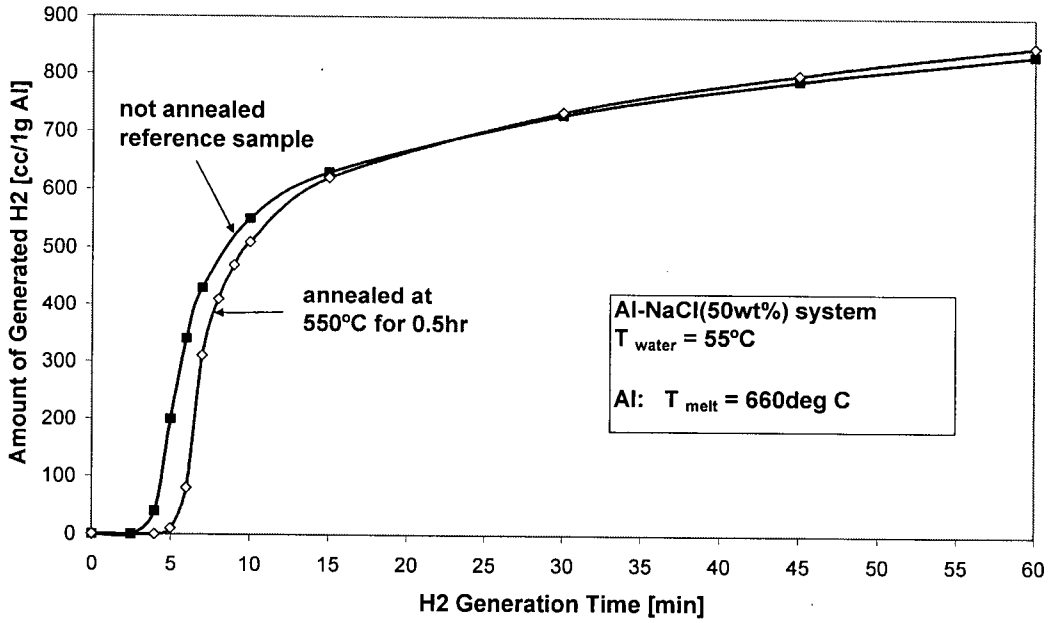

Figure 4.35 *Hydrogen generation from annealed and standard Al-NaCl(50wt%) powder mixtures. BM = 15min.*

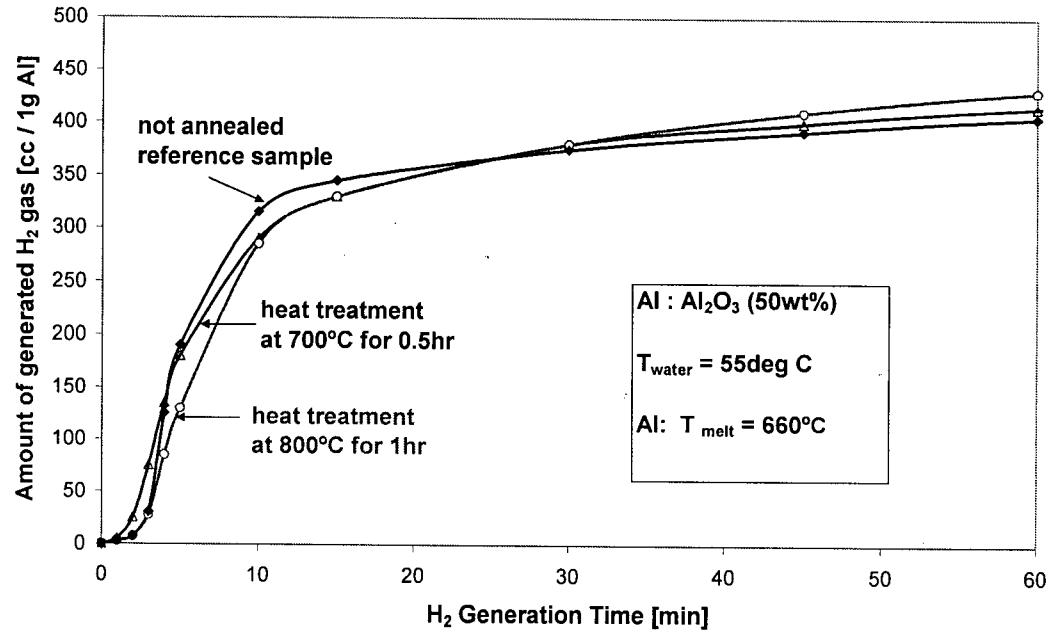

Figure 4.36 *Hydrogen generation from heat-treated (above T_{Melt} of Al) and standard Al-Al_2O_3(50wt%) powder mixtures. BM = 10min.*

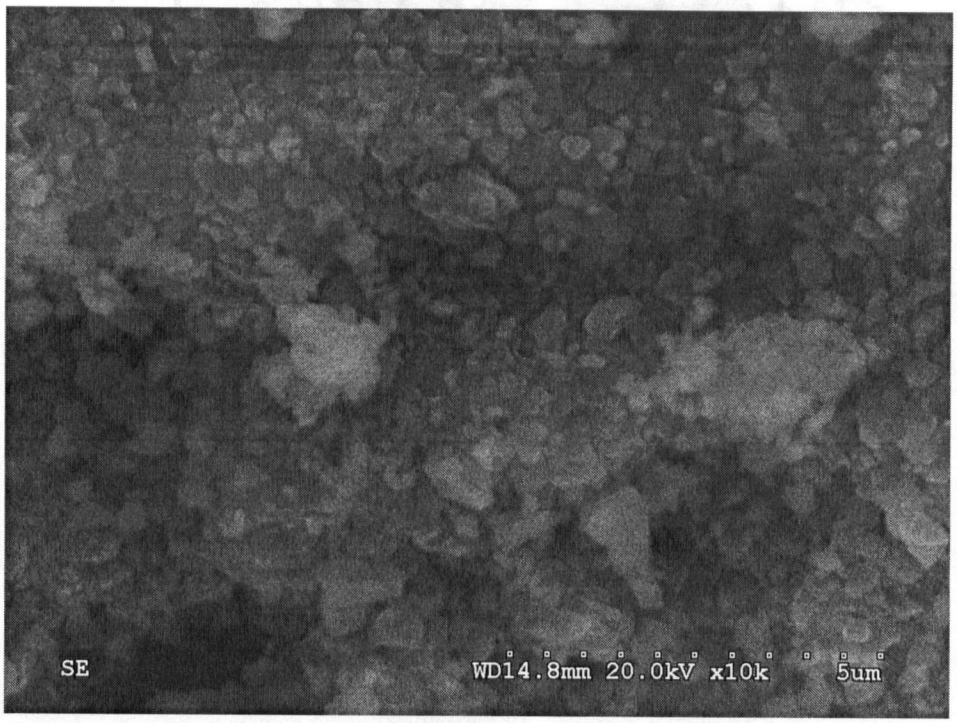

Figure 4.37-1 *Al-Al_2O_3 before heat treatment. BM = 10 min.*

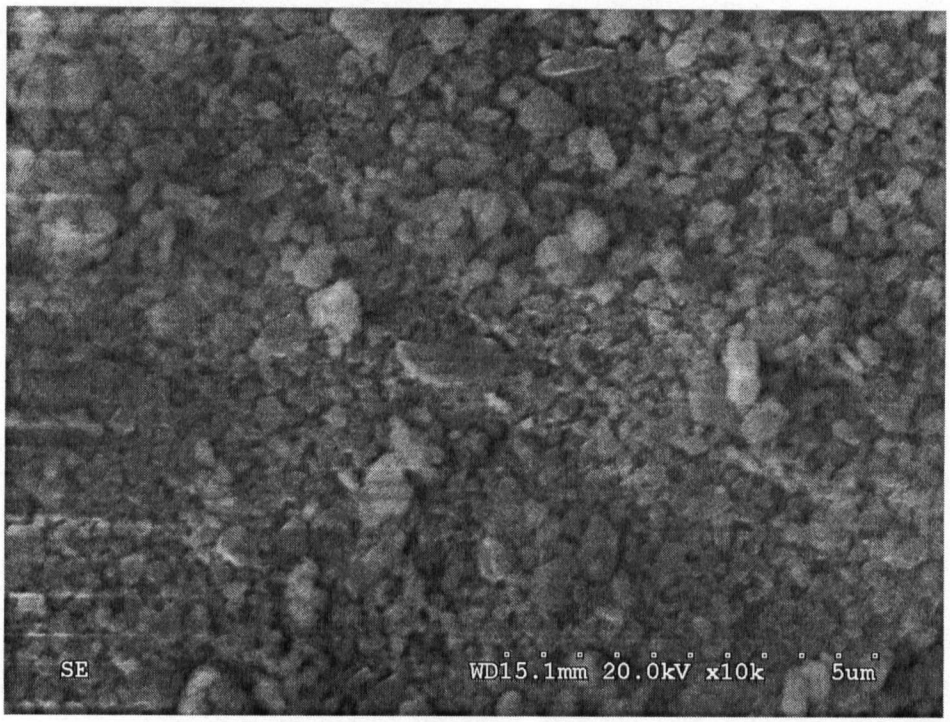

Figure 4.37-2: *Al-Al_2O_3 after heat treatment at 800°C. BM = 10 min.*

4.3.6. Influence of Temperature on Hydrogen Generation

4.3.6.1. Influence of Water Temperature

Water temperature has a considerable effect on Al corrosion and hydrogen generation. Hydrogen generation experiments in water at 22, 40, 55, 70 and 100°C were performed. The water temperature was set by thermostat. The effect of reaction heat on water temperature was negligible due to the large excess of water (~ 1000x more H_2O than Al, by mass). Table 4.9 reflects the effect of water temperature on the amount of hydrogen produced from 1g Al powder of the Al-KCl(1wt%$NaNO_3$) system, BM=15min, after 15 min and 60 min of corrosion reaction.

H_2 yield and generation rate tend to increase whereas the induction time tends to decrease with the increase of water temperature. The Al corrosion reaction progresses very slowly in cold water, with an increasing rate at moderate temperatures and very fast and completely in boiling water (T =100°C). Hydrogen was not collected in boiling water. The experiment was performed in an open system for 1 hour. It is assumed that the entire Al contained in the sample was corroded, because no Al was detected by XRD in reaction products.

Table 4.9 *Effect of water temperature on induction time and the amount of hydrogen produced from 1g Al powder of the Al-KCl(1wt%$NaNO_3$) system after 15min and 60min of Al-H_2O reaction. (BM = 15 min)*

Water Temp. [°C]	**H_2 yield after 15 min**		**H_2 yield after 60 min**		**Induction time [min]**
	[cc/1g Al]	**[%]**	**[cc/1g Al]**	**[%]**	
22	0	0	25	1.8	30
40	565	41.5	980	72.1	2.5
55	840	61.8	1050	77.3	0.25
70	1050	77.3	1210	89.0	0
100	?	?	1359*	100	0

* Value based on XRD analysis of reaction products (no elemental Al has been detected)

As seen, the Al – H_2O reaction is promoted and appreciable amounts of hydrogen are generated when water temperatures of 40°C or higher are provided. When water temperatures are low and water/powder ratio is high, the reaction heat will be dissipated and the reaction rates will be kept slow.

4.3.6.2. Influence of Reaction Heat

The Al-H_2O reaction is exothermic [3, 96, 97]. The standard enthalpies of reaction ΔH°_{rxn} were calculated in Section 3.4.1 and calorimetric measurement results are presented in Figure 4.39. Generally, only de-passivated aluminum reacts with water at neutral or near-neutral pH releasing heat to the surrounding environment. For ball-milled Al-KCl-H_2O and Al-Al_2O_3-H_2O systems the reaction heat effect on water temperature change during hydrogen generation process was investigated. Bulk water temperature changes were barely measurable when small amounts of powder (~ 1g) and excessive volume of water (~ 1000 cc) were used. By decreasing the ratio of water/powder from 1000 to 15, the approximate temperature variation during the water split reaction could be monitored even in an open system, e.g. a beaker. The results for the Al-KCl(50wt%)-H_2O and Al-Al_2O_3(50wt%)-H_2O system are presented in Figure 4.38. As starting temperature, the standard water temperature of $T_{water\ start}$ = 55°C was used. A standard hydrogen generation curve for Al-KCl and Al-Al_2O_3 was projected into Figure 4.38 from a similar experiment to correlate the reaction rate with temperature changes in the system.

When mixing Al-additive powder mixtures into water, the bulk temperature rises after 1 to 2 minutes up to 60°C for Al-Al_2O_3 and steeply up to 79°C for Al-KCl powders due to massive reaction of aluminum with water (exothermic reaction, $\Delta H^\circ_{rxn\ Bayerite}$ = - 418 kJ/mole)). During this period the hydrogen generation rate is highest. After the temperature has reached a maximum it then decreases exponentially and normalizes. The H_2 reaction rate continues to be high but will decrease steadily by time. Reaction heat is not measurable at moderate and slow

reaction rates because the heat generated at an interface dissipates to water, reaction solids and the environment. Even so, the localized temperature increase amplifies the corrosion rate and promotes the reaction and hydrogen generation.

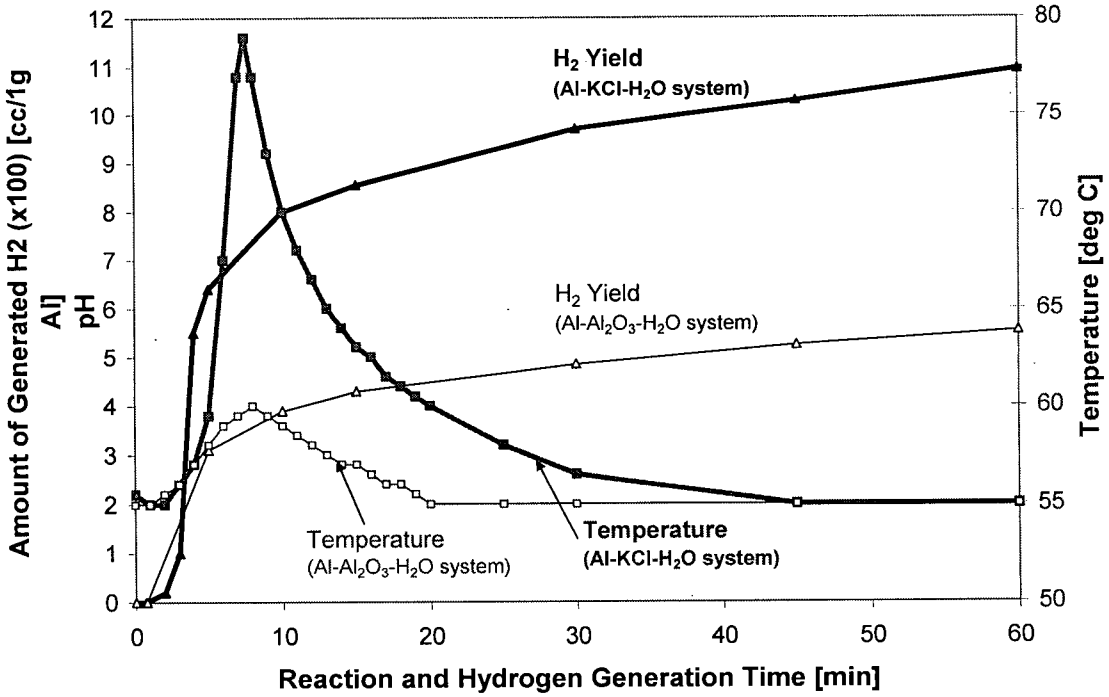

Figure 4.38 *Temperature change during the hydrogen generation reaction of the Al-KCl(50wt%) and Al-Al_2O_3 system. $T_{water\ start}$= 55°C; Volume $_{H2O}$= 30ml.*

The quantity of reaction heat (reaction enthalpy) released during the reaction of ball-milled Al-additives powders with water was determined from heat flow measurements using a differential scanning calorimeter (DSC), see Figure 4.39. The integration of the heat flow over time gives the reaction enthalpy ΔH_{rxn} for a particular system. Using the DSC graph the calculated ΔH_{rxn} for the Al-H_2O reaction are: -353.2 kJ/mole for the Al-KCl-H_2O system and -180.8 kJ/mole for the Al-Al_2O_3-H_2O system at T_{Water} = 50°C (see also Table 4.10). These values are lower then the theoretical ΔH_{rxn} for the Al-H_2O reaction because not the entire Al contained in the powder sample reacts to aluminum hydroxides. The amount of reacted Al was estimated by using DSC measurements data and ΔH_{rxn} data for a complete Al-H_2O reaction at 50°C (ΔH_{rxn}

$_{Bayerite}$ = - 421 kJ/mole at 50°C [97]). The results are presented in Table 4.10. In the Al-KCl(50wt%)-H_2O 84% and in the Al-Al_2O_3(50wt%)-H_2O system 43% of the Al contained in the powder corroded forming $Al(OH)_3$ (bayerite is the predominant aluminum hydroxide formed in Al-H_2O reactions in water temperatures up to 80°C). The results are reasonable as the H_2 yields obtained from hydrogen generation experiments are in similar range (500 cc to 600 cc H_2 for the Al-Al_2O_3(50wt%)-H_2O system and 1100 cc to 1200 cc H_2 for the Al-KCl(50wt%)-H_2O).

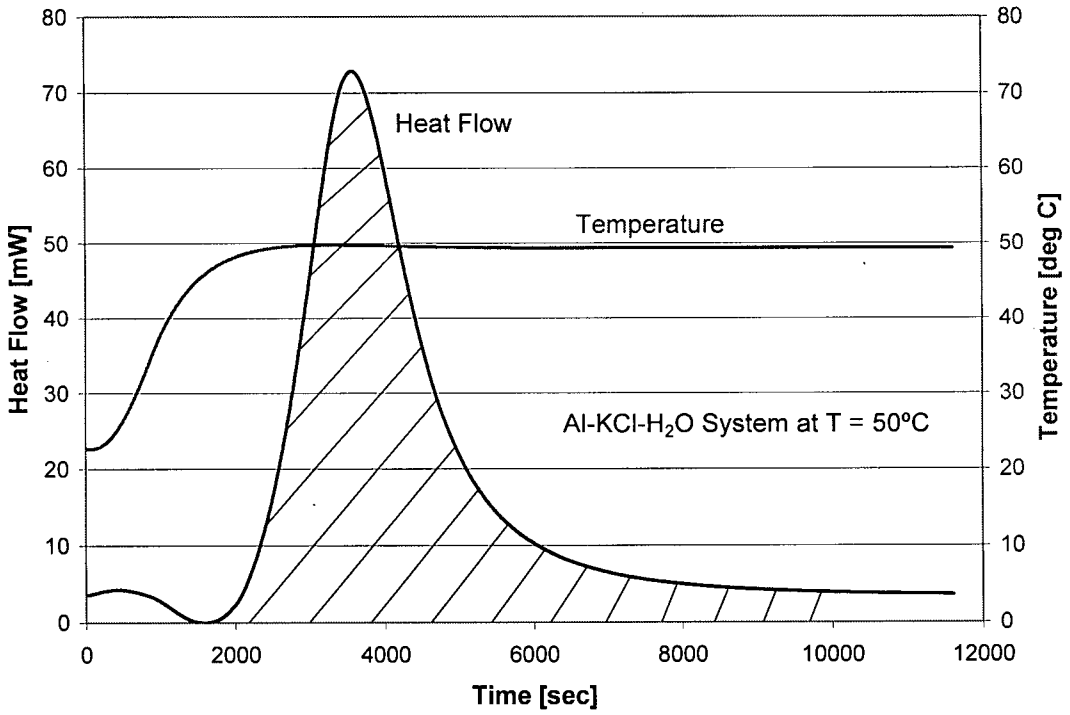

Figure 4.39 *Heat flow change as function of time during the hydrogen generation reaction of the Al-KCl(50wt%) system in 3 hours.*
m_{Al} = 0.01g; $T_{water\ start}$= 23°C; T_{water} = 50°C; Volume $_{H2O}$= 0.9 ml

Table 4.10 *Estimation of the Al amount reacted with water using DSC measurements data and ΔH_{rxn} data for complete Al-H_2O reactions at 50°C. Al-KCl(50wt%)-H_2O and Al-Al_2O_3(50wt%)-H_2O systems at 50°C.*

Sample	ΔH_{rxn} at 50°C [kJ/mole]		ΔH_{rxn} at 50°C [kJ/mole]
Al-KCl(50wt%)-H_2O	-353.2 (from DSC graph)		
		if 100% Al reacted	-421
		84% Al reacted (equivalent to 1139cc H_2/1g Al)	***-353.3***
Al-Al_2O_3(50wt%)-H_2O	-180.8 (from DSC graph)		
		if 100% Al reacted	-421
		43% Al reacted (equivalent to 583cc H_2/1g Al)	***-180.8***

4.3.7. Influence of Solution pH on Hydrogen Generation

Normally, a thin oxide film protects Al from corrosion in neutral or near-neutral pH environment [22, 23]. Corrosion rate increases in solutions of higher and lower pH. Some corrosion in as-received Al was observed in pH 10 aqueous solutions (Section 4.3.1.1, Figure 4.23). Accelerated corrosion of Al takes place in highly acidic or alkaline solutions in which aluminum oxides and hydroxides are soluble [24, 56].

For ball-milled Al-additive-H_2O systems a massive corrosion was observed when using water of neutral pH (pH = 6.5 - 7.1). The corrosion extent and progress were determined by the amount and rate of generated hydrogen. Like the reaction temperature, bulk pH changes were hardly measurable when small amounts of powder and excessive volume of water were used. However, after decreasing the ratio of water/powder from 1000 to 15 a pH variation was detected. The pH increase for the Al-KCl(50wt%)-H_2O system is presented in Figure 4.40. Figure 4.41 presents the pH change during the corrosion reaction of two additional Al-additive-H_2O systems, Al-Al_2O_3 A16 and Al-KCl(4wt%$NaNO_3$). For the Al-KCl(50wt%)-H_2O system,

see Fig. 4.40, the bulk water pH starts shifting towards higher pH right after immersion of the powder mixture into water. The pH rises steadily from pH 7 to pH 9 in the first 10 minutes of reaction. The pH stabilizes thereafter at pH 9.4 and remains constant. The other two presented systems show basically the same trend but the final pH is 8.95 for Al-Al_2O_3 and pH 10 for Al-KCl(4wt%$NaNO_3$).

The hydrogen generation reaction is typically characterized by an induction period (time during which no visible H_2 generation takes place) after the blended powders and the solution are brought together. An induction period of 2 to 3 min for Al-KCl and ~ 1 min for Al-Al_2O_3 was typically recorded at T_{Water} = 55°C. For some systems, such as the Al-KCl(4wt%$NaNO_3$), compare Fig. 4.31-1, immediate reaction was characteristic (no induction time). As the pH rises right after contact of powder with water for all the systems - regardless of H_2 evolution and the length of induction period - an immediate cathodic reaction must take place at the interface oxide/solution which leads to formation or discharge of OH^- species into the solution.

In order to further test the effect of pH on the hydrogen generation reaction, experiments in solutions of different pH (from pH 3.5 to pH 9) were conducted. The hydrogen generation from ball-milled Al-KCl(50wt%) powder mixtures in aqueous solutions of various pH as a function of reaction time is presented in Figure 4.42. The pH shift determined after the reaction of Al-KCl(50wt%) in aqueous solutions of different start pH is given in Table 4.11.

The massive reaction of ball-milled Al-KCl powders with water progresses at similar reaction rates but with a delay when using aqueous solutions of different pH. The delay rises with decreasing pH in acidic solutions: from 2 min in pH 6.8 (tap water), to 15 min in pH 5, 60 min at pH 4 and approx. 5 hrs in pH 3.5 solutions. The slightly increased volume of hydrogen released during the induction period in pH 4 and pH 3.5 solutions may be attributed to other type of corrosion, i.e. the localized pitting corrosion. A reaction delay (10 min) was also measured in pH 9 solutions.

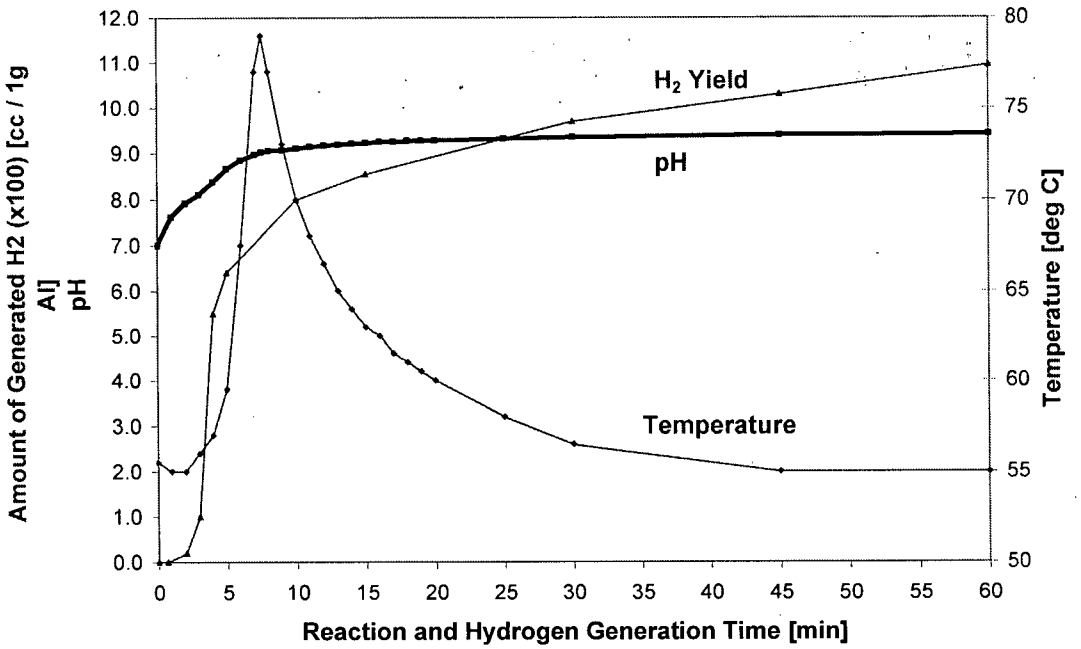

Figure 4.40 *pH and temperature change during hydrogen generation reaction of the Al-KCl(50wt%) system.*
$T_{water\ start}$= 55°C; $pH_{tap\ water}$= 7; Volume $_{H2O}$= 30ml; BM = 15 min.

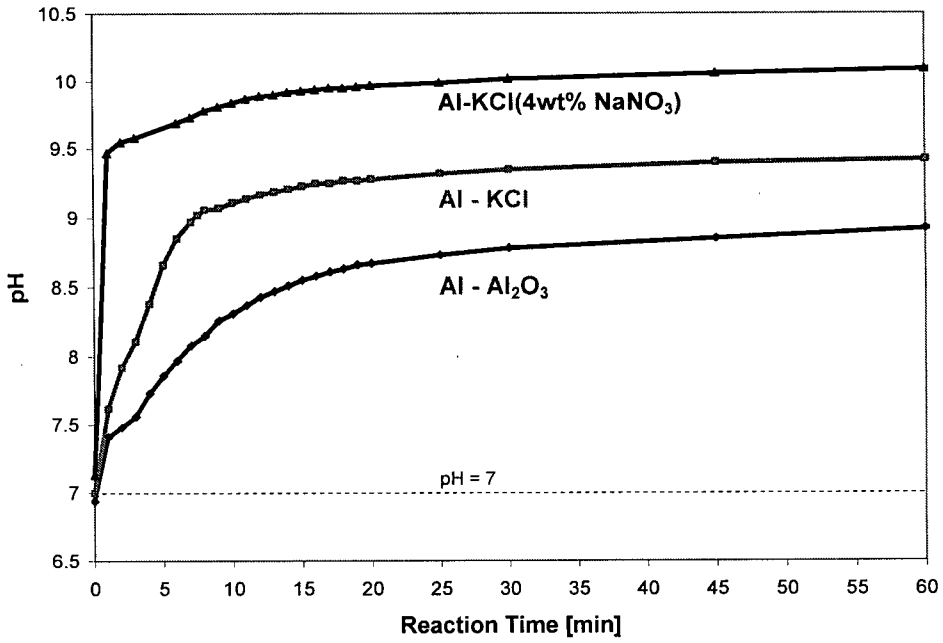

Figure 4.41 *pH shift during hydrogen generation reaction of different Al-additive-H_2O systems (Al-Al_2O_3(50wt%), Al-KCl(50wt%) and Al-KCl(4wt%$NaNO_3$).*
$T_{water\ start}$= 55°C; $pH_{tap\ water}$= 7; Volume $_{H2O}$= 30ml; BM = 15 min

As demonstrated in Table 4.11, a pH shift towards higher pH during the reaction was measured for all the systems. This indicates that some or all of the H_3O^+ species in acidic solutions have been neutralized while the concentration of the OH^- species in neutral or weak alkaline solutions have been enriched. From the pH difference the concentration of discharged OH^- species and the molarity of the bulk solution were estimated (see Table 4.11). It may be assumed, that the pH at the metal/solution interface, in pores or cavities, is locally much higher then the pH of the bulk solution. Increased local alkalinization may be one of the reasons for increased reactivity of BM Al in solutions of near-neutral pH. In an environment of pH > 11 the reaction product species as well as the protective aluminum oxide film itself are much more soluble so that Al re-passivation does not occur but a massive Al-H_2O reaction could progress.

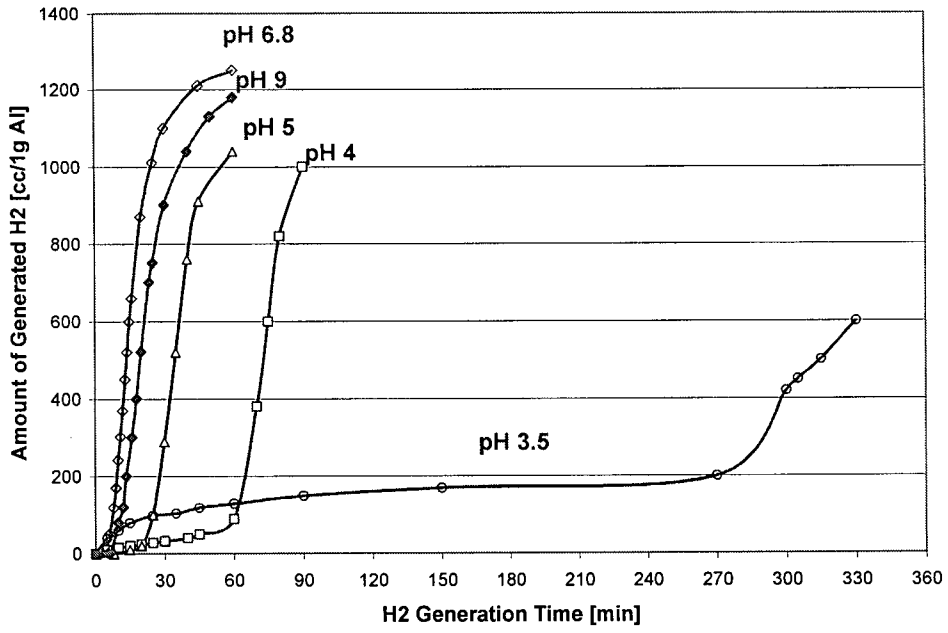

Figure 4.42 *Hydrogen generation from ball-milled Al-KCl(50wt%) powder mixtures in aqueous solutions of different pH.*
$T_{water\ start}$= 55°C; $Vol_{Solution}$= 150 ml; BM = 15 min

Table 4.11 *pH shift during Al-H_2O reaction in aqueous solutions of different start pH. T_{water} = 55°C; Volume $_{H2O}$= 150ml; Al-KCl(50wt%); 1g Al in powder mixture.*

pH at reaction start	pH at reaction end	generated $[OH^-]$ in 1 L [Molar]
9	9.8	8×10^{-6}
6.8	***9.91***	***1.2×10^{-5}***
5	9.26	4.2×10^{-6}
4	8.71	1.6×10^{-5}
3.5	6.4	4.7×10^{-5}

4.4. Characterization of Reaction Products

Besides pure but moist gaseous hydrogen and the solid or in-water dissolved additives, aluminum trihydroxides and oxyhydroxides were predicted in reaction (1) and (2), Chapter 2, and confirmed as reaction products. As far as process application is concerned, the formation of boehmite, AlOOH, is generally more favourable as it requires less water but produces the same amount of H_2 gas, i.e.:

$$2Al + 6H_2O \rightarrow 3H_2 + 2Al(OH)_3 \qquad (4.5)$$

$$2Al + 4H_2O \rightarrow 3H_2 + 2AlOOH \qquad (4.6)$$

Figure 4.43 shows XRD diffractograms obtained from dried reaction products that were formed during the reaction of Al with H_2O in water, at temperatures up to 100°C, in the presence of KCl(50wt%) as additive. Figure 4.44 presents SEM micrographs of the same powders. Depending on reaction temperature three distinctive XRD patterns were identified. The first pattern contains - in addition to KCl and some unreacted Al – only the phase bayerite, $Al(OH)_3$,

which is formed predominantly during the reaction at water temperature up to 55°C. The second pattern contains only boehmite, AlOOH, which is predominantly formed at T_{Water} = 100°C. The third pattern consists of both phases, bayerite and boehmite, which are formed in the temperature region roughly between 60°C < T_{Water} < 95°C. The bayerite peaks are sharp, indicating larger crystallites, whereas the boehmite peaks are broad and of low intensity indicating the nanocrystallinity of the material. SEM analysis confirms this, see Fig. 4.44. Bayerite (Fig. 4.44-1) forms agglomerates of partly well developed, 2 to 7 μm large crystals which vary widely in their form and appearance. In contrast, the agglomerates of boehmite (Fig. 4.44-2) consist of fine and loosely agglomerated hydroxide particles. Both reaction products are characterized by a very large surface. The specific surface area of bayerite (72 m^2/g) is slightly lower than that of boehmite (76 m^2/g). This suggests that a large fraction of nanopores, which are not visible under SEM, is present in the reaction products.

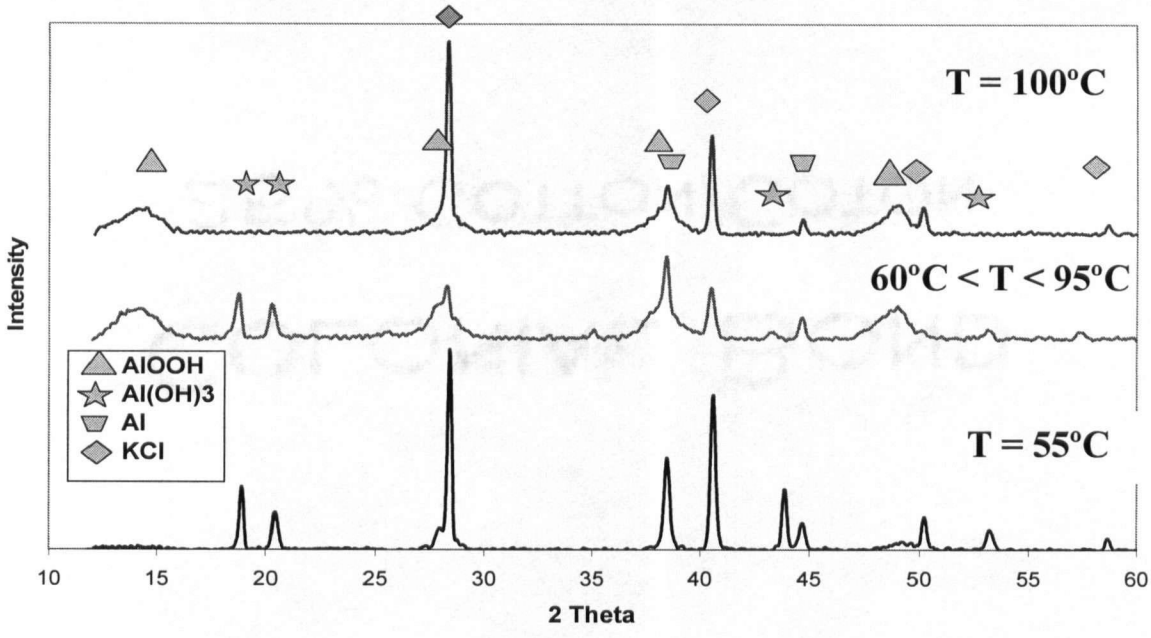

Figure 4.43 *XRD patterns of reaction products formed during the Al-KCl(50wt%)-H_2O reaction at T_{Water} = 55°C, 60°C < T_{Water} < 95°C and T_{Water} = 100°C.*

Figure 4.44-1 *SEM micrograph of reaction products formed during the Al-KCl(50wt%)-H_2O reaction at T_{Water} = 55°C. (Bayerite).*

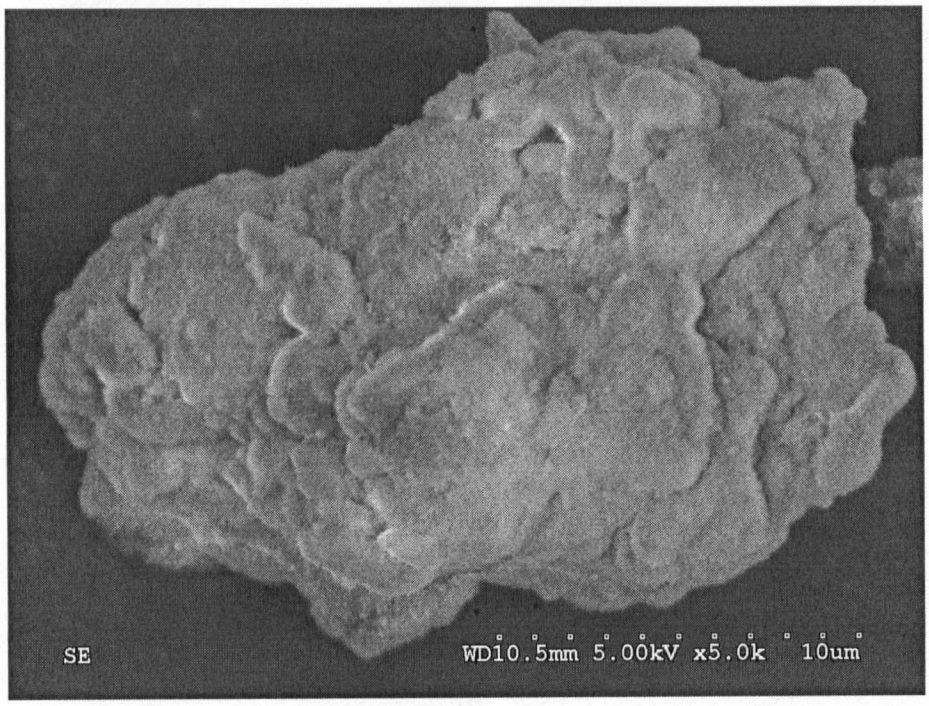

Figure 4.44-2 *SEM micrograph of reaction products formed during the Al-KCl(50wt%)-H_2O reaction at T_{Water} = 100°C. (Boehmite).*

The precipitation of bayerite or boehmite is not influenced by additives, such as sodium nitrate. Figure 4.45 shows XRD diffractograms of reacted Al-KCl-additive powders (additive amount: up to 10wt% relative to KCl) in water at 60°C < T_{Water} < 95°C. Both phases, bayerite and boehmite are found in the reaction products. However, $NaNO_3$ increases the reactivity of Al, as indicated previously (Section 4.3). This has also been found previously (section 4.3). When comparing the (200) peak of Al at 44.74° it can be seen that the intensity of this peak decreases with the increase of $NaNO_3$ in the powder mixture. Its absence indicates that the Al-H_2O corrosion reaction was completed. Comparable results were also obtained when Al-KCl-additives powders were reacted in water at 55°C and 100°C.

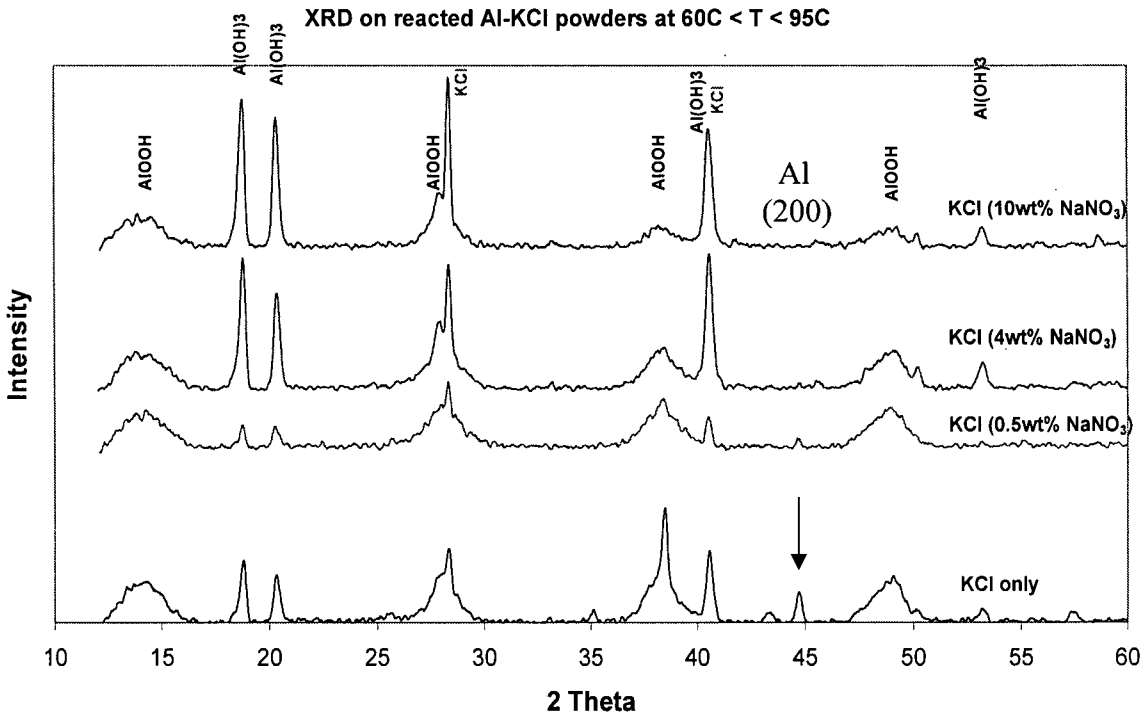

Figure 4.45 *XRD diffractograms of reacted Al-KCl-Additives powders in water at 60°C < T_{Water} < 95°C ([NaNO3] relative to KCl amount).*

5. Conclusions and Recommendations

This work demonstrates that aluminum powders ball-milled with a second phase generate exceptionally high amounts of hydrogen gas from solutions of neutral or near neutral pH, through aluminum-assisted water split reaction. The highest hydrogen yields were obtained when using water-soluble inorganic salts (WIS), such as KCl or NaCl. Using Al-WIS systems and KCl as an additive more than 80% of the aluminum present in the powder reacted to $Al(OH)_3$ and/or AlOOH after 1 hour of corrosion reaction, releasing 1095 cc H_2 gas /1g of Al. These results surpass by more than 100% the Al-additive systems found in the literature [1,2]. Crucial for the fast Al-H_2O reaction without Al re-passivation are the powder preparation, the appropriate reaction parameters as well as the reaction processes itself.

The following conclusions result from this work:

1. Powder preparation: Ball-milling of aluminum in the presence of a second phase is one of the most important process parameters. It has been shown that during the process of ball-milling the morphology of the particles and structure of aluminum changes significantly when additives are added. The degree of Al alteration is influenced strongly by milling conditions and milling time. Therefore, these parameters need to be optimized as they also affect the reaction kinetics of the Al-H_2O system and the H_2 yield. By choosing a milling atmosphere other than air, Al oxidation can be avoided.

2. The additives: Second phase particles promote crystallite refinement, inhibit cold welding of the ductile Al metal, introduce microstructural defects and strains to the Al lattice and the oxide film, and increase notably the roughness and the surface area of Al. On the other hand, additives are not required for the rapid hydrogen generation reaction from the Al-H_2O system. "Additive-free" aluminum powders retain the reaction rate and produce substantially unchanged H_2 yields. By removing the second phase (e.g. by using water-soluble system components such

as salts) aluminum exposes its entire surface area with micro- or nano-porous structure, which was attained during milling, to the reaction. Surface enlargement is considered as one of the factors which favours the water split reaction. The specific surface area of Al powder particles increased from 0.30 m^2/g before milling to 9.68 m^2/g after 15 min of milling.

3. Structure of Al: Structural defects and microstrains induced in Al are not a reason for the increased reactivity of aluminum in water. When comparing annealed and not-annealed aluminum as well as aluminum that underwent melting and solidification or re-crystallization, similar kinetics was observed and comparable amounts of hydrogen gas were generated. Defects in the oxide layer however, are largely unaffected by the relatively low temperatures (< 800°). The poor quality oxide film, which results from ball-milling with a second phase, has an enhancing effect on the Al-H_2O reaction as it is porous and therefore permeable to water. The film quality and oxide thickness are reflected mainly in the duration of the induction time.

4. Reaction parameters: Temperature, pH, the additive and its concentration, as well as impurities alter the Al-assisted water split reaction and either inhibit or accelerate the reaction kinetics and amount of generated hydrogen gas. Higher temperatures generally favour the reaction kinetics: the higher the water temperature, the higher the hydrogen generation rate and shorter the induction time. The solution pH influences primarily the induction time. Slightly alkaline (up to pH 9) or slightly acidic aqueous solutions (up to pH 3.5) delay the H_2 generation reaction (up to several hours for pH 3.5). It has been demonstrated that ball-milled Al powders have the fastest reaction response in water of neutral or near-neutral pH. A pH shift (self-induced alkalinization) observed in every system during the reaction, promotes most likely the corrosion of Al powders. The reactivity of Al powders is chiefly increased when Al is mechanically alloyed with a second phase. The higher the concentration and smaller the additive particle size the more Al reacted. Highest reactivity and H_2 yields were obtained when water soluble inorganic salts (KCl and NaCl) were used.

5. Reaction processes: Local temperature increase due to the exothermic character of the Al-H_2O reaction ($\Delta H^{\circ}_{rxn\ Bayerite}$ = - 418 kJ/mole) and local alkalinization due to the dominance of the cathodic reaction are the most influential reaction processes. The temperature at the reaction site is likely to be higher than the measured bulk temperature of the aqueous solution. Likewise, the local pH and ionic content at the oxide/solution interface could also be grossly different than the overall bulk values. Ball-milled Al-additive-H_2O systems produce a self-induced pH shift towards higher pH in the aqueous solutions (alkalinization). The corrosion reaction consequently progresses in an alkaline environment. The lack of re-passivation of the active metal surface is attributed to local alkalinization.

Future Work

As the mechanism of the massive corrosion reaction of ball-milled Al in neutral or near neutral aqueous solutions remains unclear, further studies of materials and reaction characterization are required. Much of attention should be given to the passive oxide layer, as it appears that the oxide and not the metal microstructure decides about the progress and intensity of the reaction. The characterization of the oxide film is difficult due to its low thickness (few nm) on small (few μm) particle agglomerates. However, finding evidences for the existence of "easy paths" or flaws on top of ridges in the ball-milled Al surface would explain the migration of water or ionic species through the film to the metal/oxide interface.

Further on, the origin for the self induced alkalinization is important as it reflects the processes occurring at the oxide/solution interface. If the pH is high locally, e.g. pH > 10, the oxide will dissolve and re-passivation will not occur. The knowledge of the local pH level would help to understand the effect of localized alkalinization on hydrogen generation kinetics and Al re-passivation.

Electrochemical characterization, which is in progress [JS], is essential to determine the corrosion potentials and describe the mechanism of the anodic and cathodic reaction processes.

New Al-additive systems which would allow controlling the reaction kinetics, especially at the beginning of the reaction when high reaction rates and high heat evolution are common, are desirable. Ideally a linear reaction progress versus time, until the Al-H_2O reaction is completed, is desired.

The exploration of novel and energy efficient ways of H_2 generation through Al-assisted water split is desired. The employment of scrap Al, minimization of Al processing and utilization of reaction heat will lessen the energy consumption and make the technology more competitive.

[JS] Skrovan J., PhD thesis in progress, UBC-MTRL 2006

6. References

1. Chaklader A., United States Patent No.: US 6,440,385 B1 (2002).
2. Chaklader A., United States Patent No.: US 6,582,676 (2003).
3. Holleman A., Wiberg E., *Inorganic Chemistry*, Walter de Gruyter Verlag (1985).
4. Sastri M.V.C., Viswanathan B., Srinivasa Murthy S., *Metal hydrides: Fundamentals and Applications*, Springer Verlag (1998).
5. Hatch John E., *Aluminum: Properties and Physical Metallurgy*, American Society for Metals, Ohio (1984).
6. Vargel C., *Corrosion of Aluminuium*, Elsevier (2004).
7. Czech E., Troczynski T., United States Patent Application No.: 11/103,994 (2005).
8. Ogden, J. M., *Hydrogen: The Fuel of the Future?*, Physics Today **55** (4) (2002).
9. Crabtree G. W., Dresselhaus M. S., Buchanan M. V., *The Hydrogen Economy*, Physics Today **57** (12) (2004).
10. Ogden J. M., *Prospects for Building a Hydrogen Energy Infrastructure*, Annu. Rev. Energy Environ. **24** (1999) p.227–279.
11. Kordesch K., Simader G., *Fuel Cells and Their Application*, VCH Verlag, Weinheim (1996).
12. www.eere.energy.gov
13. www.millenniumcell.com
14. Petillo P.J., Binder M., *A Safe, Portable, Hydrogen Gas Generator using Aqueous Borohydride Solution and Ru Catalys*", International Journal of Hydrogen Energy **25** (2000) p.969-975.
15. Kojima Y., Suzuki K., Fukumoto K., Sasaki M., Yamamoto T., Kawai Y., and Hayashi H., *Hydrogen Generation using Sodium Borohydride Solution and Metal Additive Coated on Metal Oxide*, International Journal of Hydrogen Energy, **27** (2002) p.1029-1034.

16. Kong V.C.Y., Kirk D. W, Foulkes F.R. and Hinatsu J. T., *Development of hydrogen storage for fuel cell generators II: utilization of calcium hydride and lithium hydride*, International Journal of Hydrogen Energy **28** (2003) p.205-214.

17. www.powerball.net

18. www.safehydrogen.com

19. Andersen et al., United States Patent No.: US 6,638,493 B2 (2003).

20. Watanabe M., United States Patent Application No.: US 20040208820 A1 (2004).

21. www.lme.co.uk (London Metal Exchange)

22. Hunter M.S. and Fowle P., *Natural and Thermally Formed Oxide Films on Aluminum*, J. Electrochem. Soc.**103** (9) (1956) p.482-483.

23. Hart R.K., *The Formation of Films on Aluminum Immersed in Water*, Transaction **53** (1956) p.1020-1027.

24. Shreir, L.L., Jarman, R.A., Burstein, G.T., *Corrosion*, 3rd Edition, Vol. 1-2, Elsevier (1994).

25. Badawy W., Al-Kharafi F., El-Azab A., *Electrochemical Behaviour and Corrosion Inhibition of Al, Al-6061 and Al-Cu in Neutral Aqueous Solutions*, Corrosion Science **41** (1999) p.709-727.

26. Davis J.R., *Corrosion of Aluminum and Aluminum Alloys*, ASM international, Ohio (1999).

27. Dignam M.J., *Oxide Films on Aluminum: Kinetics of Formation in Oxygen*, J. Electrochem. Soc. **109** (3) (1962) p.192-198.

28. Talbot D.J., *Corrosion Science and Technology*, Boca Raton, CRC Press (1998).

29. Oh H-J., Jang K-W. and Chi C-S., *Impedance Characteristics of Oxide Layers on Aluminum*, Bull. Korean Chem. Soc. **20** (11) (1999) p.1340-1344.

30. Øvari F., Tomcsanyi L., Turmezey T., *Electrochemical Study of the Pitting Corrosion of Aluminum and its Alloys – I. Determination of Critical Pitting and Protection Potentials*, Electrochimica Acta **33** (3) (1988) p.323-326.

31. Van Horn K.R., *Aluminum: Properties, Physical Metallurgy and Phase Diagrams,* American Society for Metals, Metals Park Ohio (1967).

32. Tomcsanyi L., Varga K., Bartik I., Horanyi G., Maleczki E., *Electochemical Study of the Pitting Corrosion of Aluminium and its Alloys – II. Study of the Interaction of Choloride Ions with a Passive Film on Aluminium and initiation of Pitting Corrosion*, Electrochimica Acta **34** (6) (1989) p.855-859.

33. Bunker B.C., Nelson G.C., et al, *Hydration of Passive Oxide on Aluminum*, Interfacial Chemistry and Engineering 2000 Annual Report (2000).

34. Dekker M., *The Aluminum-Water System*, R.S. Alwitt, Vol. 4, Chapter 3 (1976).

35. Szklarska-Smialowska Z., *Insight into the Pitting Corrosion Behaviour of Aluminum Alloys*, Corrosion Science **33** (8) (1992) p.1193-1202.

36. Shimizu K., Kobayashi K., Thompson G., Wood G., *The Apparent Induction Period for γ-Al_2O_3 Development in Thermal Oxide Films on Aluminum,* Oxidation of Metals **36** (1/2) (1991).

37. Lowson R., *Aluminium Corrosion Studies. IV Pitting Corrosion*, Aust. J. Chem. **31** (1978) p.943-56.

38. Shimizu K., Brown G., Kobayashi K., Skeldon P., Thompson G., Wood G., *A Novel Approach for the Study of the Migration of Cl^- Ions in Acidic Alumina*, Corrosion Science **41** (1999) p.1835-1847.

39. Dignam M.J., *Oxide Films on Aluminum: Ionic Conduction and Structure*, J. Electrochem. Soc. **109** (3) (1962) p.184-191.

40. Chao C.Y., Lin L.F., Macdonald D.D, *A Point Defect Model for Anodic Passive Films I: Film Growth Kinetics*, J. Electrochem. Soc. **128** (6) (1981) p.1187-1194.

41. Chao C.Y., Lin L.F., Macdonald D.D, *A Point Defect Model for Anodic Passive Films, II: Chemical Breakdown and Pit Initiation*, J. Electrochem. Soc. **128** (6) (1981) p.1194-1198.

42. Takahashi H., Fujimoto K., Konno H., Nagayama M., *Distribution of Anions and Protons in Oxide Films Formed Anodically on Aluminum in a Phosphate Solution*, J. Electrochem. Soc. **131** (8) (1984) p.1856-1861.

43. Brune H., Winterlin J., Trost J., Ertl G., Wiecherl J., Behm R.J., *Interaction of Oxygen with Al(111) Studied by Scanning Tunneling Microscopy*, J. Chem. Phys. **99** (3) (1993).

44. Jennison D.R., Verdozzi C., Schultz P.A., Sears M.P., *Ab initio Structural Predictions for Ultrathin Aluminum Oxide Films on Metallic Substrates*, Physical Review B **59** (24) (1999).

45. Shimizu K., Furneaux R.C., Thompson G., Wood G., Gotoh A., Kobayashi K., *On the Nature of "Easy Paths" for the Diffusion of Oxygen in Thermal Oxide Films on Aluminum*, Oxidation of Metals **35** (5/6) (1991).

46. Wu H., Zhang X., Hebert K.R., *Atomic Force Microscopy Study of the Initial Stages of Anodic Oxidation of Aluminum in Phosphoric Acid Solution*, J. Electrochem. Soc. **147** (6) (2000) p.2126-2132.

47. Brown M.G., Shimizu K., Kobayashi K., Thompson G.E., Woog G.C., *The Morphology, Structure and Mechanism of Growth of Chemical Conversion Coatings on Aluminum*, Corrosion Science **33** (9) (1992) p.1371-1386.

48. Brown M.G., Shimizu K., Kobayashi K., Thompson G.E., Woog G.C., *Further Evidence for the Presence of Residual Flaws in a Thin Oxide Layer Covering High Purity Aluminum*, Corrosion Science **34** (12) (1993) p.2099-2104.

49. Huang R., Hebert K.R., Gessmann, Lynn K.G., *Effect of Impurities on Interfacial Void Formation in Aluminum*, J. Electrochem. Soc. **151** (4) (2004) B227-B232.

50. Hebert K.R., Wu H., Gessmann T., Lynn K., *Positron Annihilation Spectroscopy Study of Interfacial Defects Formed by Dissolution of Aluminum in Aqeous Sodium Hydroxide,* J. Electrochem. Soc. **148** (2) (2001) B92-B100.

51. Caicedo-Martinex C.E., Koroleva E., Skeldon P., et al., *Behaviour of Impurity and Minor Alloying Elements during Surface Treatments of Aluminum*, J. Electrochem. Soc. **149** (4) (2002) B139-B145.

52. McCafferty E., *Sequence of Steps in the Pitting of Aluminum by Chloride Ions*, Corrosion Science **45** (2003) p.1421-1438.

53. Deltombe E., Pourbaix, M., *Electrochemical Behaviour of Aluminium - Potential pH Diagram of the System Al-H_2O at 25°C,* Corrosion **14**, (1958) 496t.

54. Lawson R.T., *Aluminum Corrosion Studies. I Potential-pH-Temperature Diagrams for Aluminum*, Aust. J. Chem. 27 (1974) p.105-127.

55. Downs A.J., *Chemistry of Aluminum, Gallium, Indium and Thallium*, Blackie Academic & Professional, Glasgow (1993).

56. Lee Hochum, Isaacs H.S., *Effect of Anion, pH and Temperature on the Dissolution of Aluminum Oxide Films*, Brookhaven National Laboratory, DE-AC02-98CH10886, (2001).

57. Aballe A., Bethencourt M., Botana F.J., Cano M.J., Marcos M., *Localized Alkaline Corrosion of Alloy AA5083 in Neutral 3.5 % NaCl Solution*, Corrosion Science 43 (2001) p.1657-1674.

58. Nisanciouglu K., *Electrochemical Behaviour of Aluminum-Base Intermetallics Containing Iron*, J. Electrochem. Soc. **137** (1) (1990) p.69-77.

59. Hurlen T. and Haug A.T., *Corrosion and Passive Behaviour of Aluminum in Weakly Alkaline Solution*, Electrochimica Acta **29** (8) (1984) p.1133-1138.

60. Van Gheem E., Vereecken J., Le Pen C., *Influence of Different Ions on the Behaviour of Aluminum in Aqueous Solutions*, J. Appl, Electrochem. **32** (2002) p.1193-1200.

61. Szklarska-Smialowska Z., *Pitting Corrosion of Aluminum*, Corrosion Science **41** (1999) p.1743-1767.

62. Stevanovic R.M., Depic A.R. and Drazic D.M., *Activation of Aluminum in Chloride Containing Solutions*, Electrochimica Acta **33** (3) (1988) p.397-404.

63. Van Gheem E., Vereecken J., Pen C., Influence of Different Anions on the Behavior of Aluminum in Aqueous Solutions, Journal of Applied Electrochemistry **32** (2002) p.1193-1200.

64. McCafferty E., *The Electrode Kinetics of Pit Initiation on Aluminum*, Corrosion Science **37** (3) (1995) p.481-492.

65. Kendig M., Addison R., Jeanjaquet S., *The Influence of Adsorbed Oxo-Cr(VI) Species on the Zeta Potential in the Porous Oxide of Anodized Aluminum*, J. Electrochem. Soc. **146** (12) (1999) p.4419-4423.

66. Bockris J.O., Minevski L.V., *On the Mechanism of the Passivity of Aluminum and Aluminum Alloys*, J. Electroanalytical Chemistry 349 (1-2) (1993) p. 375-414.

67. Berzins A., Lowson R., Mirams K., *Aluminium Corrosion Studies. III Chloride Adsorption Isotherms on Corroding Aluminium*, Aust. J. Chem. **30** (1977) p.1891-1903.

68. Beck T., *Salt Film Formation during Corrosion of Aluminum*, Electorchemica Acta **29** (4) (1984) p.485-491.

69. Silva J.W.J., Bustamante E.N., Codaro E.N., Nakazato R.S., Hein L.R.O., *Morphological Analysis of Pits Formed on Al 2024-T3 in Chloride Aqueous Solution*, Applied Surface Science **236** (2004) p.356-365.

70. DiBari G., Read H., *Electrochemical Behavior of High Purity Aluminum in Chloride Containing Solutions*, Corrosion **27** (11) (1971) p.483-493.

71. Datta J., Bhattacharya C., Sarkar D., Bandyopadhyay S., *Influence of pH and Chloride Concentration on the Corrosion Behaviour of Al-6061 Alloy*, IE Journal **84** (2003) p.79-83.

72. Pyun S-I., Moon S-M., *Corrosion Mechanism of Pure Aluminum in Aqueous Alkaline Solution*, J. Solid State Electrochem. 4 (2000) p.267-272.

73. Emergul K.C, Abbas Aksut A., *The Behaviour of Aluminum in Alkaline Media*, Corrosion Science **42** (2000) p.2051-2067.

74. Armstrong R.D., Braham V.J., *The Mechanism of Aluminum Corrosion in Alkaline Solutions*, Corrosion Science **38** (9) (1996) p.1463-1471.

75. De Salzar J.M.G., Urena A., Manzanedo S., Barrena M.I., *Corrosion Behaviour of AA6061 ad AA7005 Reinforced with Al2)3 Particles in Aerated 3.5% Chloride Solutions:Potentiodynamic Measurements and Microstructure Evaluation*, Corrosion Science **41** (1999) p.529-545.

76. Leth-Olsen H., Afseth A. and Nisancioglu K., *Filiform Corrosion of Aluminum Sheet. II. Electrochemical and Corrosion Behaviour of Bare Substrates*, Corrosion Science **40** (7) (1998) p.1195-1214.

77. Leth-Olsen H., Afseth A. and Nisancioglu K., *Filiform Corrosion of Aluminum Sheet.I II. Microstructure of Reactive Surfaces*, Corrosion Science **40** (12) (1998) p.2051-2063.

78. Afseth A., Nordlien J.H., Scamans G.M. and Nisancioglu K., *Effect of Thermo-Mechanical Processing on Filiform Corrosion of Aluminum Alloy AA3005*, Corrosion Science **44** (2002) p.2491-2506.

79. Afseth A., Nordlien J.H., Scamans G.M. and Nisancioglu K., *Effect of Heat Treatment on Filiform Corrosion of Aluminum Alloy AA3005*, Corrosion Science **43** (2001) p.2093-2109.

80. Fishkis M. and Lin J.C., *Formation and Evolution of a Subsurface Layer in a Metalworking Process*, Wear **206** (1997) p.156-170.

81. Huang D.Y., Liu Y.L. and Wambua P., *Formation of ultrafine Scale Structures in Aluminum Containing Small Amounts of Particles by Conventional Rolling Deformation*, J. Materials Science **36** (2001) p.4711-4717.

82. Suryanarayama C., *Mechanical Alloying and Milling*, Progress in Materials Science **46** (2001) p.1-184.

83. Lalande G., Denis M.C., Guay D., Dodelet J.P., Schulz R., *Structural and Surface Characterization of Nanocrystalline Pt-Ru Alloys Prepared by High-Energy Ball-Milling*, Journal of Alloys and Compounds **292** (1999) p.301-310.

84. El-Eskandarany, M.S., *Mechanical Alloying for Fabrication of Advanced Engineering Materials*, William Andrew Publishing/Noyes (2001).

85. Wang W., *Modeling and Simulation of the Dynamic Process in High Energy Ball Milling of Metal Powders*, PhD Thesis, University of Waikato (2000).

86. Janot R., Guerard D., *Ball-milling in liquid media: Applications to the preparation of anodic materials for lithium-ion batteries*, Progress in Materials Science **50** (2005) p.1–92.

87. Jangg G., Kuttner F., Korb F., *Aluminum* **51** (1975) p.641-645.

88. Manna I., Chatoopadhyay P., Banhard F., Fecht J., *Solid State Synthesis of amorphous and/or nanocrystalline AlZrSi Alloy by Mechanical Alloying*, Materials Letters **58** (2004) p.403-407.

89. Manna I., Chatoopadhyay P., Banhard F., Fecht J., *Development of Amorphous and Nanocrystalline AlCuZr alloys by Mechanical Alloying*, Materials Science and Engineering A **379** (2004) p.360-365.

90. Shaw L., Luo H., Villegas J., Miracle D., *Thermal Stability of Nanostructured AlFeCrTi Alloys Prepared via Mechanical Alloying*", Acta Materialia **51** (2003) p.2647-2663.

91. Oelerich W., Klassen T., Bormann R., *Metal Oxides as Additives for Improved Hydrogen Sorption in Nanocrystalline Mg-based Materials,* Journal of Alloys and Compounds **315** (2001) p.237-242.

92. Ivanov E., Makhlouf S., Sumiyama K., Yamauchi H., Suzuki K., Golubkova G., *Structural and Magnetic Properties of Non-Equilibrium bcc Nickel prepared by Leaching of Mechanically Alloyed* $Ni_{35}Al_{65}$, J. Alloys and Compounds **185** (1992).

93. McCafferty E. and Wightman J.P., *Determination of the Concentration of Surface Hydroxyl Groups on Metal Oxide Films by a Quantitative XPS Method*, Surface and Interface Analysis **26** (1998) p.549-564.

94. Levis D., and Northwood D.O., *Evaluation of crystallite size and microstrains in cold-worked lithium fluorite from x-ray diffraction line profiles*, Brit. J. Appl. Phys. D (1969) p.21-26.

95. Powder Diffraction File PDF-2 Database, International Centre for Diffraction Data (2004).

96. Perry R.H., Chilton C.H., *Chemical Engineers' Handbook*, Fifth Edition, McGraw-Hill (1973).

97. HSC: Chemistry 5 Database.

98. www.alcoa.com

99. Raudsepp Mati, Microbeam and Diffraction Methods for the Characterization of Minerals and Materials, Course Material (2004).

100. Chen C., Splinter S.J., Do T., McIntyre N.S., *Measurement of oxide film growth on Mg and Al surfaces over extended period using XPS*, Surface Science **383** (1997) L652-657.

101. Heusler K. E., Landolt D. and Trasatti S., *Electrochemical Corrosion Nomenclature (IUPAC Recommendations 1988,)* Pure and Appl. Chem., **61** (1) (1989) pp. 19-22

H_2 Generation: Water Electrolysis versus Al-Assisted Water Split

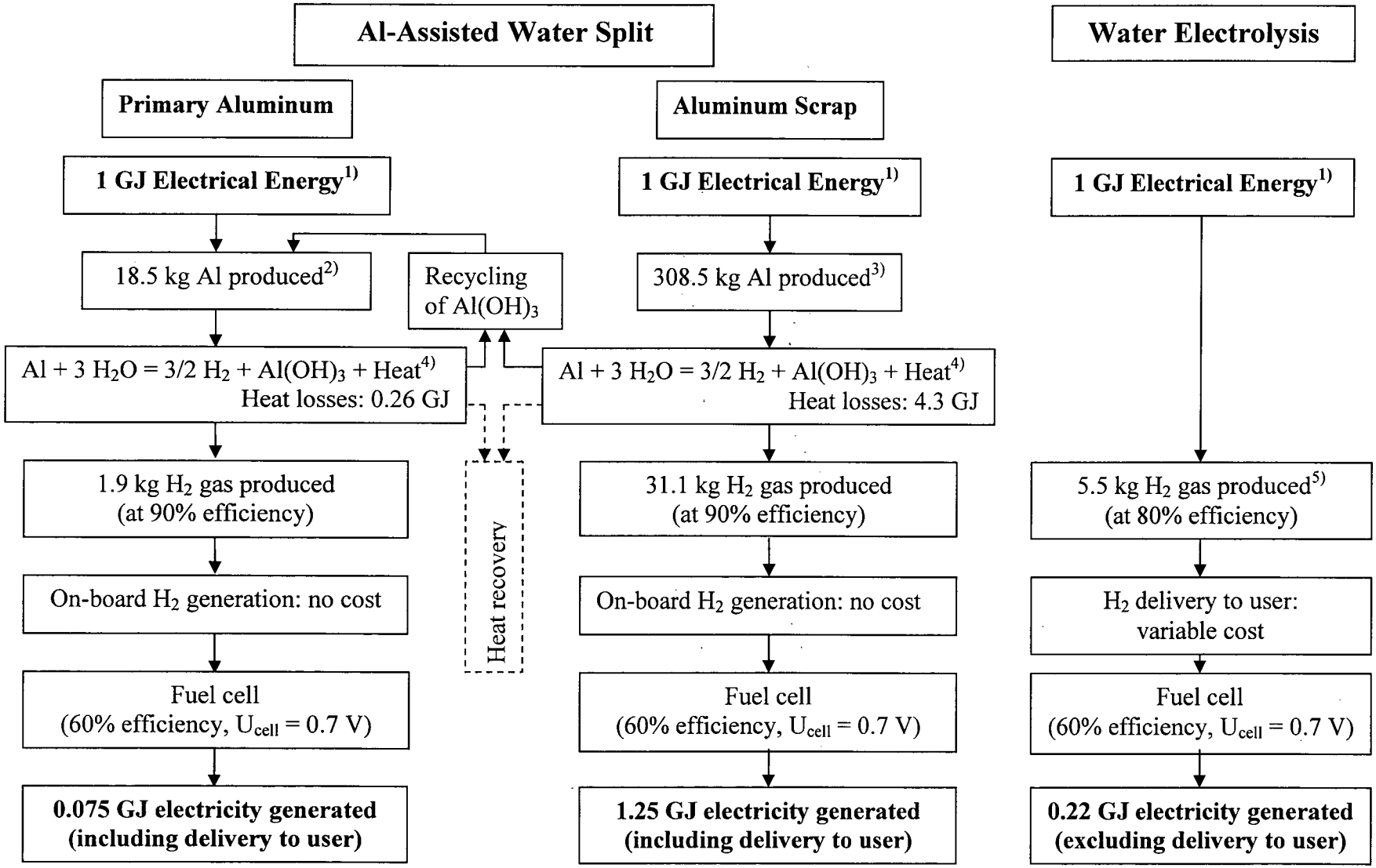

1. CAN$ 16.70 at 0.06/kWh (residential rate).

2. Total energy consumption for primary Al production (only Hall-Héroult process): 15 kWh /1 kg Al

3. Energy consumption for Al production from Al scrap is less then 6% of the energy consumed for primary Al production.

[2, 3)] *W.T. Choate, J.A.S. Green, "U.S. Energy Requirements for Aluminium Production: Historical Perspective, Theoretical Limits and New Opportunities", Report for the U.S Department for Energy, February 2003.* Processed Al is assumed.

4. Reaction enthalpy: -418 kJ/mol; may be partially recovered.

5. Water Electrolysis: 286.02 kJ + H_2O (l) = H_2 + ½ O_2
or 4.5 kWh needed to produce 1 m^3 H_2 gas [*Holleman-Wiberg*]

Appendix B

Hydrogen storage capacity in H_2O and Al-H_2O systems:

$Al + 3H_2O \rightarrow 3/2\ H_2 + Al(OH)_3$

$Al + 2H_2O \rightarrow 3/2\ H_2 + AlOOH$

H_2 storage weight ratio [%] = $[n_1 M_{Hydrogen}/(n_2 M_{Al} + n_3 M_{H2O} + m_{additive})] \times 100\ \%$

1. Hydrogen storage capacity in water:

   $\mathbf{H_2O \rightarrow\ H_2} + ½\ O_2$

   H_2 storage weight ratio [%] = 11.1 wt %

2. Hydrogen storage capacity in mechanically alloyed additive-free Al (when water not considered):

   $\mathbf{Al} + 3H_2O \rightarrow \mathbf{1.5\ H_2} + Al(OH)_3$

   H_2 storage weight ratio [%] = 11.1 wt %

3. Hydrogen storage capacity in mechanically alloyed additive-free Al-H_2O system:

   $\mathbf{Al + 3H_2O \rightarrow 1.5\ H_2} + Al(OH)_3$ or $\mathbf{Al + 2H_2O \rightarrow 3/2\ H_2} + AlOOH$

   H_2 storage weight ratio [%] = 3.7 wt % or 4.8 wt %

4. Hydrogen storage capacity in mechanically alloyed Al(50wt%)-additive(50wt%)-H_2O system:

   $\mathbf{Al + 3H_2O + additive \rightarrow 1.5\ H_2} + Al(OH)_3$ or
   $\mathbf{Al + 2H_2O + additive \rightarrow 3/2\ H_2} + AlOOH$

   H_2 storage weight ratio [%] = 2.8 wt % or 3.4 wt %

*) All calculations assume 100 % reaction conversion.